

**LOW VELOCITY IMPACT CHARACTERIZATION OF MONOLITHIC AND
LAMINATED AA 2024 PLATES BY DROP WEIGHT TEST**

**A THESIS SUBMITTED TO
THE GRADUATE SCHOOL OF NATURAL AND APPLIED SCIENCES
OF MIDDLE EAST TECHNICAL UNIVERSITY**

BY

YUNUS EREN KALAY

**IN PARTIAL FULFILLMENT OF THE REQUIREMENTS FOR THE DEGREE OF
MASTER OF SCIENCE
IN
THE DEPARTMENT OF METALLURGICAL AND MATERIALS ENGINEERING**

SEPTEMBER 2003

Approval of the Graduate School of Natural and Applied Sciences

Prof. Dr. Canan ÖZGEN
Director

I certify that this thesis satisfies all the requirements as a thesis for the degree of Master of Science.

Prof. Dr. Bilgehan ÖGEL
Head of Department

This is to certify that we have read this thesis and that in our opinion it is fully adequate in scope and quality, as a thesis for the degree of Master of Science.

Prof. Dr. Bilgehan ÖGEL
Supervisor

Examining Committee Members:

Prof.Dr. Muharrem TİMÜÇİN

Prof. Dr. Tayfur ÖZTÜRK

Prof.Dr. Orhan YILDIRIM

Prof.Dr.. Bilgehan ÖGEL

Assoc.Prof.Dr. Cevdet KAYNAK

ABSTRACT

LOW VELOCITY IMPACT CHARACTERIZATION OF MONOLITHIC AND LAMINATED AA 2024 PLATES BY DROP WEIGHT TEST

Kalay, Yunus Eren

MSc., Department of Metallurgical and Materials Engineering

Supervisor: Prof. Dr. Bilgehan ÖGEL

September 2003, 149 pages

The objective of this study was to investigate the low velocity impact behavior of both monolithic and laminated aluminum alloy plates. For this purpose, a drop-weight test unit was used. The test unit included the free fall and impact of an 8 kg hammer with an 8 mm punching rod from 0.5 m to 4 m. The relationship between the change in static mechanical properties (hardness, ultimate tensile strength, yield strength, strain hardening rate) and low velocity impact behavior of monolithic aluminum plates were investigated. Tested material was AA 2024, heat treatable aluminum alloy, which was artificially aged to obtain a wide range of mechanical properties. In the second stage of the study, the relationship between the low velocity impact behavior of laminated plates was compared with that of monolithic aluminum plates at identical areal densities. For this purpose, a series of AA 2024 thin plates were combined with different types of adhesives (epoxy, polyurethane or tape). Finally, fracture surface of the samples and microstructure at the deformation zone were examined with both scanning electron microscope and optical microscope.

It is found that the ballistic limit velocities of AA 2024 plates increase with increase in hardness, yield strength and ultimate tensile strength. It is also found that a linear relation exists between the ballistic limit velocity and strain hardening rate or hardness. When the low velocity impact behaviors of laminated and monolithic targets were compared, it was seen that monolithic targets have a higher ballistic limit velocity values for from the 2.5 to 10 mm thick targets. It was also observed that adhesives are not so effective to strengthen the low velocity impact performance. On the other hand, with increasing Charpy impact energy, penetration and perforation behaviors are getting worse in 10 to 30 joules energy range.

Different types of failure mechanisms involving, plugging, dishing, stretching and bending were determined. For high strength and thick plates plugging type deformation was led. In contrast, for thinner and weaker targets bending, stretching and dishing type failures were dominating. For laminated targets also dishing type failure was determined.

Keywords: Drop-Weight Test, Low Velocity Impact, AA 2024, Aging, Adhesives, Failure Mechanisms.

ÖZ

YEKPARE VE KATMANLI AA 2024 PLAKALARIN ÇEKİÇ DÜŞÜRME TESTİ İLE DÜŞÜK HIZLARDA DARBE KARAKTERİZASYONU

Kalay, Yunus Eren

Yüksek Lisans, Metalurji ve Malzeme Mühendisliği Bölümü

Tez Yöneticisi: Prof. Dr. Bilgehan Ögel

Eylül 2003, 149 sayfa

Bu çalışmanın temel amacı yekpare ve katmanlı alüminyum alaşımlarının düşük hızlarda darbe davranışlarının incelenmesidir. Bu amaçla çekiç düşürme test düzeneği kullanılmıştır. Test ünitesi, 8 kg ağırlığında çekice bağlı 8 mm çapında delme çubuğunun, 0.5 - 4 m arasından serbest düşüşünü ve darbesini içermektedir. Yekpare AA 2024 plakaların statik mekanik özellikleri (sertlik, çekme dayancısı, akma dayancısı, gerinim sertleşme hızı) ve düşük hızlardaki darbe dayanımları arasındaki ilişki incelenmiştir. Test edilen malzemesi olan yaşlandırılabilir AA 2024, geniş kapsamlı mekanik özellikler kazandırılmak amacıyla suni olarak yaşlandırılmıştır. Çalışmanın ikinci aşamasında aynı alan yoğunluklarına sahip, yekpare ve katmanlı alüminyum plakalarının düşük hızlardaki darbe davranışları arasındaki ilişki karşılaştırılmıştır. Bu amaçla ince AA 2024 plakalar serisi farklı cinsteki yapıştırıcılarla (epoksi, polyuretan ve bant) birleştirilmiştir. Sonunda ise numunelerin deformasyon bölgelerindeki kırılma yüzeyleri ve mikro yapıları hem tarama elektron mikroskobu hem de optik mikroskop ile incelenmiştir.

AA 2024 plakalarının balistik limit hızlarının, sertlik, çekme ve akma dayançlarındaki artış ile arttığı gözlemlenmiştir. Ayrıca balistic limit hızları ile gerinim sertleşme hızı ve sertlik arasında doğrusal bir ilişkinin var olduğu bulunmuştur. Katmanlı ve yekpare plakaların düşük hızlardaki darbe davranışları karşılaştırıldığında yekpare plakaların 2.5 mm'den 10.0 mm kalınlığa kadar olan plakalar için daha yüksek balistik limit hızlara sahip oldukları görülmüştür. Düşük hızlarda darbe performansının kuvvetlendirilmesinde yapıştırıcıların o kadar da etkili olmadığı gözlenmiştir. Ayrıca, Charpy darbe enerjisinin artması ile 10J - 30J'a kadar olan enerji aralığında nüfus etme ve delme davranışları kötüleşmektedir.

Bu çalışma sırasında ayrıca farklı tiplerdeki kırılma mekanizmaları; “*plugging*”, “*dishing*”, “*stretching*” ve “*bending*” incelenmiştir. Yüksek mukavemette ve kalın levhalarda “*plugging*” tipi deformasyon gözlemlenirken, daha ince ve düşük mukavemetteki plakalarda “*bending*” ve “*stretching*” tipi deformasyon gözlemlenmiştir. Katmanlı hedeflerde ise “*dishing*” tipi deformasyon tespit edilmiştir.

Anahtar Kelimeler: Çekiç-düşürme testi, Düşük hızlarda darbe, AA 2024, Yaşlandırma, Yapıştırıcı, Kırılma Mekanizmaları

To Birgöl & Mustafa Kalay

ACKNOWLEDGEMENTS

First of all, I would like to express sincere appreciation to my supervisor Prof. Dr. Bilgehan Ögel for his guidance and insight throughout the thesis.

I also want to express sincere thanks to Prof. Dr. Orhan Yıldırım for his valuable suggestions.

I wish to thank Dr. Qingming Li, instructor of the department of Mech. Aero. and Manuf. Engng. in Manchester University England, for his valuable comments and suggestions on my experimental data.

I want also thank to Ahmet Tokmakçiođlu, chief of process control and fabrication Insp./NDI department TAI Aerospace Industries Inc., and Tolay Özer, regional representative, Sika® construction, for their valuable suggestions for surface preparation and adhesive application of AA 2024 plates. Thanks are also due to technical staff of the Metallurgical and Materials Engineering and Mechanical Engineering Departments.

Finally, thanks to my family; my father and my mother, for all their love and support. Special thanks go to my sweet love, İlkay Saltođlu, without whom I would not have been able to do anything at all.

TABLE OF CONTENTS

ABSTRACT	iii
ÖZ	v
DEDICATION	vii
ACKNOWLEDGEMENTS	viii
TABLE OF CONTENTS	ix
LIST OF TABLES	xiii
LIST OF FIGURES	xv
NOMENCLATURE	xix
CHAPTERS	
1. INTRODUCTION	1
2. THEORY	5
2.1. DEFINITION OF BALLISTICS.....	5
2.1.1. Interior Ballistics.....	5
2.1.2. Exterior Ballistics.....	7
2.2. TERMINAL BALLISTICS.....	8
2.2.1. The Projectile.....	11
2.2.2. Projectile and Trajectory Orientation.....	16
2.2.3. Penetration and Perforation.....	17
2.2.4. Ballistic Limit.....	21
2.2.5. Target Material Physical Characteristics.....	23
2.3. IMPACT TESTS.....	24
2.3.1. High Velocity Impact Testing.....	24
2.4. DROP WEIGHT TEST.....	27
2.4.1 Determining Nil Ductility Temperature.....	27
2.4.2 Metal Working Operations.....	30
2.4.3 Ballistic Testing.....	31

2.5. ALUMINUM ALLOYS.....	32
2.5.1 Alloy and Temper Designation System.....	32
2.5.2 Phases in Aluminum Alloys.....	36
2.5.3 Strengthening by Heat Treatment.....	38
2.5.4 Age Hardening of AA 2024.....	40
2.6. ADHESIVES.....	42
2.6.1 Epoxy Adhesives.....	43
2.6.2 Polyurethane (Urethane) Adhesives.....	45
2.6.3 Surface Preparation of Aluminum before Adhesive Bonding.....	46
3. EXPERIMENTAL PROCEDURE.....	49
3.1. EXPERIMENTAL SET-UP.....	50
3.1.1. Drop Weight Testing Machine.....	50
3.1.2. Test Set-Up Modifications.....	53
3.1.3. Drop-Weight Testing	55
3.2. SPECIMEN PREPARATION.....	61
3.2.1. Heat Treatment of AA 2024 Target Plates.....	61
3.2.2. Preparation of Laminated Targets.....	63
3.2.2.1 Surface Preparation for Adhesive Bonding.	65
3.2.2.2 Application of Adhesive.	66
3.3. STATIC MECHANICAL CHARACTERIZATION.	68
3.3.1. Hardness Test of AA 2024 Plates.....	69
3.3.2. Tensile Testing of AA 2024 Plates.....	69
3.3.3. Tensile Testing of Adhesives.....	70
3.4. MICROSTRUCTURAL CHARACTERIZATION...	74
3.5.DYNAMIC.MECHANICAL.CHARACTERIZATION	74
3.5.1 Notched-Bar Impact Test.....	74
3.6. NOTATION FOR TARGET PLATES.....	75

4. EXPERIMENTAL RESULTS	77
4.1. MICROSTRUCTURAL CHARACTERIZATION OF AA 2024.....	78
4.2. EFFECT OF FPL TREATMENT ON SURFACE MORPHOLOGY OF AA 2024	81
4.3. STATIC MECHANICAL TESTS.....	87
4.3.1 Hardness Test.....	87
4.3.2 Tensile Testing.....	90
4.4. DYNAMIC MECHANICAL TESTS.....	93
4.4.1 Charpy Impact Test.....	93
4.4.2 Determination of Ballistic Limits of AA 2024 Plates.....	94
4.5 MACROSCOPIC INSPECTIONS.....	102
4.5.1 Macroscopic Inspection of Projectile.....	102
4.5.2 Macroscopic Inspection of Monolithic Targets....	104
4.5.3 Macroscopic Inspection of Laminated Targets....	106
4.6. MICROSCOPIC INSPECTIONS.....	109
5. DISCUSSION	114
5.1 FAILURE MECHANISMS.....	115
5.1.1 Failure Mechanisms in Monolithic Targets.....	116
5.1.2 Failure Mechanisms in Laminated Targets.....	119
5.1.3.Effects of Artificial Aging on Failure Mechanisms.....	121
5.2.FACTORS.AFFECTING.BALLISTIC PERFORMANCE.....	123
5.2.1 Effect of Hardness.....	124
5.2.2 Effect of Tensile and Yield Strength.....	124
5.2.3 Effect of Strain Hardening Rate.....	129
5.2.4 Effect of Charpy Impact Energy.....	130
5.2.5 Effect of Thickness and Lamination.....	131

6. CONCLUSION.....	137
REFERENCES.....	139
APPENDICES.....	147

LIST OF TABLES

TABLE

Chapter 2

2.1	Impact Response of Materials.....	10
2.2	Projectile Characteristics.....	14
2.3	The basic temper designations.....	34
2.4	The basic temper designations (continued).....	35
2.5	Temper Designations for Strain-Hardened Alloys.....	36
2.6	Possible Phases in AA 2024.....	38
2.7	Advantages of Adhesives.....	42
2.8	Disadvantages of Adhesives.....	43

Chapter 3

3.1	Nominal Chemical Compositions of AA 2024 targets.....	61
3.2	Monolithic AA 2024 T6 aging to compare mechanical properties.....	62
3.3	Monolithic AA 2024 T6 aging to compare dynamic properties with laminated AA 2024 T6 plates.....	63
3.4	Heat treatment of laminated type targets.....	63
3.5	Chemicals used in surface preparation of AA 2024.....	66
3.6	Notations for tensile and lap-shear tests of adhesives.....	72
3.7	Keller's Reagent.....	74
3.8	Charpy V-notch impact test parameters.....	75
3.9	Notation for Monolithic Targets.....	75
3.10	Notation for Monolithic Targets (continued).....	76
3.11	Notation for Laminated Targets.....	76

Chapter 4		
4.1	Tensile and lap-shear tests results for polyurethane.....	85
4.2	Tensile and lap-shear tests results for epoxy.....	85
4.3	Brinell hardness values of AA 2024 at 220°C.....	87
4.4	Brinell hardness values of AA 2024 at 190°C.....	88
4.5	Tensile test values of AA 2024 at 220°C.....	90
4.6	Impact energy values of AA 2024.....	93
Chapter 5		
5.1	Experimental parameters used in Equation 5.1.....	127
5.2	Comparison of experimental results with analytical model of Chen and Li.....	128
5.3	Comparison of experimental results with analytical model of Woodward and Cimpoeru.....	135
Appendices		
App.3	Unit Conversion Factors.....	149

LIST OF FIGURES

FIGURE

Chapter 2

2.1	Pressure/ velocity/ space curve	7
2.2	Forces acting on the Projectile	8
2.3	Examples of kinetic energy penetrators	13
2.4	Examples of projectiles with warheads.....	14
2.5	Types of angle of incidence	16
2.6	Permanent deformation of a thin target element showing bulging and dishing	18
2.7	Perforation Mechanisms	20
2.8	Target failure features in homogeneous plates	21
2.9	Definitions of perforation and partial penetration for defining the ballistic limit.....	22
2.10	Phase diagram for projectile impact	26
2.11	Fracture appearances vs. temperature for explosion-crack- starter test.....	28
2.12	Schematic view of a drop-weight machine	30
2.13	Equilibrium binary solid solubility as a function of temperature for alloying elements most frequently added to aluminum.....	36
2.14	The principal aluminum alloys	37
2.15	Effect of aging on tensile strength of AA 2024	41
2.16	Effect of aging on percent elongation of AA 2024	41
2.17	Polyurethane reaction	46
2.18	Simple urethane reaction	46

Chapter 3

3.1	Gravity Drop Weight Testing Machine.....	51
3.2	Drop Weight Setup and Modifications.....	56

3.3	Calibration Chart for Drop Weight Test Unit.....	59
3.4	(a) Hammer with blunt penetrator	
	(b) Target (40 x 30 x 5 mm AA 2024).....	60
3.5	Muffle Furnace	64
3.6	Oil Bath.....	64
3.7	AA 2024 plates bonded with epoxy adhesive	67
3.8	AA 2024 plates loosely held with adhesive tape.....	68
3.9	Epoxy adhesive preparation	68
3.10	Dimensions of the Tensile Test Specimen.....	69
3.11	Dimensions of Tensile Test Specimen for Adhesives.....	71
3.12	Dimensions of Lap Shear Test Specimen for Adhesives.....	71
3.13	Specimens used in adhesive tensile tests.....	72
3.14	Specimen used in adhesive lap-shear test.....	73
3.15	Grips prepared for tensile test of adhesives.....	73
Chapter 4		
4.1	AA 2024-O (200X).....	79
4.2	AA 2024-T6 (200X).....	79
4.3	AA 2024-T6, showing rosettes formed by eutectic melting. Solidus temperature was exceeded during solution heat treating (200X).....	80
4.4	AA 2024-T6, SEM picture showing eutectic melting.....	80
4.5	AA 2024-T6, as ground with 100 grit abrasive paper.....	82
4.6	AA 2024-T6, as FPL etched for 2 minutes.....	82
4.7	AA 2024-T6, as FPL etched for 10 minutes.....	83
4.8	AA 2024-T6, as FPL etched for 15 minutes.....	83
4.9	AA 1050 and AA 2024, as FPL etched for 15 minutes	84
4.10	The surfaces of jigs of FPL applied (a) and not applied (b) specimens.....	86
4.11	Aging curve of AA 2024 at 220°C.....	89

4.12	Aging curve of AA 2024 at 190°C.....	89
4.13	The change in UTS of AA 2024 plates after aging at 220 °C	91
4.14	The change in yield strength of AA 2024 plates after aging at 220 °C.....	91
4.15	Comparison of hardness values of AA 2024 plates after aging at 190 and 220 °C.....	92
4.16	Comparison of tensile and yield strength values of AA 2024 plates after aging at 220 °C.....	92
4.17	Impact energy versus aging time.....	93
4.18	The change in ballistic limit of AA 2024 with respect to hardness.....	96
4.19	The change in ballistic limit of AA 2024 with respect to tensile strength.....	96
4.20	The change in ballistic limit of AA 2024 with respect to yield strength.....	97
4.21	The change in ballistic limit of AA 2024 with respect to SHR.....	97
4.22	The change in ballistic limit of AA 2024 with respect to impact energy.....	98
4.23	Ballistic limit versus Thickness (Monolithic).....	100
4.24	Ballistic limit versus Thickness (Laminated).....	100
4.25	Ballistic limit versus Thickness (Both monolithic and laminated).....	101
4.26	Penetrators after the impact.....	103
4.27	Ballistic limit reached after an impact. The plug could not be separated.....	103
4.28	Sectioned AA 2024-O target after impact.....	105
4.29	Front face of AA 2024-T6 with 2.5 mm thickness.....	105

4.30	Notation of layers with respect to impact side.....	107
4.31	Two layers AA 2024-T6 after impact.....	107
4.32	The sectioned view of an impacted 10 mm thick plates.....	108
4.33	(a) The sectioned view of an impacted AA 2024-O plate (50X) (b) The crack propagation at a higher magnification (200X).	110
4.34	AA 2024-T6 plates. Intense Shear Zone (200X).....	112
4.35	AA 2024-T6 plates and plug. Shear and Compression Zone.	112
4.36	AA 2024-T6 laminated plate. (Front Faces).....	113
4.37	AA 2024-T6 laminated plate. (Plug and Rear Faces).....	113
Chapter 5		
5.1	Schematic views of failure mechanisms investigated.....	115
5.2	Shear localization.....	118
5.3	Schematic view of failure mechanisms by pure shear plugging.....	118
5.4	Schematic view of failure mechanisms by bending and plugging.....	119
5.5	Micrographs of (a) monolithic and (b) laminated targets close to perforation.....	121
5.6	AA 2024 target solution heat treated at 540°C impacted under drop-weight test machine.....	122
5.7	Comparison of experimental results with analytical model of Chen and Li.....	128
5.8	Ballistic limits versus Thickness (Monolithic).....	132
5.9	Ballistic limits versus Thickness (Laminated).....	132
5.10	Simple force equilibrium model for plugging.....	134
Appendices		
App.1	Three Dimensional Phase Diagram of Al-Cu-Mg	147
App.2	Ternary Phase Diagram of Al-Cu-Mg	148

NOMENCLATURE

A	$\frac{2}{3} \left\{ 1 + \ln \left[\frac{E}{3(1-\gamma)\sigma_y} \right] \right\}$
B	1.5
d	diameter of the projectile (mm)
E	Young's modulus of the target material (GPa)
H	thickness of the plate (mm)
H_p	thickness of the plug (mm)
H_i	depth of indentation (mm)
M	mass of the projectile (g)
K	constraint factor for quasi-static indentation of metals (K=2,7)
SHR	strain hardening rate (MPa)
STD	standard deviation
V_{BL}	ballistic limit (m/s)
UTS	ultimate tensile strength (MPa)
%EL	percent elongation
χ	$\frac{H}{d}$ dimensionless thickness of the plate
γ	Poisson's ratio of the target
η	$\frac{\rho H \pi d^2}{4M}$
ρ	density of the target material (g/cm ³)
σ_y	yield strength of the target material (MPa)
Y	flow stress (MPa)
τ	shear stress (MPa)
σ_{sdt}	dynamic shear strength of the target (MPa)
$\dot{\epsilon}$	strain rate (s ⁻¹)
Y_p	yield strength of the projectile body (MPa)

CHAPTER 1

INTRODUCTION

Ballistic has been the most attractive science for human beings since the prehistoric ages. Terminal ballistic, which is one of the major subclass of ballistic science, deals with all interactions between the projectile and target. From the primitive form of armors made up of wood to light-weight composite protection, terminal ballistic technology was always developed for the same aim, which is the protection.

At one time terminal ballistic was primarily of concern to the military. However, during the last few decades, enormous strides have been made in civilian technology. Safe designs of transportation vehicle for hazardous materials, nuclear-reactors, or even protection of spacecraft from meteoroid impact were extremely important besides military applications. Of course armor system designs for protection of police officers, government and military personnel have still the biggest share in terminal ballistic science.

Projectile and target interaction involve highly complex processes which have been investigated experimentally for a long time. Analytical and especially numerical simulations due to the innovations in computer science are most recent investigations in terminal ballistic. Many of the analytical models are single mechanism models that have so far enjoyed limited applications. Even only for the penetration and perforation of targets by kinetic energy projectiles

eight possible perforation mechanisms for brittle and ductile targets in a range of target thickness. Also more than one perforation mechanism may lead in a target under impact loading. As far as numerical simulations were considered, they are successful in predicting the response of targets but they have to be still developed in reflecting all target and projectile properties. Also they still require considerable resources in terms of computing time.

Aluminum alloys, due to their specific strength, are very important ballistic materials. In contrast to the wide use of steel armors, light weight armors like aluminum alloys started to be investigated recently. It has been demonstrated various idealized failure mechanics for homogeneous aluminum plates by various projectiles with a blunt tip. Shear plugging was usually observed for thick plates and dishing was dominating for laminated targets. Multi-stage models have been proposed to study the perforation of relatively thick plates. Penetration of a plate target was divided into two stages; deceleration of the effective mass of the projectile and shear plug formation. This model was improved by considering the reduction of the shear force in the second stage. Then this two-stage model was extended to a three-stage model and modified to a five stages model. In another five stage model plastic wave propagation in both the thickness and radial directions of the plate is considered. Recent analytical models indicate ballistic limit velocities for shear plugging deformation by non-deformable projectile. However they are based on some assumptions therefore great care must be taken in using them.

Experimental investigations in penetration and perforation studies can roughly be divided into three major categories related to the impact velocity of the projectile. The first category covers low velocity impact ($V_i < 50$ m/s) where target plates are normally hit by heavy projectiles using a drop hammer or a pneumatic accelerator. The second category covers the subordnance and ordnance velocity regime ($50 < V_i < 1300$ m/s) where projectiles of arbitrary mass and shape are launched from compressed gas guns or powder guns. The

last category covers the other extreme that is high velocity penetration ($V_i > 1300$ m/s). Second and third categories have received much attention however there isn't enough information for low velocity impact in the literature especially for AA 2024 which is a potential candidate material in terminal ballistic science. Also the effect of age hardening parameters in penetration and perforation by a blunt tip non deformable projectile is not clear for AA 2024 metal targets. Another debate is for using metallic laminates substitute for monolithic metal targets. Metallic laminates have some potential advantages over monolithic metallic armors including the ability to be fabricated into thicker structures than is possible with homogeneous plates of the same material for a given strength level. Monolithic and laminated targets have different failure modes. In spite of differences in failure modes, homogeneous targets were found to be as effective as or more effective than laminates. Some studies showed that the response of multi-layered targets depends on plate thickness. They concluded that layering weakened thin targets and monolithic targets were more effective against perforation than equal weight multi-layered targets.

The benefits of replacing monolithic targets with multi-layered ones are not clear. Moreover the effect of adhesion used to create laminated target in ballistic limit is missing. On the other hand, the information about the effect of artificial aging of AA 2024, on low velocity impact behavior is weak. There are some studies on the correlation of analytical and numerical data with experimental ones, but the correlation of those data with low velocity impact data are almost uncovered. Therefore this study will be mainly focused on the debates mentioned above.

In this study a drop-weight test machine with a blunt tip non deformable projectile held on an 8 kg hammer was used. AA 2024 metal targets, with different mechanical properties supplied by artificial aging, were tested under drop weight test machine. The relationships between low velocity impact

behavior and mechanical properties were determined. . Ballistic limit data were also compared with some analytical models. Moreover, in order to investigate the effect of lamination, a series of laminated and monolithic targets were impacted at low velocities. Different types of adhesives (Epoxy, polyurethane, tape) were used to analyze the effect of adhesives. AA 2024 targets were also investigated under optical and scanning electron microscope. Different types of failure mechanisms were determined after macro and micro examination.

In conclusion, determination of the factors affecting low velocity impact behavior, including artificial age hardening, lamination and adhesion, may provide valuable information in the terminal ballistic science. Although this study was mainly focused on AA 2024 plates, the results most probably can be used for other monolithic and laminated metal targets especially having the same failure mechanisms.

CHAPTER 2

THEORY

2.1. DEFINITION OF BALLISTICS

Ballistics is the science that treats of the motion of projectiles, and is a particular branch of applied mechanics [1]. Actually the time interval from the instant the trigger is squeezed until the projectile crashes into a nearby target is less than the time it takes to blink an eye. Yet, in that brief fraction of a second, a large number of complex phenomena have all taken place. For convenience, the study of these various phenomena is known collectively as ballistics. This term, however, has become a little too general, and so ballistics is now broken down into three distinct and separate technologies:

- *Interior Ballistics*: Science and technologies which is concerned with what takes place inside the barrel;
- *Exterior Ballistics*: Science and technologies which is concerned with the aerodynamic forces acting on the projectile during its flight; and
- *Terminal Ballistics*: Science and technology which is concerned with the dynamics of target impact [2].

2.1.1. Interior Ballistics

Interior ballistics includes a study of the mode of combustion of the powder, the pressure developed, the velocity of the projectile along the bore, and the

calculation of the dimensions of the powder chamber and of the powder which, for any particular design of gun and projectile, will give the required muzzle velocity while not exceeding the permissible interior pressure. Having determined the powder-pressure curve for the gun, the thickness of wall of the gun to withstand the expected pressure at each point may be determined by the principles of the gun construction [1].

At the instant that the charge is ignited the propellant begins to burn in the confined space the forward and rearward limits of which are defined by the driving band of projectile and whatever method of obturation is used to prevent the rearward escape of gases. The rate of burning increases in proportion to the rate of increase in pressure until the gas reaches "shot start pressure". Shot start pressure is the pressure at which the projectile is moved forward. As the projectile moves down the barrel the space available for gases increases thus reducing the rate of increase in pressure. The point of maximum pressure is reached when the pressure loss caused by the space increase is equal to the pressure increase from the burning propellant. Thereafter the pressure in the bore begins to drop. Meanwhile the projectile continues to accelerate and continues to accelerate even after the charge is all burnt; however, the rate of acceleration decreases until retardation occurs just outside the muzzle. **Figure 2.1** shows the relationship between pressure, distance traveled by the projectile and velocity of the projectile. During the period of projectile travel in the bore about 25-35% of the energy produced by the charge is consumed. The remainder is discharged into the atmosphere after the projectile leaves the muzzle [3].

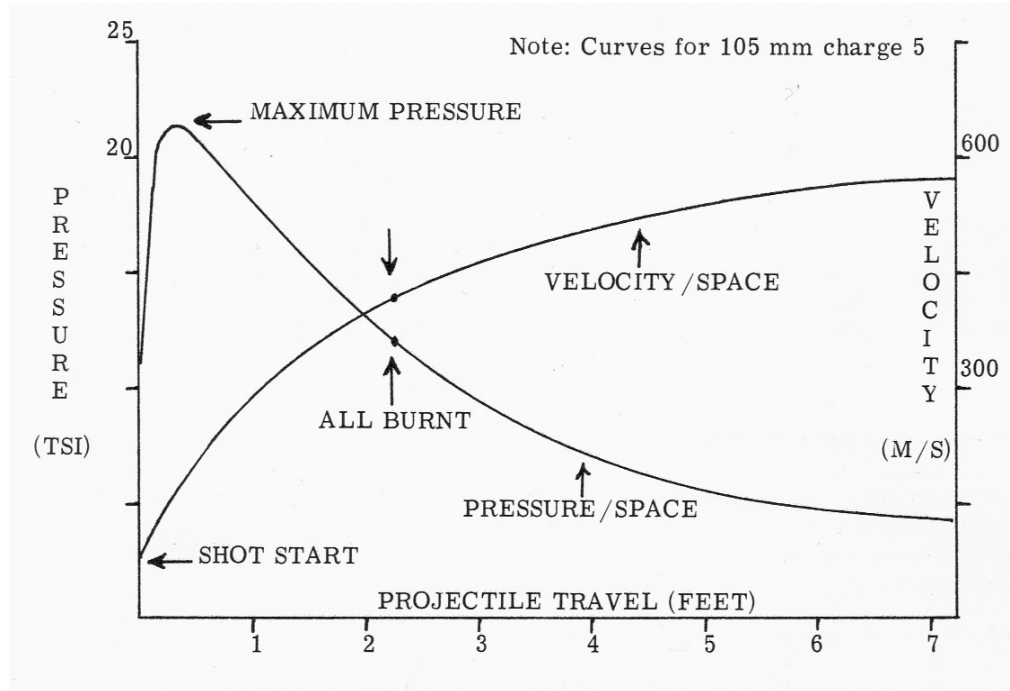


Figure 2.1. Pressure/ velocity/ space curve [3].

2.1.2. Exterior Ballistics

Exterior ballistics is a branch of physics which deals with the motion of projectiles through the air and their behavior during flight. The term projectile is used in a broad sense to designate any rigid body which is projected or thrown at a target. It includes such missiles as rifle bullets, artillery projectiles, airplane bombs, etc.

Consider a projectile moving in still air shown as shown in **Figure 2.2** with its axis making an angle δ with the direction of motion. It will be acted on by gravity W , acting vertically downward, and an air force R , which will depend upon the velocity, the characteristics of the air and of the projectile, and upon the presentation of the projectile with respect to the direction of motion.

If δ were zero and the projectile symmetrical about its axis, R would point in a direction opposite to the direction of motion. In general, δ is not zero and thus

R intersects the direction of motion [1]. Then, exterior science and technology deals with this kind of aerodynamic forces acting on the projectile during its flight.

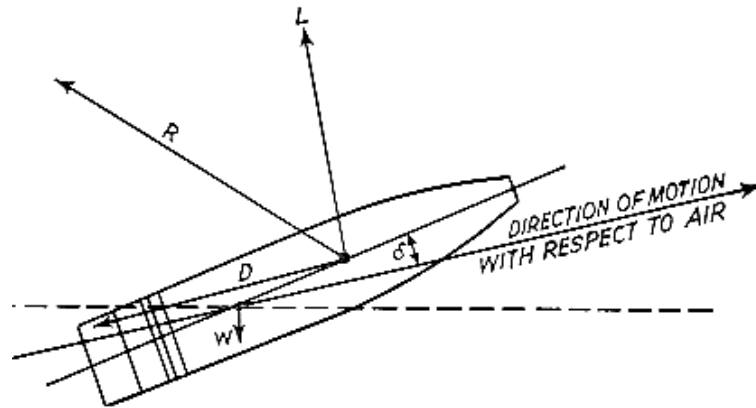


Figure 2.2 Forces acting on the projectile [1].

2.2. TERMINAL BALLISTICS

Terminal Ballistics deals with the study of the projectile's effect on the target, or the counter-effect of the target on the projectile. Yet, it is concerned with the dynamics of target impact.

Situations involving impact – the collision of two or more solids – are currently receiving widespread attention. At one time, impact problems were primarily of concern to the military. Now, however, as civilian technology grows more sophisticated, severe demands are being made on the behavior of materials under very short duration loading. Safe and cost-effective design demands a rigorous understanding of the behavior of materials and structures subjected to intense impulsive loading for such diverse applications as:

1. Safe demolition of prestressed concrete structures,
2. The transportation safety of hazardous materials,
3. Crashworthiness of vehicles and protection of their occupants or cargo,
4. Safety of nuclear-reactor containment vessels subjected to missile impact from external sources (tornadoborne debris, aircraft) or internal ones (extremes pressures from reactor excursions, debris, and fragments from failed components),
5. The design of lightweight armor systems, including fabric body armors, for protection of police officers, executives in business, and government and military personnel,
6. The vulnerability of military vehicles, aircraft, and structures to impact and explosive loading,
7. Protection of spacecraft from meteoroid impact,
8. Explosive forming and welding of metals [4].

The study of impact phenomena involves a variety of classical disciplines. In the low-velocity regime ($< 50\text{m/s}$) many problems fall in the area of structural dynamics. Local indentations or penetrations are strongly coupled to the overall deformation of the structure. Typically, loading and response times are in the millisecond regime. As the striking velocity increases ($0.5\text{-}2\text{ km/s}$) the response of the structure becomes secondary to the behavior of the material within a small zone (typically 2-3 projectile diameters) of the impact area. A wave description of the phenomena is appropriate and the influences of velocity, geometry, material constitution, strain rate, localized plastic flow, and failure are manifest at various stages of the impact process. Typically, loading and reaction times are on the order of microseconds. Still further increases in impact velocity ($2\text{-}3\text{ km/s}$) result in localized pressures that exceed the strength of the material by an order of magnitude. In effect, the colliding solids can be treated as fluids in early stages of impact. At ultra-high

velocities ($> 12\text{km/s}$) energy deposition occurs at such a high rate that an explosive vaporization of colliding materials results [4].

Table 2.1 Impact response of materials [5].

$\dot{\epsilon}$	V_s	Effect	Method of Loading
10^8	$>12 \text{ kms}^{-1}$	Explosive Impact Colliding Solids Vaporized	-
10^6	$3-12 \text{ kms}^{-1}$	Hydrodynamic Material Compressibility not Ignorable	Explosive Acceleration
	$1-3 \text{ kms}^{-1}$	Fluid Behavior in Materials; Pressures Approach or Exceed Material Strength; Density a Dominant Parameter	Powder Guns, Gas Guns
10^4	$500-1000 \text{ ms}^{-1}$	Viscous-Material Strength Still Significant	Powder Guns
10^2	$50-500 \text{ ms}^{-1}$	Primarily Plastic	Mechanical Devices, Compressed Air Gun
10^0	$<50 \text{ ms}^{-1}$	Primarily Elastic Some Local Plasticity	Mechanical Devices, Compressed Air Gun

2.2.1. The Projectile

Any item capable of being launched can become a projectile. Military projectiles are probably the most familiar, but they form only a small subset of possible missiles. During the demolition of buildings made of prestressed concrete, scabs or spall fragments may be formed as a result of rapid unloading.

Classification

Projectiles can be characterized according to the method of launching and the commodity that is delivered. The means of setting them in motion are projection from guns (bullets, shells, grenades), drops from a parent vehicle (bombs, mines), and self-projecting devices (missiles, rockets, torpedoes). The commodity to be delivered by a projectile solely designed to penetrate is its kinetic energy. It is explosive or incendiary warhead for projectiles that are intended to approach but not penetrate a target. It is a combination of both kinetic energy and warhead for penetrating weapons that count on explosive or incendiary effects to contribute to the dysfunction of the target [6].

Kinetic Energy Penetrators

Kinetic energy projectiles of all sizes and shapes have been used since man first discovered that a thrown object could be a lethal weapon. The effectiveness of a kinetic energy projectile is based, as the name indicates, on the kinetic energy of the projectile when it reaches the target. That energy is a function of the mass and the velocity of the projectile. When that energy is expended on a small area of the target, the projectile is capable of penetrating the target.

Examples of projectiles that are designed for efficiency of penetration of targets are shown in **Figure 2.3**. Armor-piercing projectiles have a hard core to which other components are attached that serve exterior and interior ballistic purposes, i.e. a rotating band for spin stabilization, a windscreen for

aerodynamic efficiency, and a tracer unit to make the trajectory visible. These parts of the projectile increase its range and assure a favorable orientation at impact but tend to degrade performance slightly compared to a bare core striking under the same conditions. The projectile parameters that are required to determine the *ballistic limit in regions of the phase diagram* (**Figure 2.10**) where the projectile remains intact are the projectile mass m , its dimensions of length L_A , diameter D , and the nose shape and length L_N , and the density of the penetrator ρ_p . This set of parameters constitutes a minimum description of the penetrator. In order to determine the deformation and breakup limit curves, a further characterization of strength of the projectile is needed [6].

Projectiles with Warheads

Example of a design of projectile that is intended to deliver a warhead with significant penetration into a target is shown in **Figure 2.4**. The body of these projectiles and their high explosive content are the principal elements of the penetrator, but the fuse is the vital functioning elements of the warhead. The penetrator must achieve some degree of entry to target without dysfunction of the warhead such as, fuse malfunctioning or premature initiation of the explosive system. The design of penetrating projectiles with warheads must have a compromise between penetration and warhead performance. This compromise can be expressed by determining the minimum thickness, h_w , for the warhead case such that, the case will not fail in perforation of plates of known thickness, h_t . For flat ended projectiles, the case thickness, h_w , is estimated as [6];

$$h_w = h_t \left(\frac{\sigma_{sdt}}{Y_P} \right) \left(\frac{\hat{m}}{M} \right) \dots \dots \dots \text{Equation 2.1}$$

where \hat{m} is the mass of the projectile to the rear of section at which failure occurs which is a region just beyond the flat nose section, σ_{sdt} is the dynamic

shear strength of the target element, and Y_p is the yield strength of the projectile body.

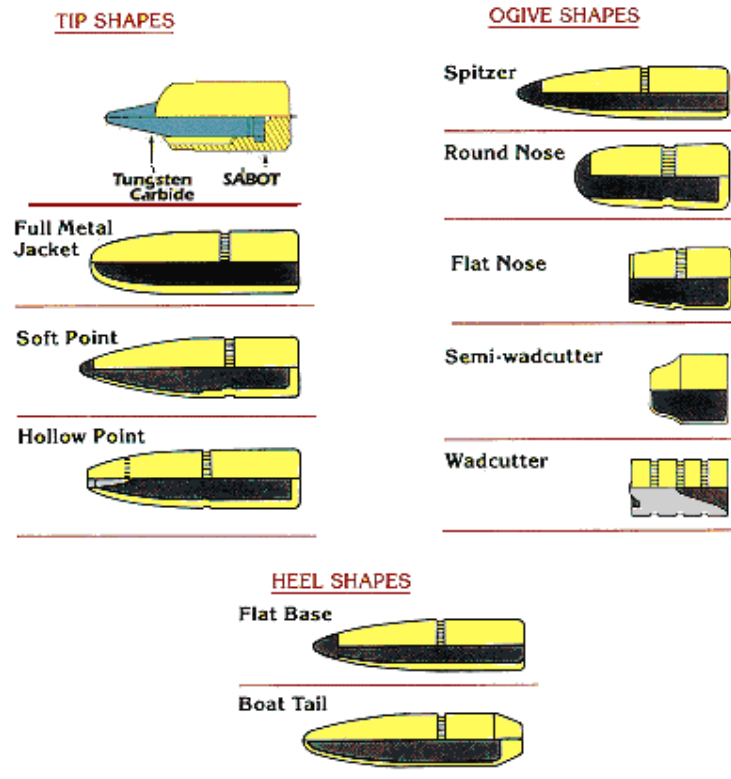


Figure 2.3 Examples of kinetic energy penetrators [12].

Table 2.2 Projectile characteristics [4].

Geometry			
<i>Basic Shape</i>	Solid Rod Sphere Hollow Shell Irregular Solid	<i>Nose Configuration</i>	Cone Ogive Hemisphere Right Circular Cylinder
Material			
<i>Density</i>	Lightweight	Wood, Plastics, Ceramics, Aluminum	
	Intermediate	Steel, Copper	
	Heavy	Lead, Tungsten	
Flight Characteristics			
<i>Trajectory</i>	Straight (Stable) Curved (stable) Tumbling (unstable)	<i>Impact Condition</i>	Normal Oblique
Final Condition			
<i>Shape</i>	Undeformed Plastically Deformed Fractured Shattered	<i>Location</i>	Rebound Partial Penetration Perforation

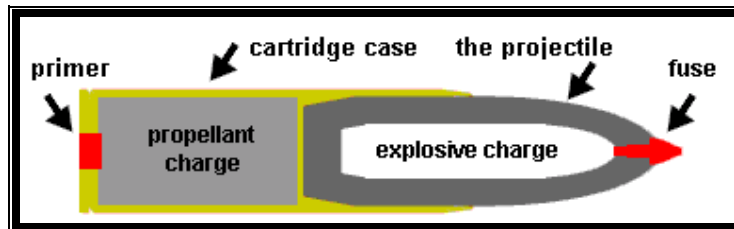


Figure 2.4 Examples of projectiles with warheads.

Projectile Parameters

Penetrator shape is significant in determining the mode of perforation and the resistance of a target element to penetration. Pointed penetrators exhibit a piecing mode of perforation in which target failure centers about the projectile axis. Blunt shapes, on the other hand, exhibit a plugging mode of perforation

in which target failure occurs over either a cylindrical or a roughly conical surface. The transition depends on penetrator shape, but the relationship between configuration and material properties that is needed to define that transition is only known approximately. This correlation of shape to mode of perforation for target elements of intermediate thicknesses has been investigated both experimentally and by analyses that estimate the compressive, inertial, and frictional forces on a projectile [7]. For conical projectiles, sharp and blunt shapes are defined as follows:

sharp.....for nose half-angles.....14°

blunt.....for nose half-angles.....90°

and definitions of “pseudo-sharp” and “pseudo-blunt” are given between these definitions in terms of a critical angle that varies from 30 to 50°. The concept of a criterion for “sharp” and “blunt” shapes has been more simply stated in [8] by requiring that $L_n/d_p \geq 1$ for “sharp” and $L_n/d_p < 1$ for “blunt”, where L_n is projectile nose length. The flight orientation ϕ , the angle between the velocity vector and projectile axis, is an additional parameter that influences the mode of perforation and this is treated as another aspect of shape [8]. An impact by a sharp projectile with $\phi \leq 10^\circ$ becomes blunt, i.e. it is assumed that perforation occurred in the plugging mode.

It is desirable that a penetrator be long, but two disadvantages appear with increased length: (1) increased susceptibility to bending mode failures, and (2) exterior ballistic instability for spin-stabilized projectiles. Projectile designs that use aerodynamic stabilization by tail fins avoid the latter problem. Many projectiles that are used to penetrate soils are bombs for which fin-stabilization and length of the projectile tend to overcome the inherent instability problems.

2.2.2. Projectile and Trajectory Orientation

The well establish convention for designating the direction of approach by a projectile to a target element is based on the choice of motion perpendicular to the front surface of the target element in zero obliquity. Thus, the obliquity, θ , of a projectile is the angle between its velocity vector and the normal into the front surface.

The flight orientation of a projectile is the angular displacement between the axis of symmetry and instantaneous line of flight impact of a projectile to the target occurs in four types of angle of incidence [6]:

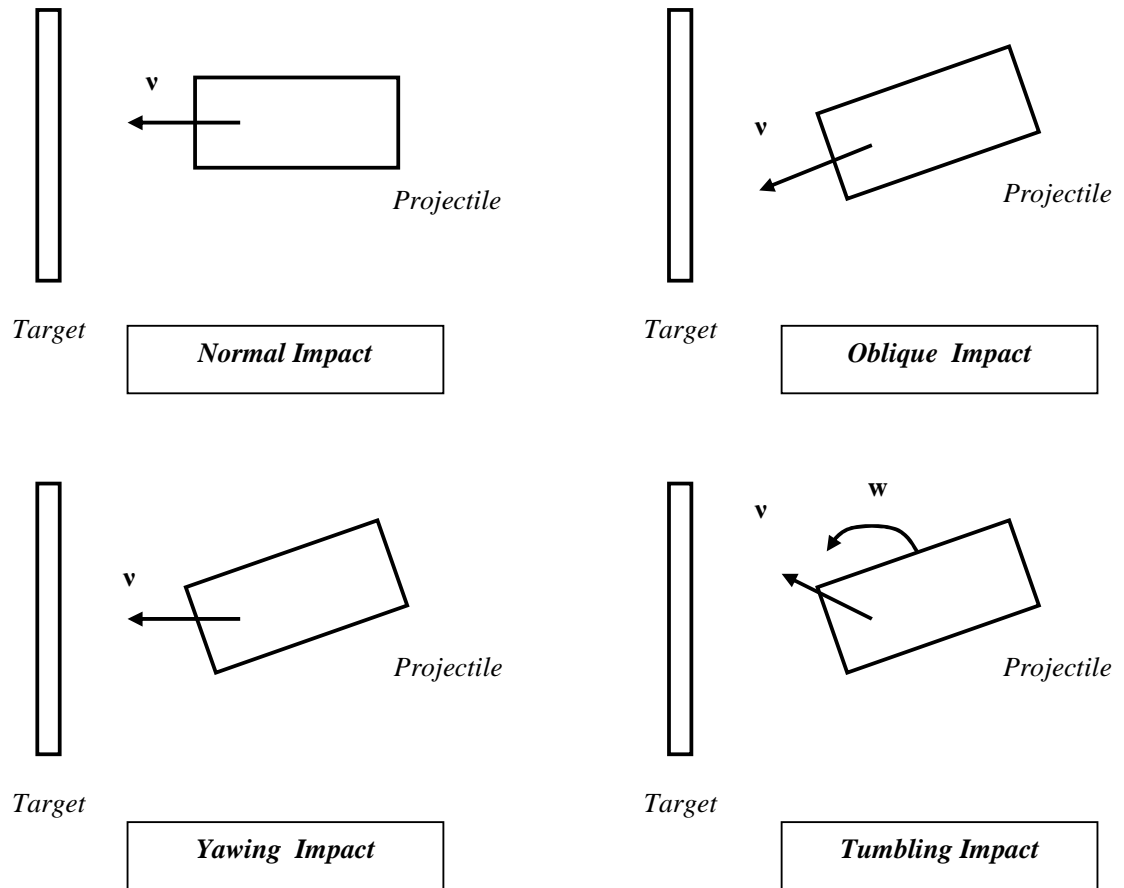


Figure 2.5 Types of angle of incidence.

2.2.3. Penetration and Perforation

Penetration may be defined as the entry of the penetrator into any region of the targets, i.e. the object struck by the penetrator and identified by structural and functional unity. Penetration in this sense will involve perforation, embedment, and ricochet in the course of the sequence of impacts. These terms will be reserved for interaction with target elements and have the following meanings: *Perforation* means that the penetrator passed through the target element, *Embedment* means that the penetrator is stopped during contact with the target element, and *Ricochet* means that the penetrator is deflected from the target element without being stopped or perforating [6].

Permanent deformations may involve variety of mechanical processes, either singly or in combination. The actual mechanisms depend on such variables as material properties, impact velocity, projectile shape, method of target support, and relative dimensions of projectile and target as mentioned before. Non-perforating failure modes consist of two types of transverse displacement of thin elements due to plastic deformation: (a) That in contact zone called bulging, where the element conforms to the shape of the penetrator nose, and (b) That induced by bending, termed dishing, which may extend to considerable distances from the impact area. These types of failures are shown in **Figure 2.6**. As the target thickness increases, non-perforating deformation type changes. Highly localized deformation, cratering occur in both the front and the rear surface of the target.

Knowledge of the failure conditions is useful in designing a target with the minimum areal density to defeat a projectile and in designing projectiles to defeat a given target with minimum energy. To achieve these goals it is necessary to have information about the important material properties and how they relate to the failure mechanisms during the perforation process.

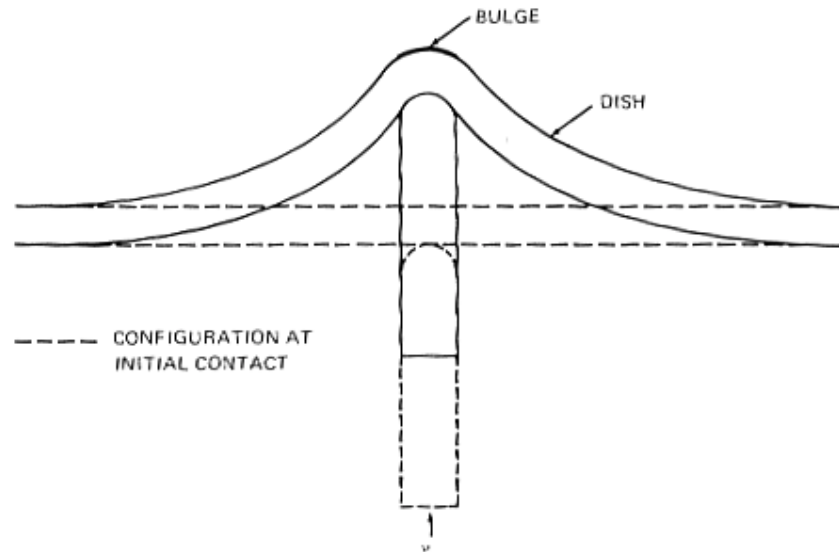


Figure 2.6 Permanent deformation of a thin target element showing bulging and dishing [6].

Failure involving fracture results in the perforation of thin or intermediate targets. These failures are due to interaction of a variety of mechanisms with one predominating, depending on material properties, geometric characteristics and impact velocity. The most frequent types are fracture resulting from the initial compressive wave, fracture in the radial direction, spalling, scabbing, plugging, front or rear petalling, fragmentation in the case of brittle targets and ductile hole enlargement [6].

Fracture due to an initial stress wave in excess of the ultimate compressive strength, σ_{UC} , could conceivably occur in weak, low density targets, while radial cracking is common in materials such as ceramics where their corresponding compressive strengths are higher than their tensile strength.

Spalling is tensile material failure and is a commonplace phenomenon under explosive loading. *Scabbing* has a similar appearance, but the fracture is produced by deformation and its surface is determined by local inhomogeneities and/or anisotropies such as the rolling direction.

Plugging develops as the results of a nearly cylindrical slug of approximately the same diameter as the bullet being set in motion by the projectile. Failure occurs due to large shears produced around the moving slug. Heat generated by the shear deformation is restricted to a narrow annulus in which it decreases the material strength resulting in instability; this is called an adiabatic shearing process. Plugging is most frequently found when blunt penetrators strike intermediate or thin, hard plates. Its presence is sensitive to velocity and the angle of obliquity of pointed projectiles.

Petalling is produced by high radial and circumferential tensile stresses after passage of the initial wave occurring near the lip of the penetrator. This deformation is the result of bending moments created by the forward motion of the plate material being pushed ahead of the striker, and by inhomogeneities or planes of weakness of the target. It is most frequently observed in thin plates struck by ogival or conical bullets at relatively low impact velocities or blunt projectiles near the ballistic limit.

A combination of ductile failure and spalling seems to be characteristics for the perforation of the thick plates of medium or low hardness. In addition to target element failure, projectile damage may also occur by plastic deformation, shattering, bursting of shells or component malfunction. Furthermore, the plug generated by failed targets or projectiles must be considered as a penetrator when considering any subsequent target element.

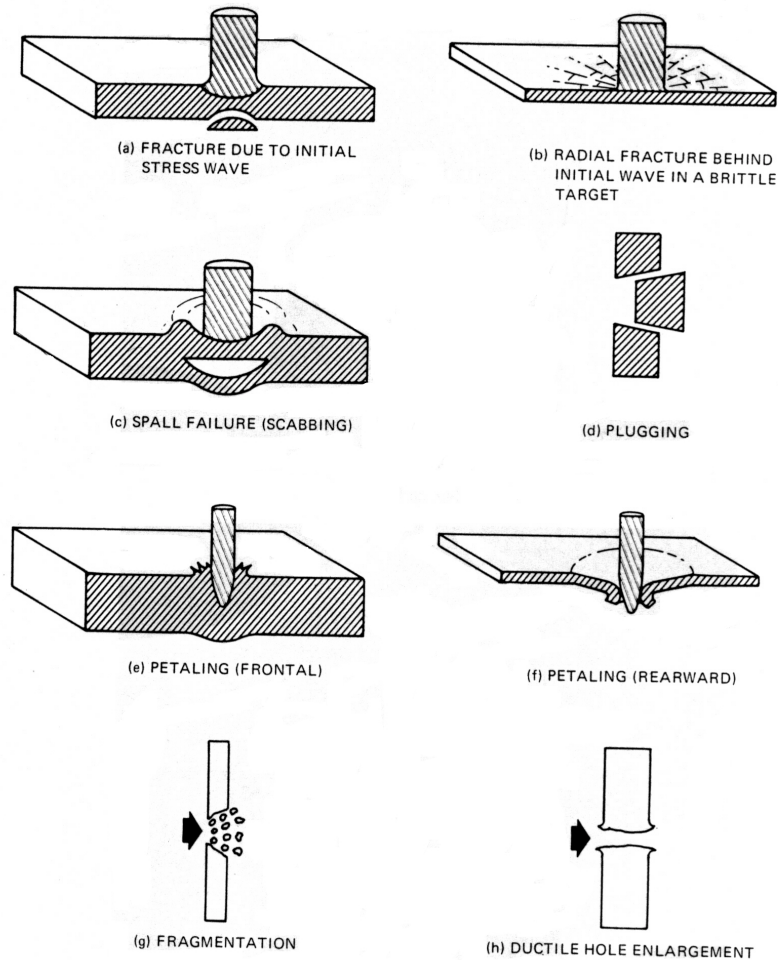


Figure 2.7 Perforation mechanisms [6].

In the case of high strength aluminum alloys, shear plugging is generally observed for relatively thick targets. Discing failure is also observed in thick targets of high strength aluminum alloys [9]. In the case of discing, shear cracks develop in the plane of the plate as a consequence of in-plane shear stresses induced by bending. Both metallurgical inclusions and inhomogeneities in the plane of the plate, as well as adiabatic thermal softening effects associated with the high rate of deformation contribute to discing failure. For thinner plates where bending is favored, the stretching of the sheet

can lead to tensile failures at the edges with a plug ejected, or the plug folded away attached to one of the petals, or necking and tearing in the form of a star pattern from the center of impact [10].

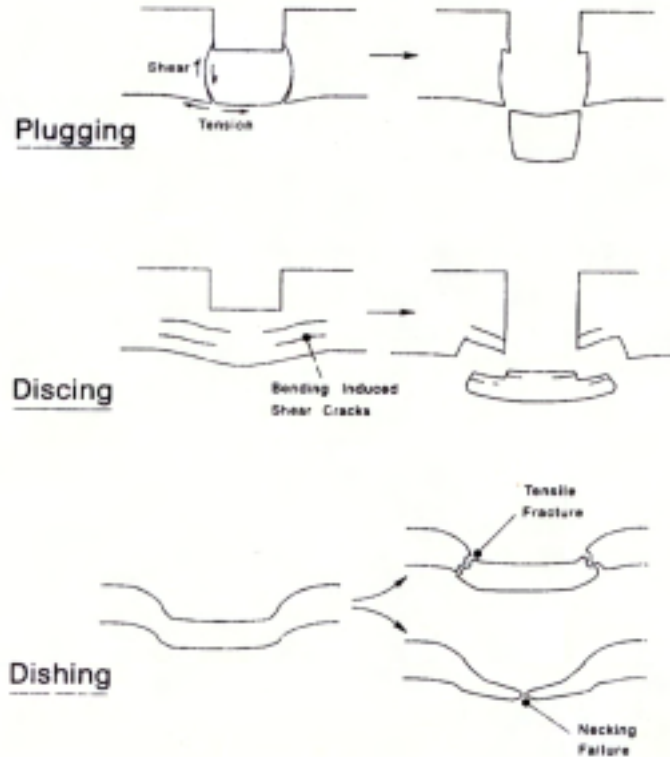


Figure 2.8 Target failure features in homogeneous plates [10].

2.2.4. Ballistic Limit

One of the problems encountered in the study of impact phenomena is the determination of a velocity below which an object will fail to perforate a barrier or some type of protective device. This determination is of prime importance in the design of protective structures, in evaluation of the effectiveness of military vehicle armor, and in any problem area where an impact can cause damage. This velocity is commonly referred to as a critical

impact velocity or *ballistic limit* [4]. This concept is formally defined in ordnance science; for example, the following definition is given in [11].

“Ballistic Limit – The average of two striking velocities, one of which is the highest velocity giving a partial penetration and the other of which is the lowest velocity giving a complete penetration. There are several measures used in rating the resistance of armor or other materials to penetration, the three most widely used criteria are: (1) *the Army*, (2) *protection*, and (3) *the Navy ballistic limits*.”

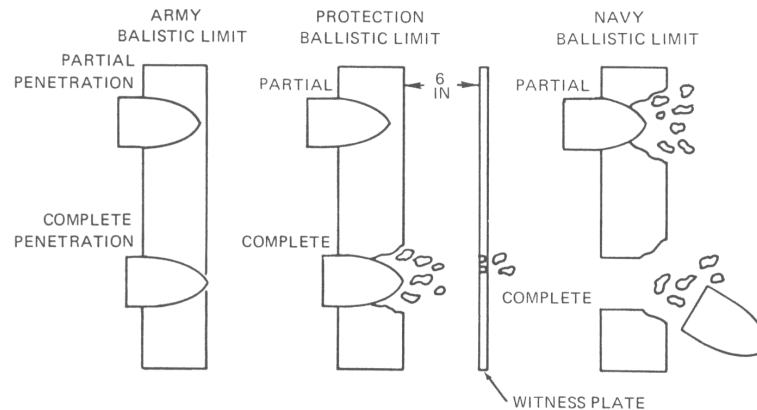


Figure 2.9 Perforation and partial penetration for defining the ballistic limit [6].

The techniques available to determine this velocity can be classed as either deterministic or probabilistic. In the former category, a limit velocity is determined from physical principles (the conservation laws and material constitutive relations) but because of complexity of governing partial differential equations, simplifications are introduced that generally require empirical determination of one of two constants. In the probabilistic approach, models are built relying a substantial base of data consisting of the object’s striking velocity and either its residual velocity or a statement of either defeat or nondefeat of the barrier. The resulting critical velocity is most commonly expressed as a V_{50} , that is , a striking velocity for which there exists a 50%

probability of perforation of the barrier. In V_{50} determinations, a statistical approach is employed where the response is quantal and sensitivity test can be applied to the data [4].

2.2.5. Target Material Physical Characteristics

Penetration mechanics is properly concerned with interactions between penetrators and target elements. The analytical process for reducing targets into appropriate elements requires many methods and data that are not part of penetration mechanics; however, the criteria for the size of the target element and the parameters that are needed to describe it depend directly on penetration-mechanical considerations [6]. The material properties of the target play a very important role in penetration mechanics. The three physical properties of armor which have the greatest influence on its ballistic properties are:

1. **Hardness:** The ability of the armor to resist indentation.
2. **Toughness:** The ability of the armor to absorb energy before fracturing.
3. **Soundness:** The absence of local flaws, cavities, or weaknesses in the armor. Unsoundness is not so often found in rolled armor as in cast armor, because of the mechanical working which has been done during the hot-rolling process [12].

The search for increased ballistic performance of armors within restrictive weight requirements has led inevitably away from monolithic homogeneous metallic to high performance non-metallic materials, composites and complex armor configurations. Metallic laminates have some potential advantages over monolithic metallic armors, including the ability to be fabricated into thicker structures than is possible with homogeneous plates of the same material for a given strength level. Laminates also have increased damage tolerance if plane stress conditions are met in the layered structure [13], and increased ballistic resistance if the plates are optimally configured.

2.3. IMPACT TESTS

In view of the complexity of penetration processes, it is not surprising that the bulk of the work in this area is experimental in nature. High-velocity impact test techniques, aside from routine proof tests, vary mainly in the degree of instrumentation provided and hence the amount of data retrieved. The most common types of testing have as their objective the determination of [4]:

1. The velocity and trajectory of the projectile prior to impact.
2. Changes in configuration of projectile and target as a result of impact.
3. Masses, velocities, and trajectories of fragments generated by the impact process.
4. The ballistic limit.

2.3.1. High Velocity Impact Testing

High-velocity impact is a very energetic process. Some of the incident energy is converted into light that obscures the impact event. Further problems are caused by debris ejected at the impact face and at the rear of the target once the projectile has broken through. Conventional optical techniques, such as high speed cameras, are therefore quite limited for such applications. To overcome these problems, most experimental facilities rely on x-ray illumination of energetic interaction events. Frequently, both x-ray and optical methods are used to record impact phenomena.

Projectile trajectories may be determined in a number of ways; high-speed photography, orthogonal-flash radiography, or yaw-card measurements. Yaw cards are thin paper or plastic sheets located along the anticipated trajectory. The striking velocity is determined from a measurement of transit over fixed distances. The time of arrival at predetermined locations is established by the

closing or opening of electrical circuits, interruption of light beams, synchronized photography, or flash radiography of the projectile [4].

Post-mortem measurements on projectile and target include determination of principal dimensions of the target crater such as depth, diameter, and crater volume (or entrance and exit diameters for a perforation) as well as the final length, diameter, and mass of the projectile and other massive fragments [14].

In summary, the data extracted from conventional high-velocity impact tests consists of the following:

1. Speed and orientation of the projectile prior to impact.
2. Speed and orientation of major projectile pieces after perforation.
3. Speed, mass, and spatial distributions of fragments behind the target.
4. Hole size and mass loss in the target.

Graphical representations of high-velocity impact data concern relationships among such variables as velocity, target thickness, angle of obliquity, total projectile yaw, impact-kinetic energy, impulse, force, and time. For such plots, physical and geometric characteristics of projectile and target (excepting target thickness) are held constant. Since plots are two-dimensional, the curves represent relationships between one dependent variable and one independent variable. **Figure 2.10** from [6] is an example of a phase diagram portraying the behavior of a 6.35 mm ogival-nosed projectile striking a 6.35 mm aluminum target.

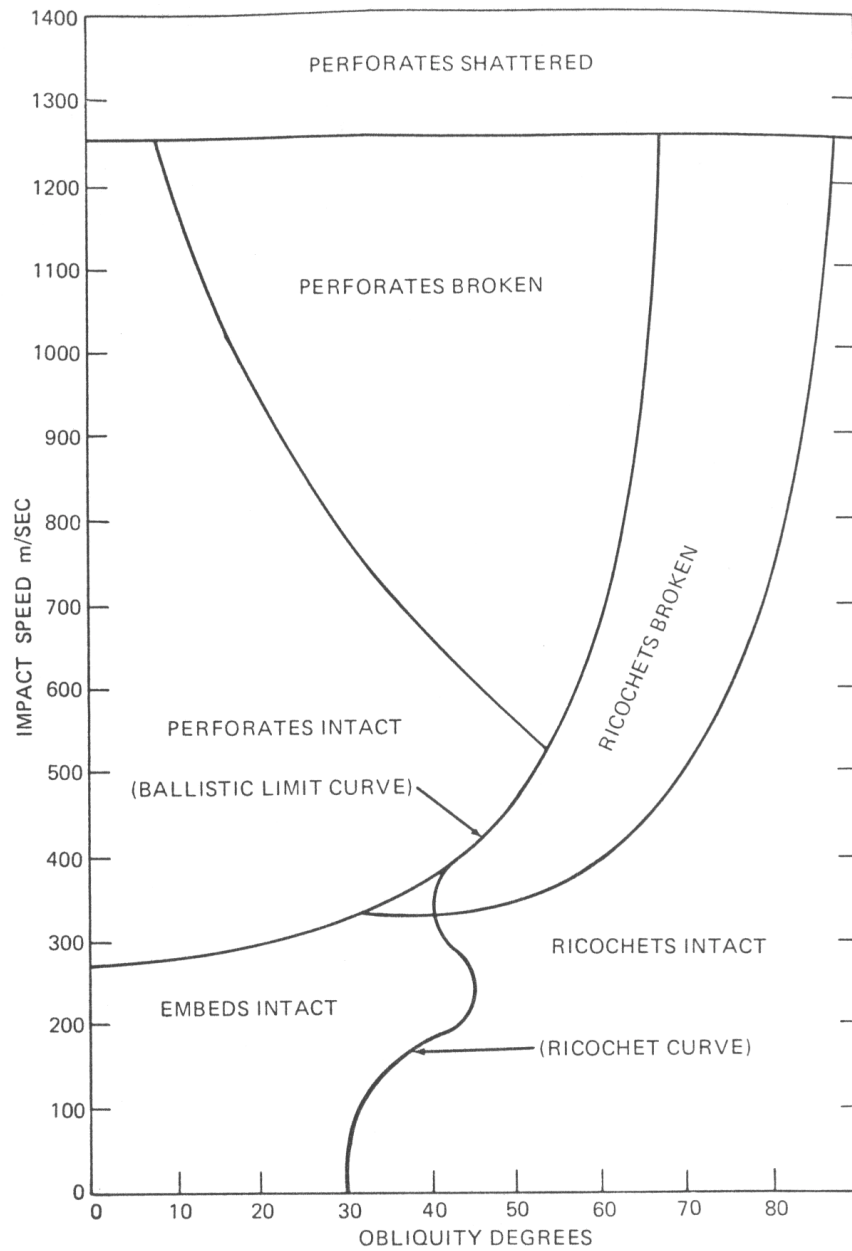


Figure 2.10 Phase diagram for projectile impact [6].

2.4. DROP WEIGHT TEST

The drop weight test was developed specifically for the determination NDT (nil ductility temperature) on full thickness plates [15]. Drop-weight can also be used as metal forming operations since it is simple and economical in design. Recently, it is also started to be used as a ballistic test method.

2.4.1 Determining Nil Ductility Temperature

Probably the chief deficiency of the Charpy impact test is that the small specimen is not always a realistic model of the actual situation. Not only does the small specimen lead to considerable scatter, but a specimen with a thickness of 10 mm cannot provide the same constraint as would be found in a structure with a much greater thickness. At a particular service temperature the standard Charpy specimen shows a high shelf-energy, while actually the same material in a thick-section structure has low toughness at the same temperature.

The most logical approach to this problem is the development of tests that are capable of handling specimens at least 25 mm thick. The basic need for large specimen resulted from the inability to produce fracture in small laboratory specimens at stresses below the gross yield stress, whereas brittle fractures in ship structures occur at service temperatures at elastic stress levels.

The first development was the explosion-crack-starter test, which featured a short, brittle weld bead deposited on the surface of a 350 x 350 x 25 mm steel plate. The plate was placed over a circular die and dynamically loaded with an explosive charge. The brittle weld bead introduces a small natural crack in the

test plate similar to weld-defect crack. Tests are carried out over a range of temperature and the appearance of the fracture determines the various transition temperatures. Below the nil ductility temperature (NDT) the fracture is a flat (elastic) fracture running completely to the edges of the test plate. Above the NDT a plastic bulge forms in the centre of the plate, but the fracture is still a flat elastic fracture out to the plate edge. At still higher temperature the fracture does not propagate outside of the bulged region. The temperature at which elastic fracture no longer propagates to the edge of the plate is called the fracture transition elastic (FTE). The FTE marks the highest temperature of fracture propagation by purely elastic stresses. At yet higher temperature the extensive plasticity results in a helmet-type bulge. The temperature above which this fully ductile tearing occurs is the fracture transition plastic (FTP) (Figure 2.11).

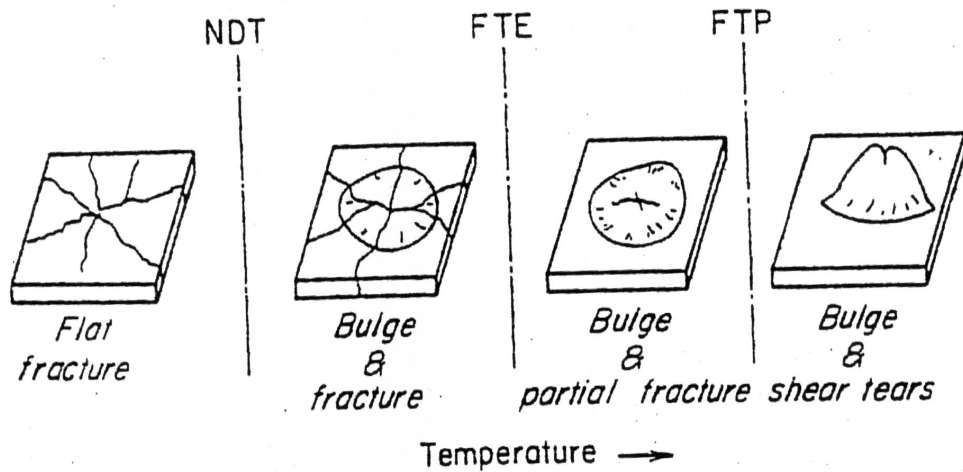


Figure 2.11 Fracture appearances vs. temperature for explosion-crack-starter test [16]

The drop-weight test (DWT) was developed specifically for the determination of the NDT on full thickness plates. A short bead of brittle weld metal is deposited on the surface of a plate, typically 90 x 350 x 15 to 25 mm in thickness. A small notch is introduced in the weld bead and the specimen supported as a simple beam in a constant temperature bath. The brittle weld bead is fractured at near yield-stress levels as a result of dynamic loading from

a falling weight. The anvil stop restricts the deflection of the specimen. Since the specimen is a wide beam loaded in three-point bending, this restriction limits the stress on the tension face of the plate to a value that does not exceed the yield stress. If the starter-crack propagates across the width of the plate on the tension surface to the edges, the test temperature is below the NDT. Complete separation on the compression side of the specimen is not required. The NDT is the highest temperature at which a nil ductility break is produced. The test is quite reproducible and the NDT can be determined to the nearest 5° C [16].

2.4.2 Metal Working Operations

Most of the metals forming operations such as bar cropping, sheet metal operations, and upsetting can be performed by using the constructed drop hammer. The drop-weight is constructed with the limited work shop facilities but it can fulfill experimental needs.

Metal forming energies and impact velocities with several magnitudes are available since dropping of the ram from a required height is possible. In addition to these, the work capacity of the drop-weight can be increased easily, by simple increasing the weight of the ram.

A drop-weight consists of an anvil carrying bottom die and top support which guides a falling weight and a device to raise the falling weight to the desired height. The falling weight generates required energy by falling from the raised height. A simple drop weight machine can be seen in **Figure 2.12**.

Some of the energy is lost in the guides due to opposing frictional forces. The machine frame absorbs certain amount of the energy due to vibration of different parts. This is because of the transfer of the momentum from the ram.

The specimen will also absorb certain amount of the energy in the form of plastic deformation.

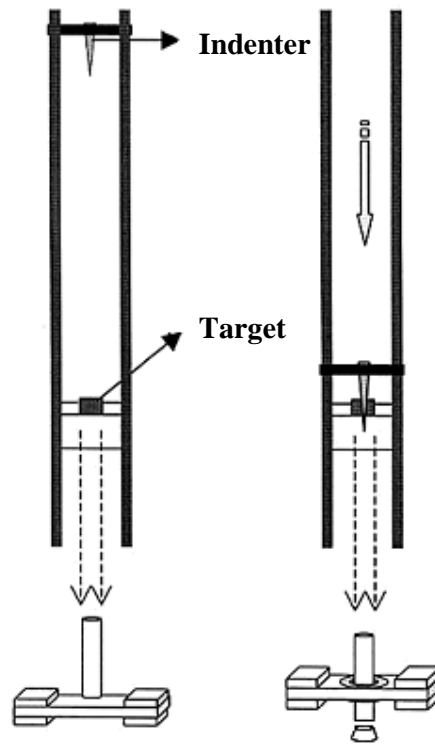


Figure 2.12 Schematic view of a drop-weight machine.

It is clear that, in gravity drop hammer the acceleration of the ram is slightly less than the gravitational acceleration ($a < g$), due to frictional losses. And the acceleration of the ram is directly proportional to the weight of the ram [17].

2.4.3 Ballistic Testing

The aim of the test is to supplement existing ballistic testing procedures and to establish a consistent and reliable means of evaluating the resistance to sharp instrument penetration of body armor. This test is intended to reflect the effect of hand delivered impact of sharp, pointed instruments whose point or tip is

not offset more than 19.05 mm from the centre-line of the fist(s) delivering the impact [18].

The basis of these procedures is the creation of a consistent and repeatable sharp instrument impact, which is representative of:

- a typical sharp instrument which may be used to defeat the protection of ballistic body armor
- the maximum energy with which such an instrument could be hand delivered by a healthy, athletic male with no physical infirmities.

As a result 18 kg weight dropped from a stationary position located 121 cm above the test impact surface is suitable for the test. Such that the resultant theoretical kinetic energy is 13 joule, the resultant theoretical translational momentum is 9 kg-seconds, and the resultant theoretical striking velocity is 484 cm per second. These values are theoretical, in as much as the calculations assume the potential energy to be wholly-transformed into kinetic energy, disregarding that portion of the potential energy actually transformed into friction, heat, sound, etc. [18].

2.5. ALUMINUM ALLOYS

Aluminum, the second most plentiful metallic element on earth, became an economic competitor in engineering applications as recently as the end of 19th century. It was to become a metal for its time. The emergence of three important industrial developments would, by demanding material characteristics consistent with the unique qualities of aluminum and its alloys, greatly benefit growth in the production and use of the new metal [19].

Aluminum and its alloys are widely used almost is everywhere in the industry. The areas of the usage can be categorized as follows;

- Aerospace Industry
- Road, Rail and Sea Transport
- Cooking and Packaging
- Constructions
- Electrical Applications
- Medicine
- Defense Industry

2.5.1 Alloy and Temper Designation System

It is convenient to divide aluminum alloys into two major categories: casting compositions and wrought compositions. A further differentiation for each category is based on the primary mechanism of property development.

Cast and wrought alloy nomenclatures have been developed. The Aluminum Association system is most widely recognized. Their alloy identification system employs different nomenclatures for wrought and cast alloys, but

divides alloys into families for simplification. For wrought alloys a four-digit system is used to produce a list of wrought composition families as follows [19]:

- **1xxx** Controlled unalloyed (pure) composition used primarily in the electrical and chemical industries,
- **2xxx** Alloys in which copper is the principal alloying element, though other elements, notably magnesium, may be specified. 2xxx series alloys are widely used in aircraft,
- **3xxx** Alloys in which manganese is the principal alloying element. Used as a general purpose alloy for architectural applications and various products,
- **4xxx** Alloys in which silicon is the principal alloying element. Used in welding rods and brazing sheet,
- **5xxx** Alloys in which magnesium is the principal alloying element. Used in boat hulls, gangplanks, and other products exposed to marine environments,
- **6xxx** Alloys in which magnesium and silicon are principal alloying elements. Commonly used for architectural extrusions.
- **7xxx** Alloys in which zinc is the principal alloying element, but other elements such as copper, magnesium, chromium, and zirconium may be specified. Used in aircraft structural components and other high-strength applications,
- **8xxx** Alloys including tin and some lithium compositions, characterizing miscellaneous compositions,
- **9xxx** Reserved for future use.

Historically, all major industrialized countries developed their own standard designations for aluminum and aluminum alloys. These are now being grouped under systems of the American National Standards Institute,

The International Organization for Standardization and the European Committee for Standardization.

Major subdivisions in the T series of tempers employ numerals 1 through 10 to distinguish among major variations in the sequence of operations. Additional digits are assigned to tempers of stress-relieved wrought products, to tempers that differ in amount and type of cold work applied after quenching or between quenching and artificial aging, and to tempers produced by special practices to control such characteristics as resistance to corrosion or dimensional stability [10].

Table 2.3 The basic temper designations [20].

F	<i>As fabricated.</i> Applies to wrought products that acquire some temper from shaping processes in which no special control is exercised over the amount of strain hardening or thermal treatment. For wrought products in this temper, there are no mechanical-property limits. Applies to castings in the as-cast condition if the alloy is also regularly produced in heat treated tempers.
O	<i>Annealed (wrought products only).</i> Applies to the softest temper of wrought products.
W	<i>Solution heat treated.</i> An unstable temper applicable only to alloys that age at room temperature after solution heat treatment. The designation is specific only when the period of natural aging is indicated; for example : W(0.5 hr).
T	<i>Heat treated to produce stable tempers other than F or O.</i>

Table 2.4 The basic temper designations (continued) [20].

T1	<i>Naturally aged to a substantially stable condition.</i> Applies to products in which partial solution of alloying elements is provided by elevated-temperature, rapid-cool fabrication.
T2	<i>Annealed (cast products only).</i> Designates a temper produced by a type of annealing treatment used to improve ductility and increase dimensional stability of castings.
T3	<i>Solution heat treated, cold worked, and naturally aged to a substantially stable condition.</i> Applies to products that are cold worked to improve strength, or in which the effect of cold work associated with flatter or straightening recognized in applicable specifications. Different amounts of cold work are denoted by a second digit.
T4	<i>Solution heat treated and naturally aged to a substantially stable condition.</i> Applies to products that are not cold worked after solution heat treatment, or in which the effect of cold work associated with flatter or straightening may not be recognized in applicable specifications.
T5	<i>Artificially aged only.</i> Applies to products that are artificially aged after an elevated-temperature, rapid cool fabrication process, such as casting or extrusion, to improve strength and/or dimensional stability.
T6	<i>Solution heat treated and artificially aged.</i> Applies to products not cold worked after solution heat treatment, or in which the effect of cold work associated with flatter or straightening may not be recognized in applicable specifications.
T7	<i>Solution heat treated and overaged.</i> Applies to products that are solution heat treated and artificially aged beyond the condition of maximum strength, to provide controlled special characteristics, such as dimensional stability, lower residual stresses, or improved resistance to corrosion.
T8	<i>Solution heat treated cold worked, and artificially aged.</i> Applies to products that are cold worked to improve strength, or in which the effect of cold work associated with flatter or straightening is recognized in applicable specifications.
T9	<i>Solution heat treated, artificially aged, and cold worked.</i> Applies to products that are cold worked as a final operation, to improve strength.
T10	<i>Artificially aged, and cold worked.</i> Applies to products that are artificially aged after an elevated-temperature, rapid-cool fabrication process, such as casting or extrusion, and then cold worked to improve strength.

Table 2.5 Temper Designations for Strain-Hardened Alloys [20].

F	<i>As fabricated.</i> No control over the amount of strain hardening; no mechanical property limits.
O	<i>Annealed, recrystallized.</i> Temper with the lowest strength and greatest ductility.
H1	<i>Strain hardened.</i>
H2	<i>Strain hardened and partially annealed.</i>
H3	<i>Strain hardened and stabilized.</i>
H112	<i>Strain hardened during fabrication.</i>
H321	<i>Strain hardened during fabrication.</i> Amount of strain hardening controlled during hot and cold working.

2.5.2 Phases in Aluminum Alloys

The elements that are most commonly present in commercial aluminum alloys to provide increased strength – particularly when coupled with strain hardening by cold working or with heat treatment, or both – are copper, manganese, silicon, and zinc. These elements all have significant solid solubility in aluminum, and in all cases the solubility increases with increasing temperature as indicated in **Figure 2.13** [26].

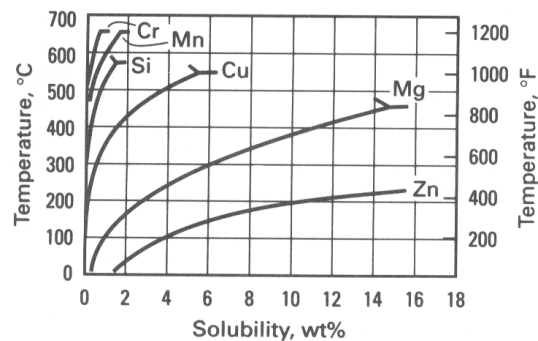


Figure 2.13 Equilibrium binary solid solubility as a function of temperature for alloying elements most frequently added to aluminum [26].

Of all the elements, zinc has the greatest solid solubility in aluminum (a maximum of 66.4 at .%). In addition to zinc, the solid solubilities of silver, magnesium, and lithium are greater than 10 at %.(in order of decreasing maximum solubility). Gallium, germanium, copper, and silicon (in decreasing order) have maximum solubilities of less than 10 but greater than 1 at .1%. all other elements are less soluble. With the one known exception of tin (which shows a retrograde solid solubility between the melting point of aluminum and the eutectic temperature, 228.3 °C, with a maximum of 0.10% at approximately 660 °C), the maximum solid solubility in aluminum alloys occurs at the eutectic, peritectic, or monotectic temperature. With decreasing temperature, the solubility limits decrease. This decrease from appreciable concentrations at low temperatures is one fundamental characteristic that provides the basis for substantially increasing the hardness and strength of aluminum alloys by solution heat treatment and subsequent precipitation aging operations [21].

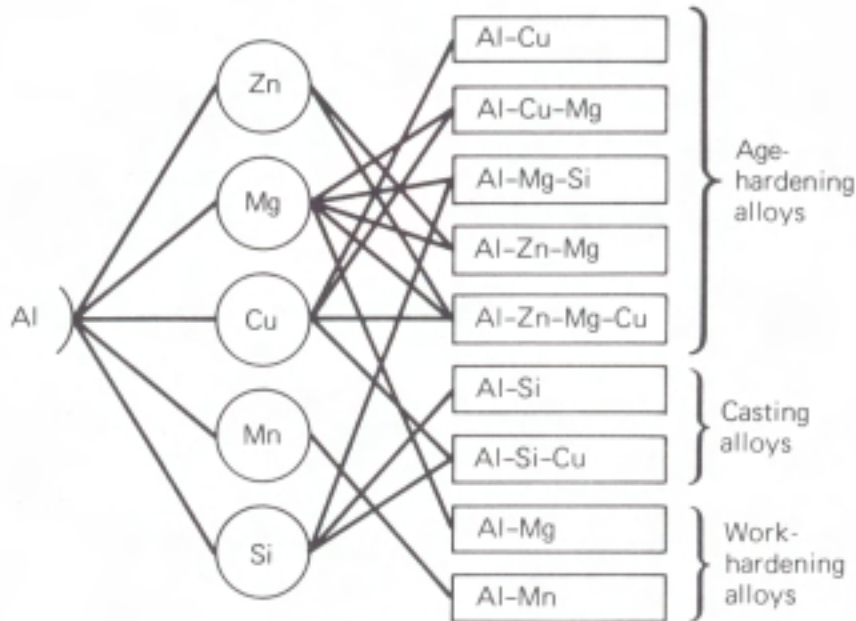


Figure 2.14 The principal aluminum alloys [21].

Table 2.6 Possible Phases in AA 2024 [19].

<i>Alloy System</i>	<i>Examples of Alloy</i>	<i>Alloy Form</i>	<i>Phases</i>
Al-Cu-Fe-Si-Mg-Mn	2024	Ingot	(Fe,Mn)Al ₃ , (Fe,Mn) ₃ SiAl ₁₂ , Mg ₂ Si, CuAl ₂ , CuMgAl ₂ , Cu ₂ FeAl ₇
		Wrought	(Fe,Mn) ₃ SiAl ₁₂ , Mg ₂ Si, CuMgAl ₂ , Cu ₂ FeAl ₇ , Cu ₂ Mn ₃ Al ₂₀

2.5.3 Strengthening by Heat Treatment

Many important properties of aluminum alloys such as their mechanical strength, toughness, creep, and stress-corrosion cracking are largely affected by the presence of precipitated particles of a second phase. The basic requirement for an alloy, necessary for age-(or precipitation) hardening, is a decrease in the solid solubility of one or more of the alloying elements with decreasing temperature.

Heat treatment to increase the strength of aluminum alloys is a three-step process:

- Solution heat treatment : dissolution of soluble phases
- Quenching : development of supersaturation
- Age hardening : precipitation of solute atoms either at room temperature (natural aging) or elevated temperature (artificial aging or precipitation hardening)

Solution Heat Treating

To take advantage of the precipitation hardening reaction, it is necessary first to produce a solid solution. The process by which this is accomplished is called solution heat treating, and its objective is to take into solid solution the

maximum practical amounts of the soluble hardening elements in the alloy. The processes consist of soaking the alloy at a temperature sufficiently high and for a time long enough to achieve a nearly homogeneous solid solution.

Quenching

Quenching is in many ways the most critical step in the sequence of heat-treating operations. The objective of quenching is to preserve the solid solution formed at the solution heat-treating temperature, by rapidly cooling to some lower temperature, usually near room temperature. The solute atoms that precipitate either on grain boundaries, dispersoids, or other particles, as well as the vacancies that migrate (with extremely rapidity) to disordered regions, are irretrievably lost for practical purposes and fail to contribute to the subsequent strengthening.

Age Hardening

After solution treatment and quenching, hardening is achieved either at room temperature (natural aging) or with a precipitation heat treatment (artificial aging). In some alloys, sufficient precipitation occurs in a few days at room temperature to yield stable products with properties that are adequate for many applications. These alloys sometimes are precipitation heat-treated to provide increased strength and hardness in wrought or cast products. Other alloys with slow precipitation reactions at room temperature are always precipitation heat-treated before being used.

In some alloys, notably those of 2xxx series, cold working of freshly quenched material greatly increases its response to later precipitation heat treatment [19, 22].

2.5.4 Age Hardening of AA 2024

Relatively few commercial alloys based on the binary Al-Cu system are actually used at present, although the sequence of the precipitation process, particularly GP zone formation, have been studied until recently in greater detail for this system than any other system.

An addition of Mg to Al-Cu alloys accelerates and intensifies the natural aging. From the investigation of ternary equilibrium, the existence of five phases i.e., (Al), θ -Al₂Cu, S-Al₂CuMg, Al₆CuMg₄, and Al₃Mg₂, in ternary Al-rich solid phase equilibrium diagram has been clarified. The precipitation sequences are divided into two processes as follows [38];

- (1) (SSSS) – GP(1) – GP(2) – θ' -CuAl₂ – θ -CuAl₂
- (2) (SSSS) – GPB(1) – GPB(2) - S'-Al₂CuMg – S-Al₂CuMg

The first process proceeds in the alloy of Cu/Mg = 8, and the first and second processes advance simultaneously in the alloys of 4 < Cu/Mg < 8. In the range of 1.5 < Cu/Mg < 4, the quasi-equilibrium of Al-S-Al₂CuMg may be established, and thus appreciable age hardening occurs in these alloys. GPB(1) and GPB(2) correspond to GP(1) and GP(2) containing Mg as well as Cu [39]. GPB consisting of Cu and Mg atoms may be formed on {110} matrix planes. The apparent acceleration of this formation may result from either complex interactions between vacancies and the two solute atoms or some preliminary pairing of Cu and Mg atoms. The coherent precipitation of S'-Al₂CuMg plays an important role in age hardening at elevated temperatures, such as with AA 2024-T6.

Artificial aging has a great effect on mechanical properties of AA 2024. Some of these effects are summarized from **Figure 2.15- Figure 2.16**.

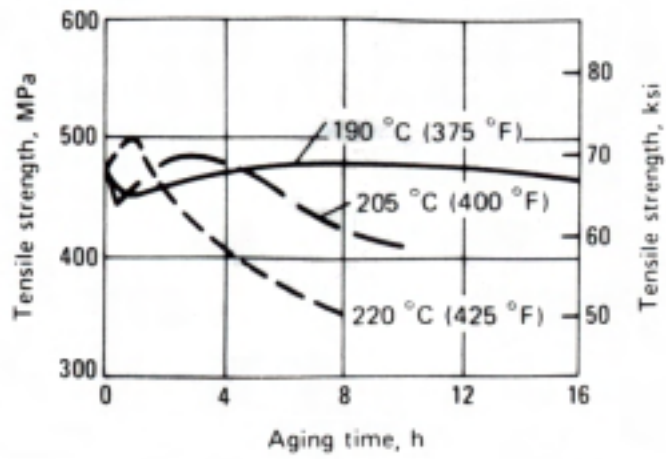


Figure 2.15 Effect of aging on tensile strength of AA 2024 [19].

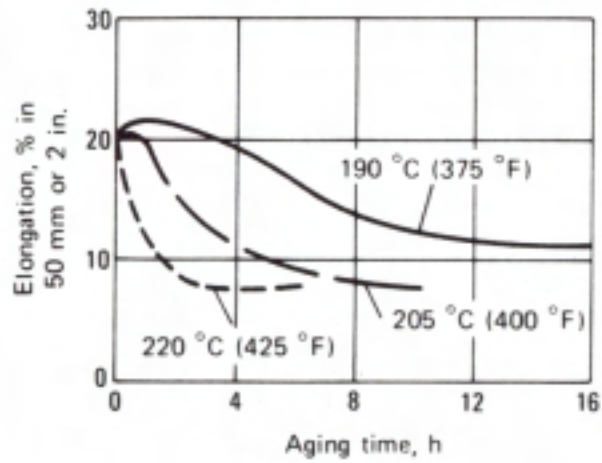


Figure 2.16 Effect of aging on percent elongation of AA 2024 [19].

2.6. ADHESIVES

Adhesive bonding is more than a mere substitute for other joining techniques. It has inherent characteristics that make it especially valuable for a great number of applications in cases where other methods cannot be used, or where it has proved its superiority [23].

When one surveys the many uses of adhesives, the question always presents itself as to what factors influence a choice to use adhesives, and what design principles dictate the type of adhesive for a particular application. A few of these advantages is given in **Table 2.7** and disadvantages in **Table 2.8**.

Table 2.7 Advantages of Adhesives [24].

Allows Fabrication of Smoother Parts and Assemblies	Adhesives do not break through or deform the surface of an assembly or product.
Permits Use of Light-weight Materials	
Serves as a Vibration Damper	Better stress distribution leads better fatigue resistance under vibration loads.
Joins Dissimilar Materials	In all probability this is one of the best single arguments for the use of adhesives.
Permits Easier Fabrication of Unique Contours and Miniature Components	Many contoured surfaces that would be difficult to join by other methods may be adhesively joined satisfactorily.

Table 2.8 Disadvantages of adhesives [24].

Temperature Disadvantages	Where high strengths are necessary at elevated temperatures, an elevated-temperature cure is usually necessary, and the adherents may be affected.
Joint Design	This is important and sometimes requires added attention as compared with conventional modes of fastening.
Services Life	This is often shorter than for other fastening techniques.
Inspection and Quality	After a part has been fabricated, quality determination is difficult.

2.6.1 Epoxy Adhesives

Like unsaturated polyesters, epoxies (EP) are thermosetting and can be defined as any molecule containing more than one a-epoxy group (whether situated internally, terminally, or on cyclic structures) capable of being converted to a useful thermoset form. The term is used to indicate the resins in both thermoplastic (uncured) and thermoset (cured) states [25]. Because of similarities, epoxies and unsaturated polyesters often are used for the same purposes, but the somewhat more complex curing and fabricating process and higher cost of epoxies mean they are generally employed in building when polyester will not do. Epoxy resins, also known as epoxides, are monomers (low modulus) and prepolymers (high modulus) that further react with curing agents to yield the desirable flexible, semi-rigid, or rigid thermosetting plastics. Epoxy resin selection is usually based on performance properties, reactivity, handling characteristics, availability, and cost. The curing agent, also known as the hardener, chemically brings about the change from liquid,

paste, or mortar consistency to a solid plastic. It is in this state that the system is usually used—there is limited usage in the uncured, non-cross-linked state.

Because of their brittleness, unreinforced epoxies cannot be used structurally, but when reinforced with glass fibers and other fibrous, laminar, or particulate reinforcements, they provide excellent structural materials. Adhesion to many substrates is excellent. Consequently, the most common building applications for reinforced epoxies are reinforced plastics, laminates, crack fillers, industrial and decorative (i.e., terrazzo) flooring, and adhesives for metals, masonry, and concretes. A major use is heavy-duty protective coatings. Epoxy formulations are widely used as flooring systems, thin-film and build-up coatings, penetration sealers (with or without decorative surface films), epoxy sand-filled grouts, patching compounds, and mortar overlays. They provide excellent anti-skid surfaces, chemical resistance, and weatherability.

Epoxy formulations during the design stage are categorized by lowest-temperature cure, moisture content of substrate (dry, moist, or underwater abilities of application and adherence), solid content, reactivity, and consistency or viscosity (liquid, paste, or mortar) for a specific use. Conditions of application, the desired form of protection, and the physical properties (such as compressive, tensile and flexural strengths, the modulus of elasticity, and the coefficient of thermal linear expansion, etc.) determine the compatibility of a substrate. After cure and use are determined, the epoxy resin and curing agent types are selected. Then it is a relatively routine task to develop the formulation to meet the desired goal [26].

2.6.2 Polyurethane (Urethane) Adhesives

In recent years, the use of polyurethane sealants and caulks in the construction market has shown a dramatic increase. Sealants are important in present-day construction technology, and a wide variety of materials is available, with highly different properties and applications. The unique versatility of urethane technology allows for the formulation of a wide range of products for the construction industry [27]. Urethane polymers are among the most widely used in both new and remedial construction markets. Sealing of joints is an important part of the modern building process. Polyurethane was developed in 1937 in Germany by Dr. Otto Bayer, who discovered the polymerization reaction of polyisocyanates that leads to the production of high molecular weight products. The rapid popularity it has attained throughout Europe and the United States was stimulated by shortages of several natural rubber materials during World War II.

It is usually necessary to seal joints to avoid penetration of air, water, vapor, odors, noise, insects, and so forth. Sealing against air, water, and vapor is considered most important although the requirements might not differ much. Successful sealing can be achieved by the selection of the right sealant and including sensible details in the design. The second point can be as important as the first one.

All urethane prepolymers are manufactured by the reaction of a polyisocyanate with a polyol, in the presence of a catalyst, which results in the formation of stable chemical links or bonds creating a urethane polymer. There can be many variations to the reaction to achieve various degrees of polymer quality and performance success. The polymer then is compounded with various other raw materials to create the desired finished product.

The basic reaction on which polyurethane chemistry is based was discovered more than 140 years ago. In 1849, Wurtz reacted isocyanates with compounds containing hydroxyl groups into esters of carbamic acid, which were named urethanes [28].

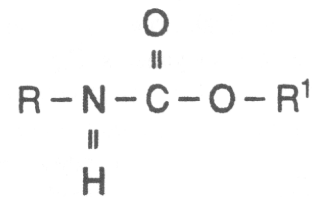


Figure 2.17 Polyurethane reaction [26].

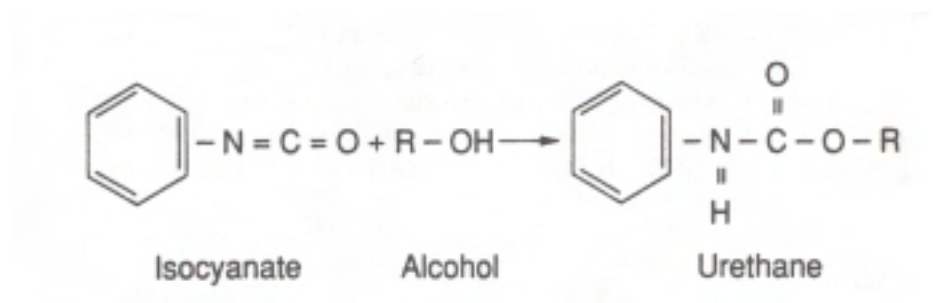


Figure 2.18 Simple urethane reaction [26].

2.6.3 Surface Preparation of Aluminum before Adhesive Bonding

In bonding aluminum (as well as other adherents) the surface preparation of faying surfaces stands alone as a basic absolute requirement for success [24]. The degree to which aluminum must be pretreated is related to the service application and the ultimate bond strength desired. If optimum strength is not

a determinant, an adhesive of lower bond strength may be employed, and simple surface cleaning by vapor degreasing is usually adequate. Where maximum strength, good bond reproducibility and maximum resistance to deterioration are required, a more thorough surface pretreatment is necessary [23].

Commonly used preparations result in microtough adherent morphologies, which have been shown to yield the best overall bond durability. Four of these surface preparations, the Forest Products Laboratory (FPL) etching procedure, P2 etching procedure, phosphoric acid anodization (PAA), and chromic acid anodization (CAA), are described below [19].

The FPL

The FPL and other chromic-sulfuric acid etching procedures are the oldest surface pretreatments for aluminum adherents, with the exception of simple degreasing or mechanical abrasion. Variations of chromate-containing solutions (e.g., NaHSO_4 instead of H_2SO_4) are used for low-stress applications. For the best results etching solutions should be freshly prepared. Etched surfaces should be free from striations and hold a break-free water film [36]. In addition to being used as a complete adherent pretreatment, FPL is also frequently used as the first step in other pretreatments, such as PAA and CAA [29]. FPL was developed by Forest Products Laboratory in 1950 and since then it has been widely used in structural application. This standard was also taken place in the ASTM standards [37].

The P2 etch

The P2 etch, a recently developed process, avoids the use of toxic chromates, but it still provides the complex oxide surface morphology that is crucial to a mechanically interlocked interface and strong bonding. Ferric sulfate is used

as an oxidizer in place of sodium dichromate [30]. The P2 solution produces oxide morphology very similar to that seen on chromic-sulfuric acid etch surfaces over a broad range of time-temperature solution concentration conditions [31]. Mechanical testing confirms that P2-prepared surfaces are equivalent to FPL-prepared specimens. Thus, the P2 solution appears to have great promise as a less hazardous replacement for the chromic-sulfuric acid etches [19].

Phosphoric acid anodization

Phosphoric acid anodization was developed by the Boeing Company in the late 1960s and early 1970s to improve the performance of bonded primary structures [32]. Bonds formed with PAA-treated adherents exhibit durability during exposure to humid environments that is superior to those formed with FPL-treated adherents, especially when epoxy adhesives are used. In addition, PAA bonds are less sensitive than FPL bonds to processing variables such as rinse-water chemistry and time before rinsing.

Chromic acid anodization

Chromic acid anodization [33] is widely used to improve the corrosion resistance of aluminum surfaces (e.g., for window frames and other architectural applications). Similarly, it was thought that the use of a good protective coating on the aluminum would protect the metal interface and thereby increase the bond durability of the joint. Although CAA is not as popular as FPL and PAA treatments in the United States, it has been extensively developed and is widely used for aerospace applications in Europe [19, 34, 35].

CHAPTER 3

EXPERIMENTAL PROCEDURE

In this study, low velocity impact behavior of both monolithic and laminated AA 2024 targets was investigated. Low velocity ballistic characterization of monolithic AA 2024 targets was carried out in three major steps. Firstly, AA 2024 targets were aged in different conditions. Second step was the static mechanical characterization of variously aged AA 2024 samples. Third step was determination of dynamic impact properties of these samples with the help of drop-weight test machine. Low velocity ballistic characterization of laminated AA 2024 targets was performed in four major steps. First step was aging of these targets at identical conditions to obtain improved mechanical properties. Second step was surface treatment of these metal targets before adhesion application. Third step was the adhesion bonding of the AA 2024 target materials. Finally, dynamic impact properties were determined using drop-weight testing. The adhesives that were used in this study were further studied and their static mechanical properties were determined. All tested samples were also examined under optical and electron microscope to obtain information about failure mechanism.

3.1. EXPERIMENTAL SET-UP

A simple gravity drop weight test set-up constructed in METU, Mechanical Engineering Department work-shop, was used for the purpose of this study.

3.1.1. Drop Weight Testing Machine

A simple gravity drop-weight machine has been constructed in a previous study in Mechanical Engineering Department, METU [17]. The set-up was designed to have a maximum 5 m of drop height. However the maximum effective drop height of the ram is 4 to 4.5 m. Main parts of the set-up can be defined as following [17]:

Base

The complete set-up is mounted on a concrete pedestal. It was produced from a 450 x 500 x 400 mm reinforced concrete. To increase the impact resistance of the concrete, a steel structure was formed and S-shape bended wires were mixed randomly into concrete.

Anvil

Anvil was produced from a 350 x 400 x 75 mm steel block. It was constructed heavily to take severe shock loads, as well as to have moderate blow efficiency. Anvil is secured to base by four bolt-nut combinations.

A 350 x 400 x 5 mm rubberized pad was installed between the anvil and base to damp out vibrations. Four T-slots and six M 10 threaded holes were provided on the anvil for easy engagement and removal of bar-cropping, forging and similar die-sets. Two 35 mm in diameter holes were drilled to guide the columns in axial direction.



Figure 3.1 Gravity drop weight testing machine [METU].

Frame of the Hammer

Frame of the hammer consists of upper plate, spreader block and two circular cross-section guides. The guides are 5800 mm in length and 35 mm in diameter St 60 bars. Upper plate is 8 mm in thickness and is fixed to the ceiling with the aid of an L-shaped structure and seven M 14 bolt-nut combination. Guides are suspended by using two pins. Upper plate, centering plate, together with anvil supply the rigidity and parallelism of the columns.

Stairs having same height with set-up were constructed to make the working easy during the tests. Also flash shield, 1800 mm in height was constructed for safety of the personnel.

Guide Connections

Two guide connections with 100 mm in outside diameter, 35 mm inside diameter and 80 mm in height were manufactured. Polyamide was used as a material in order to reduce opposing frictional force and to keep the guide weight minimum.

Damper

In order to absorb excess energy of the guide after impact and to prevent the failure of set-up from shock waves, rubberized pads were installed around the columns on the anvil.

The quick release mechanism

A positive action quick-release mechanism was selected to release the falling weight from the desired height. This mechanism released a tongue, which was connected to the falling weight. While the ram was being raised, the weight tried to close the clamps of the quick-release mechanism. If release lever was pulled downward, the same weight tried to open the clamps of the mechanism.

So, unless the release lever was pulled, the mechanism could not release the falling weight.

The raising and dropping mechanism

Hosting of falling weight and quick-release mechanism was done by pulley, steel rope and drum assembly. Pulley was produced from polyamide to minimize opposing friction. In order to raise the weight with applying small force, drum mechanism with positive drive clutch was manufactured. By using this positive drive clutch, accidental drops were avoided.

3.1.2. Test Set-Up Modifications

Drop-weight testing machine was actually designed for metal forming operations such as bar cropping sheet [17]. However, in some previous studies, it was redesigned for low velocity ballistic characterization purposes [40]. As can be seen from **Figure 3.2**, six new pieces were designed. Those modifications can be cited as follows:

Hammer and Penetrator

An 8 kg steel part was used as a drop-weight hammer. A cylindrical rod penetrator having a diameter of 8 mm was fixed at the bottom of the steel hammer. The impact on the specimen was achieved with the help of this 8 mm-diameter rod. The rod penetrator has blunt tip geometry with 130 mm total length and 110 mm buckling length.

The rod penetrator was made of 115CrV3 steel (**No.1 in Figure 3.2**). It was in hardened and tempered condition. It was austenitized at 1040 °C for 1 hour in a muffle furnace (**Figure 3.5**) then quenched and tempered at 200° in a silicon oil bath (**Figure 3.6**). At the end the projectile has a hardness value of 56 HRC.

Shock Absorber

In order to prevent damage to the guides and to absorb the excess energy of the falling weight after penetration, an aluminum pipe having a diameter of 50 mm, a height of 55 mm and a thickness of 2 mm were used as a shock absorber. **(No.2 in Figure 3.2)**

Fixing Plate

The aim of the fixing plate was to hold the aluminum pipe and to fix the specimen. Also this part would serve as preserver for the guides in the case where A1 pipe were deformed. **(No.3 in Figure 3.2)**

Specimen

It is fixed between fixing **(No.3 in Figure 3.2)** and bottom **(No.5 in Figure 3.2)** plates. **(No.4 in Figure 3.2)**

Bottom Fixing Plate

A rectangular steel holder with dimensions 40 x 30 x 20mm and with a hole 20 mm diameter, was used to fix the specimen. The 20mm diameter hole was drilled so that the punch could pass through the part after hitting the specimen. **(No.5 in Figure 3.2)**

Holder

Beneath the holder, a cylindrical steel part was used as a back holder. A 20mm hole was also drilled to this cylindrical part, so the rod could pass until the weight was stopped by A1 pipe. **(No.6 in Figure 3.2)**

Vice

This part is consisted of two parts. Vice was fixed to the anvil by four bolts. It holds the other parts and the excess energy of the falling weight is transmitted to the anvil through the vice. Since the shape of the inner cavity of the part is

just like a close box all the broken pieces of the specimens recovered after the perforation. (No.7 in Figure 3.2)

3.1.3. Drop-Weight Testing

All the prepared monolithic and laminated AA 2024 targets were tested under a drop weight test machine. During the test, blunt tip penetrators are used. In drop weight test, the weight (hammer) falls from a definite height and the penetrator rod, which is attached in front of the hammer, punches the fixed armor specimen. This impact, results in either plugging; disc shape removal or dishing. In laminated targets delamination may also occur. Therefore, the result of the test is simply whether or not:

- 1) The armor plate penetrated
- 2) The armor plate could not be penetrated
- 3) Laminated target was delaminated

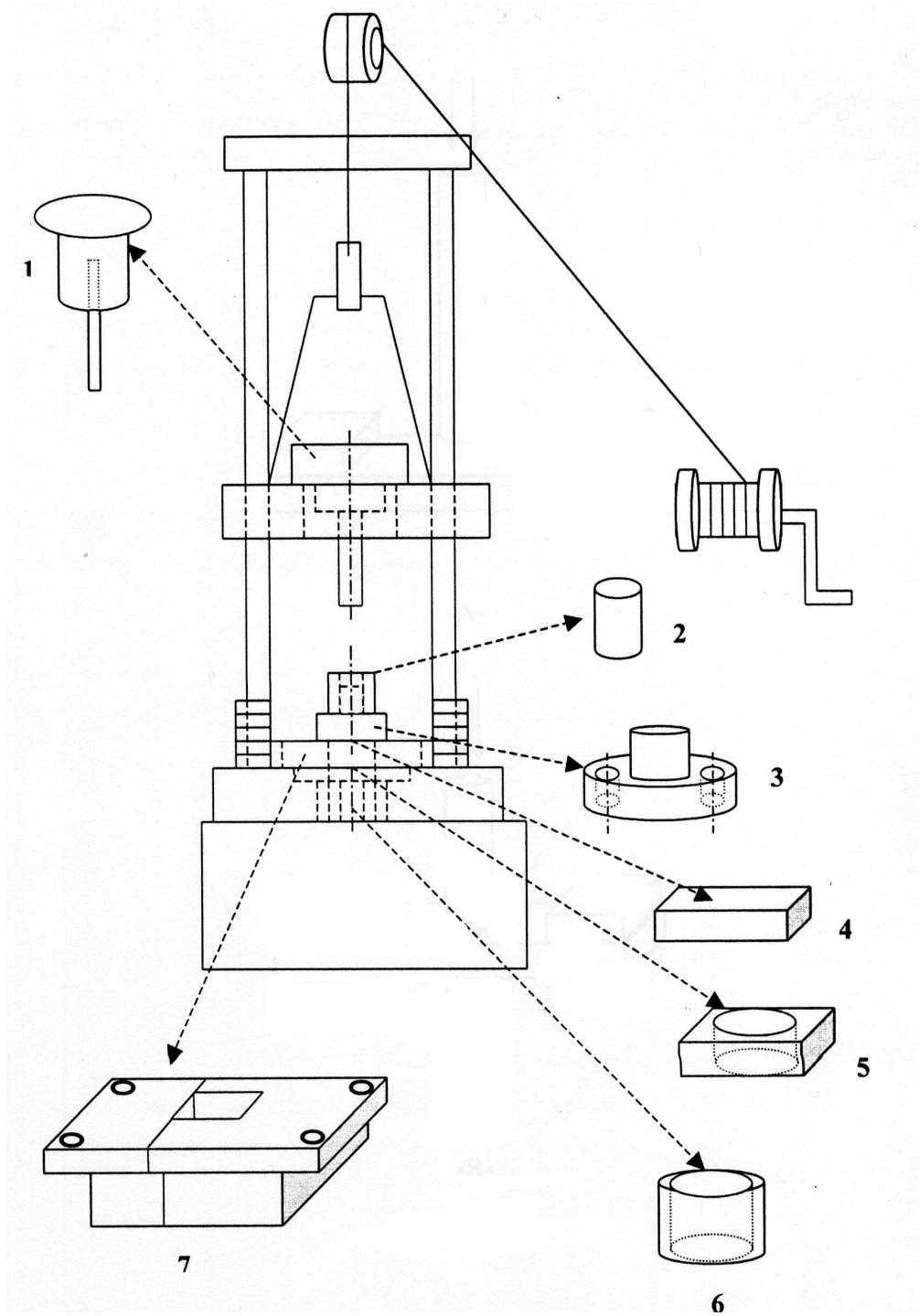


Figure 3.2 Drop Weight Setup and Modifications

During the tests, the hammer was 8 kg. The drop height was in the range of 0.5 m – 4.5 m.

In this study, the drop hammer test is used to find the `ballistic limit` as a material property. *Ballistic Limit Velocity is the minimum striking velocity at which perforation occurs for a projectile – armour system.* In other words, it is the minimum velocity to create a hole through armour, yet not necessarily to cause any fragments to be displacing from the rear plate.

In this study, for each category of target plate specimens, ballistic limit is determined using bisection method. This method involves punching of target plate from the mid-height of perforation case and no perforation case. Procedure is iterated till the determination of the ballistic limit. This procedure is applied to decrease the number of experiments, rather than punching from gradually increasing or decreasing heights to ensure the determination of ballistic limit, after this step, 5 samples are hit at ballistic limit velocity (i.e. same height). If more than 50% (i.e. 3 samples) behaved similarly as in the first stage, the value is determined as ballistic limit. This process is carried out since ballistic failure has somewhat chaotic nature especially in brittle specimens. This may be due to the fact that brittle specimens are more sensitive to defects. The ballistic limit which is determined as the height of the hammer is converted to velocity using the calibration chart in **Figure 3.3** in order to obtain information about impact momentum and energy. Some of the energy is lost in the guides due to opposing frictional forces. The machine frame absorbs certain amount of the energy due to vibration of different parts. This is because of the transfer of the momentum from the ram. The specimen will also absorb certain amount of the energy in the form of plastic deformation.

The impact velocity (V) is calculated as:

$$V := \sqrt{2 \cdot a \cdot h} \dots \dots \dots \text{Equation 3.1}$$

where ,

h : Stroke Height

a : Acceleration of the Ram

If R is the frictional force, W is the falling weight and P is the constant vertical force (For gravity drop-weight P=0), acceleration of the ram is equal to;

$$a = (W+P-R) / m = (W-R) / (W/g) = g - (R/m) = g - (R / (W/g)) \text{Equation 3.2}$$

It is clear that in the drop-weight test acceleration is slightly less than the gravitational acceleration ($a < g$), due to frictional losses. Moreover, it can be seen that acceleration of the ram is directly proportional to the weight of the ram [17]. According to this fact a height versus velocity graph for 8 kg hammer was previously drawn in [40] for ballistic aimed studies. However, this graph was based on several theoretical relationships (**Equation 3.1, Equation 3.2**).

For measuring the impact velocity of the hammer, and constructing the height versus velocity graph especially for this study, a digital camera capable of taking 30 frames per second was used. The series of photographs of 8 kg hammer falling down from different height were transmitted to an image analyzer program. Finally results were determined in MathCAD[®] software program. The modified height versus velocity graph can be seen in **Figure 3.3** as a dash line.

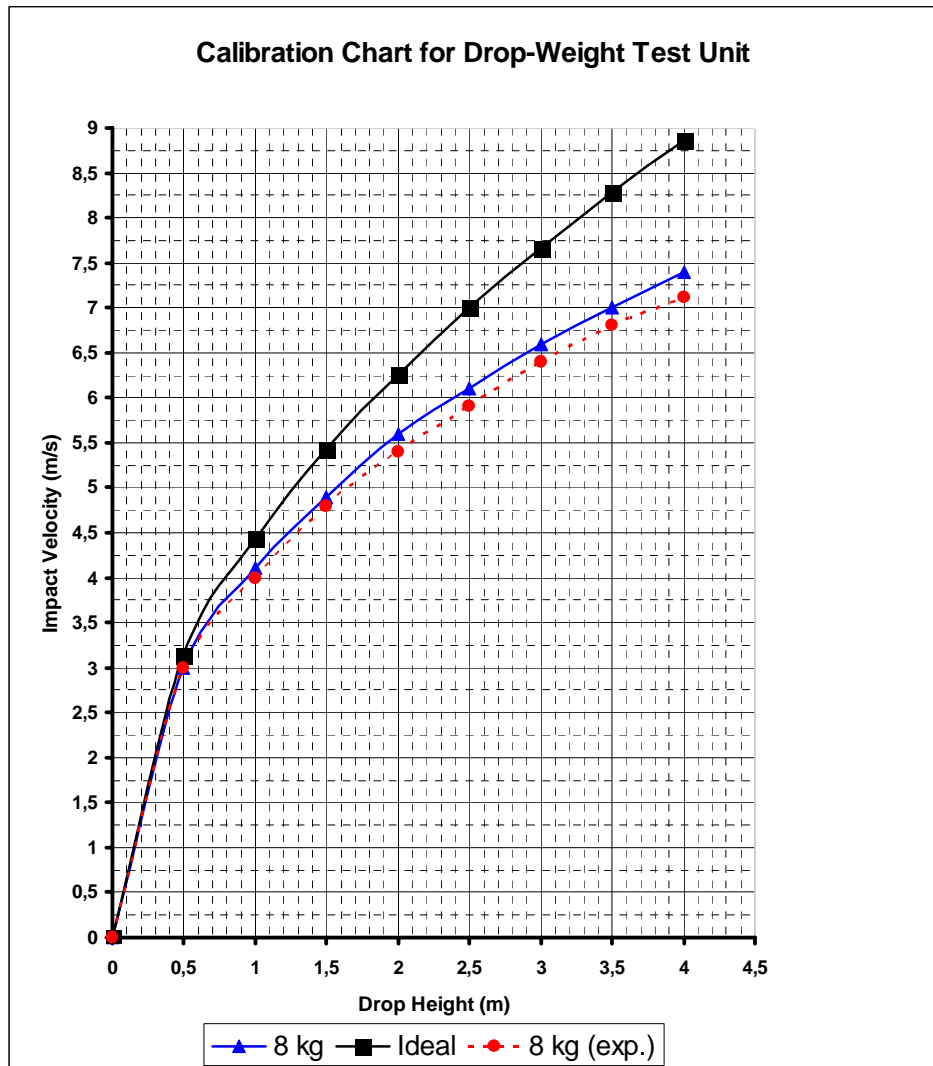
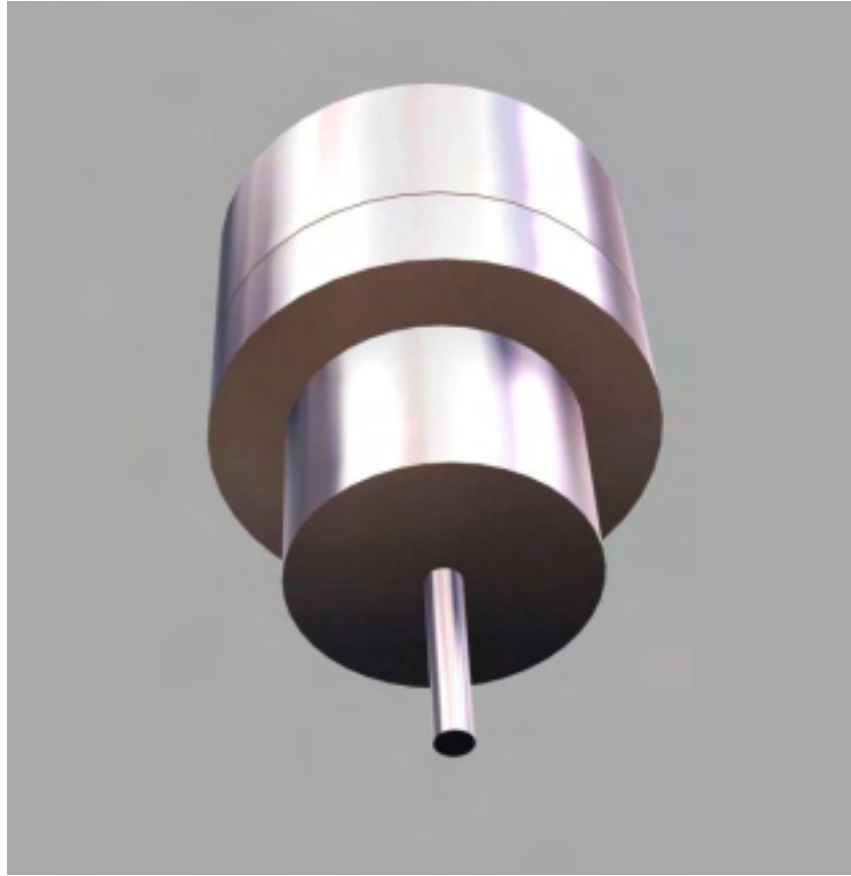
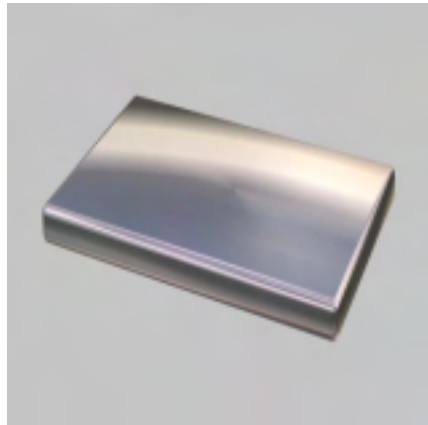


Figure 3.3 Calibration chart for drop weight test Unit.



(a)



(b)

Figure 3.4 (a) Hammer with blunt penetrator (b) Target (40 x 30 x 5 mm AA 2024).

3.2. SPECIMEN PREPARATION

Monolithic and layered AA 2024 plates were used as a target.

3.2.1. Heat Treatment of AA 2024 Target Plates

As a target plate AA 2024 type grade aluminum alloy for which nominal composition can be seen in **Table 3.1**, was used. The commercial AA 2024 plates were received in “0” condition and with dimensions 2000mmx1000mm. The thicknesses of the plates were 2.5, 5.0, 7.5 and 10.0 mm. 40mmx30mm rectangular specimens were cut from these plates for testing at various thickness values. Monolithic target plates were prepared in the form of 2.5, 5.0, 7.5 or 10.0 mm thick specimens. Laminated target plates were constructed from 2.5 mm thick plates with different number of layers.

Mechanical properties of AA 2024 can be improved by heat-treatment. One of these methods is artificial aging. The monolithic AA 2024 targets were heat treated to their peak strength values. Different combination of temperature and time was also used during aging to yield specimens having a wide range of strength values.

Table 3.1 Nominal chemical compositions of AA 2024 targets [19].

	<i>%Cu</i>	<i>%Mg</i>	<i>%Mn</i>	<i>%Si</i>	<i>%Fe</i>	<i>%Zn</i>	<i>%Cr</i>	<i>%Ti</i>	<i>%Al</i>
AA2024	3.80	1.20	0.30	0.50	0.50	0.25	0.10	0.15	bal.
	4.90	1.80	0.90	<i>max</i>	<i>max</i>	<i>max</i>	<i>max</i>	<i>max</i>	

Initially, the heat treatment response of the AA 2024 plate was investigated using 5 mm thick plate. For this purpose target plates were solution heat treated at 490 °C for 50 minutes to obtain a solid solution in a muffle furnace (**Figure 3.5**). Here both the temperature and soaking times (the time at the nominal solution heat-treating temperature) are very critical. Care was taken to avoid exceeding the initial eutectic melting temperature for Al-Cu-Mg system (*Relevant phase diagrams are given in appendices*). Secondly, solution heat treated targets were quenched into the water. After solution treatment and quenching, artificial aging was performed at either 220 or 190°C. Artificial aging was performed in a silicon (viscosity: 1000) oil bath (**Figure 3.6**) for different time intervals.

Low velocity impact tests under drop weight testing machine were carried out on heat treated 2.5, 5.0, 7.5 and 10.0 thick plates.

The experimental procedure for heat treatment of AA 2024 target plates are summarized in the **Table 3.2** and **Table 3.3**.

Table 3.2 Monolithic AA 2024 T6 aging to compare mechanical properties.

<i>Thickness (mm)</i>	<i>Solution Heat Treatment Temperature (C°)</i>	<i>Solution Heat Treatment Duration (minutes)</i>	<i>Artificial Aging Temperature (C°)</i>	<i>Artificial Aging Duration (hour)</i>
5	490	50	190	From 1 to 150
5	490	50	220	From 1/2 to 24

Table 3.3 Monolithic AA 2024 T6 aging to compare dynamic properties with laminated AA 2024 T6 plates.

<i>Thickness (mm)</i>	<i>Solution Heat Treatment Temperature (C°)</i>	<i>Solution Heat Treatment Duration (minutes)</i>	<i>Artificial Aging Temperature (C°)</i>	<i>Artificial Aging Duration (hour)</i>
2.5	490	40	220	1
5	490	50	220	1
7.5	490	65	220	1
10	490	70	220	1

3.2.2. Preparation of Laminated Targets

Laminated targets were prepared from 2.5 mm thick AA 2024 plates by bringing different number of plates together. These target plates were hold together either by a loosely adherent tape wound outside or by a very strong adhesive applied between each layer. The experimental procedure for heat treatment of laminated targets is summarized in **Table 3.4**.

Table 3.4 Heat treatment details of laminated targets

<i>Number of Layers</i>	<i>Thickness (mm)</i>	<i>Solution Heat Treatment Temperature (C°)</i>	<i>Solution Heat Treatment Duration (minutes)</i>	<i>Artificial Aging Temperature (C°)</i>	<i>Artificial Aging Duration (hour)</i>
1	2.5	490	40	220	1
2	2 x 2.5	490	40	220	1
3	3 x 2.5	490	40	220	1
4	4 x 2.5	490	40	220	1



Figure 3.5 Muffle furnace.



Figure 3.6 Oil bath.

3.2.2.1 Surface Preparation for Adhesive Bonding

In high-strength applications, particularly where aluminum is to be bonded to itself, the chemical pretreatment of the surfaces is mandatory. In order to construct laminar target plates, the surface treatments of AA2024 plates were performed. The procedure applied can be summarized as follows:

1. The 40x30x2.5 mm plates were solution-heat treated and artificially aged to T6 temper.
2. Plates were grinded with 100-grit sandpaper and immersed in tap water.
3. The surfaces of the plates were cleaned with toluene (solution no.1[†]) soaked cellulose tissues and air dried.
4. Plates were immersed for 10-12 minutes in a tap-water solution of an aqueous alkaline cleaner solution (Turco 4215[®]).
5. Plates were rinsed thoroughly in water and air dried.
6. Plates were immersed in an acid solution containing sodium dichromate (solution no.2[†]) at 60-65 °C for 15 minutes.
7. The treated surfaces were flushed with fresh water and air-dried.

As the solution no.2 was highly acidic, a polyvinyl-chloride-lined tank was used and solution was gently stirred with a stainless steel mixer. Moreover, some severe precautions (acid proof gloves, eyeglasses, acidic and organic gas proof mask) were taken while working.

Table 3.5 [†] Chemicals used in surface preparation of AA 2024.

[†] Chemical formulas of these solutions are given in **Table 3.5**.

Solution No.	Chemicals	Formulas	Composition by Weight
1	Toluene (Methylbenzene, phenyl methane)	$C_6H_5CH_3$	-
2	Sulfuric Acid (95-98%)	H_2SO_4	10 parts
	Sodium Dichromate	$Na_2Cr_2O_7 \cdot 2H_2O$	1 part
	Distilled Water	H_2O	30 parts

3.2.2.2 Application of Adhesive

The layers of the laminated targets were brought together with three different methods.

First set held together with a two-component commercial epoxy adhesive. Four different total thicknesses including, 2.5, 5.0, 7.5 and 10.0 mm, were established using 40 x 30 x 2.5 mm dimension plates (**Figure 3.7**). A commercial epoxy (Sikadur 32N[®]) based adhesive was used. The procedure applied for epoxy adhesive application on AA 2024 target surfaces is summarized below:

1. Plates were surface treated.
2. Epoxy and its hardener were mixed with a weight ratio of Epoxy/Hardener: 2 (**Figure 3.9**).
3. Adhesive was applied to the surface.
4. Surfaces held together under 40 kPa pressures. Excess adhesive overflowed from the edges were cleaned before complete curing.
5. Complete curing was performed at room temperature at 168 hours.

For the second set of AA 2024 plates a two-component commercial polyurethane (Bison®) adhesive was used. Four different thicknesses including, 2.5, 5.0, 7.5, 10.0 mm, were established using 40 x 30 x 2.5 mm dimension AA 2024 T6 plates. Almost the same procedure like epoxy, applied to polyurethane practice. However, polyurethane/curing reagent ratio was 3.

Third set AA 2024 plates were loosely held together with an adhesive tape. Surface preparation was not applied to these samples as no adhesion bonding was present. The aim was to hold specimens loosely. Again four different thicknesses including 2.5, 5.0, 7.5, 10.0 mm, were established using 40 x 30 x 2.5 mm dimension AA 2024 T6 plates (**Figure 3.8**).



Figure 3.7 AA 2024 plates bonded with epoxy adhesive.

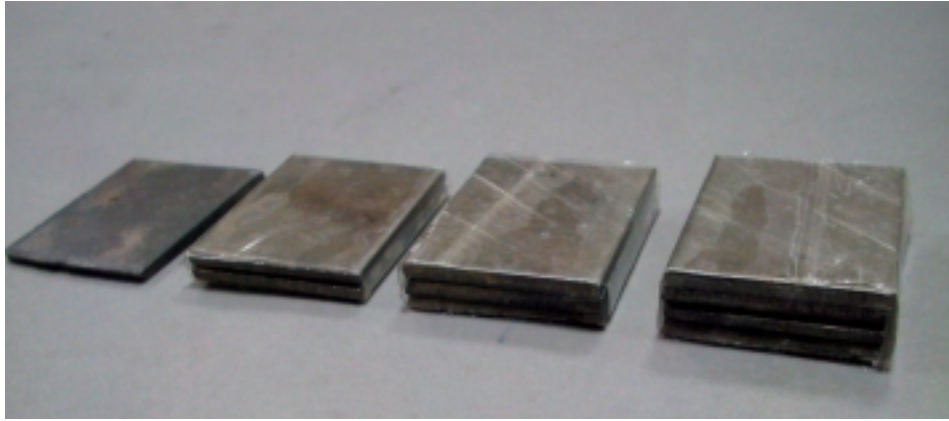


Figure 3.8 AA 2024 plates loosely held with adhesive tapes.



Figure 3.9 Epoxy adhesive preparation.

3.3. STATIC MECHANICAL CHARACTERIZATION

Static mechanical characterization basically consists of conventional hardness testing and tensile testing. Results obtained from those tests are important for investigating the relationships between static mechanical properties and dynamic properties under low velocity impact.

3.3.1. Hardness Test of AA 2024 Plates

Hardness tests were carried out with Brinell hardness tester with 2.5 mm steel ball indenter under 613 N or 1839 N loads depending on the hardness level. For each aging condition, 5 indentations were taken from each sample and for each case 5 samples were used. While taking the indentations it was paid attention to leave sufficient space between indentations to prevent strain hardening. Before hardness test, all the test specimens were ground with 100 grit emery paper to obtain a flat surface.

3.3.2. Tensile Testing of AA 2024 Plates

Tensile test specimens were prepared from AA 2024 plates according to ASTM E8M [41]. The dimension of the test specimen is given in **Figure 3.10**.

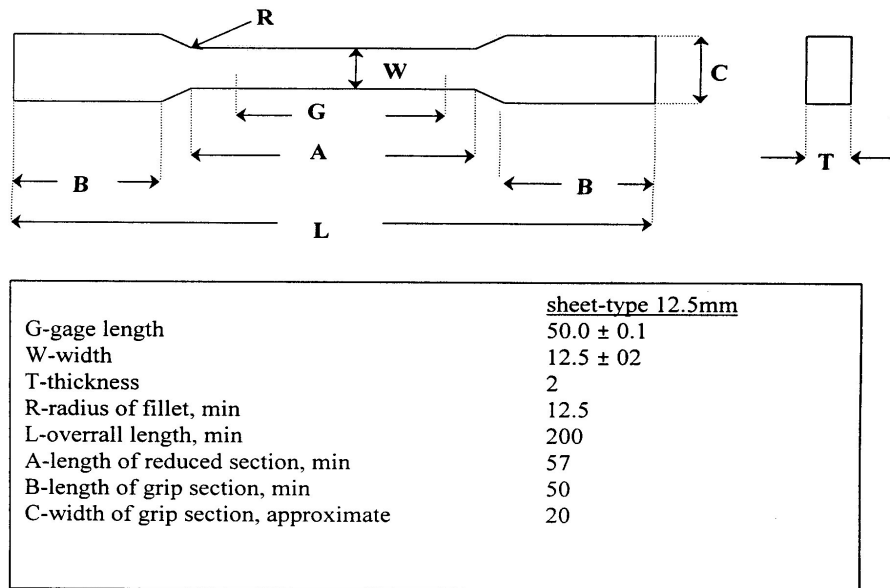


Figure 3.10 Dimensions of the tensile test specimen [41].

In order to obtain the same static mechanical properties between the target plates under drop-weight test and the tensile test specimens, identical aging procedure was applied to tensile test specimens and target plates.

3.3.3. Tensile Testing of Adhesives

The adhesion strength of both epoxy and polyurethane adhesives were investigated by two major tests; tensile and lap-shear tests. The aim of measuring these quantities was:

- (1) To compare the adhesion strength of these two adhesives,
- (2) To investigate the effect of surface treatments and,
- (3) To compare the behavior of adhesives under dynamic and static loading.

The tensile tests of adhesives were carried out according to ASTM D897-78 standard [42]. In this test, the adhesive is applied between the surfaces of two jigs. The jigs are pulled parallel apart until adhesive fails. The measured load before failure is recorded. The adhesive strength of three specimens which were not surface treated (but only ground), and three specimens of FPL [29] etched (surface treated) were compared. Material used as a specimen was AISI 1020 cold finished bar according to ASTM D897-78 standards. The dimension of the test specimen is given in **Figure 3.11**.

In order to perform these tensile tests, test grips were constructed again according to ASTM D897-78 standards.

Apart from tensile strength, strength properties of adhesives in shear by tension loading were also investigated according to ASTM D1002-72 standards [43]. The adhesive shear strength of three specimens which were not surface treated (but only ground), and three specimens of FPL [29] etched

(surface treated) were compared. Material used as a specimen was AA 2024 T3 bar according to ASTM D1002-72 standards. The dimension of the test specimen is given in **Figure 3.12**.

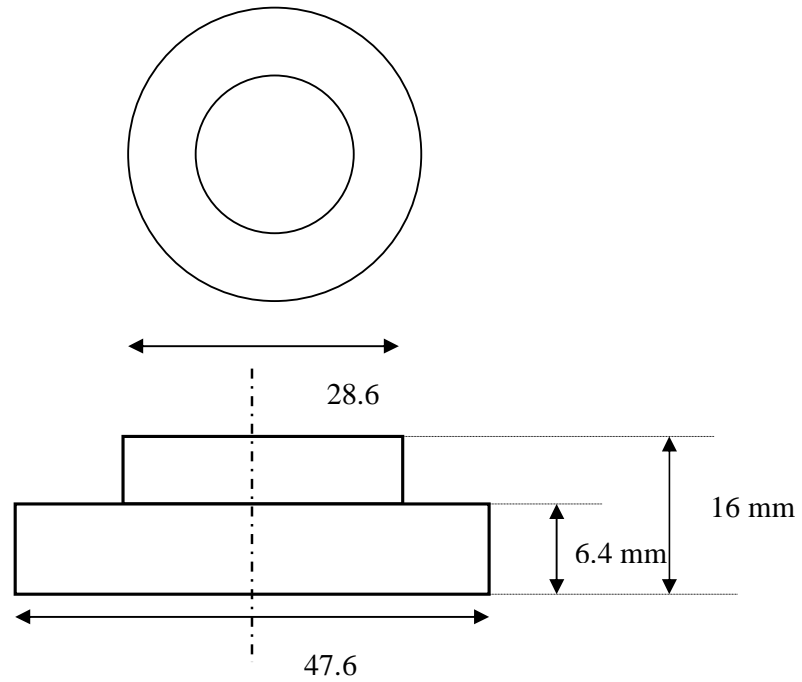


Figure 3.11 Dimensions of tensile test specimen for adhesives [42].

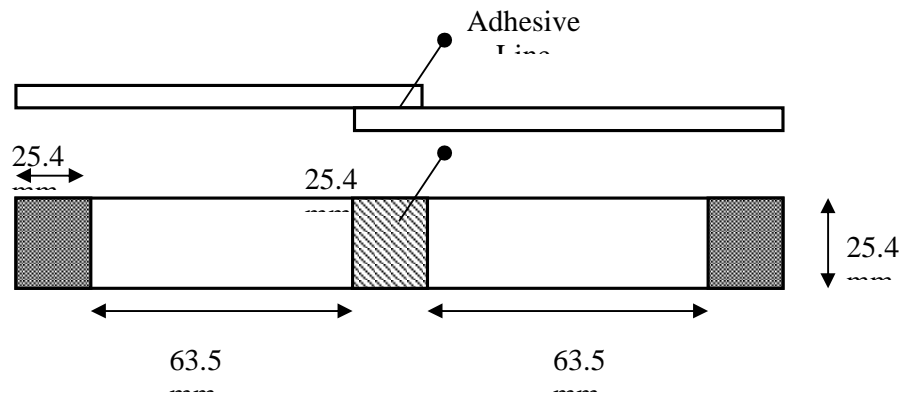


Figure 3.12 Dimensions of lap shear test specimen for adhesives [43].

In order to investigate the effects of surface preparation on adhesion strength, the specimens with notations indicated in **Table 3.6** were prepared

Surface	E1	E2	E3	P1	P2	P3
Preparation						
Grinding (100 grit-abrasive)	√	√	√	√	√	√
Toluene	-	√	√	-	√	√
FPL	-	-	√	-	-	√
Adhesives						
Epoxy	√	√	√	-	-	-
Polyurethane	-	-	-	√	√	√

Table 3.6 Notations for tensile and lap-shear tests of adhesives.

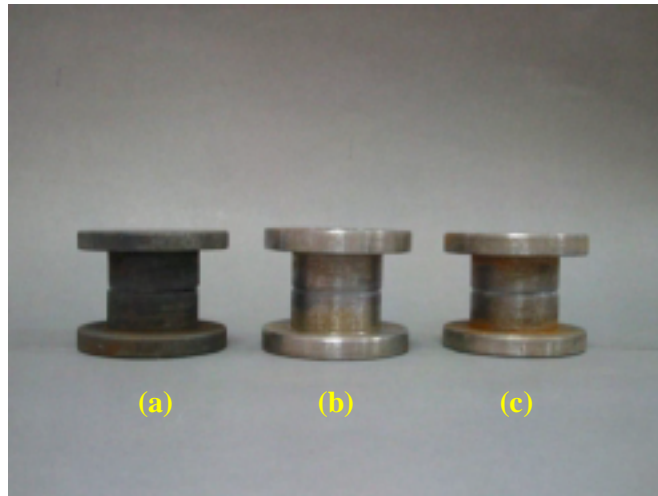


Figure 3.13 Specimens used in adhesive tensile tests

(a) Surface Treated (FPL) (b) Grounded + Toluene (c) Only Grounded

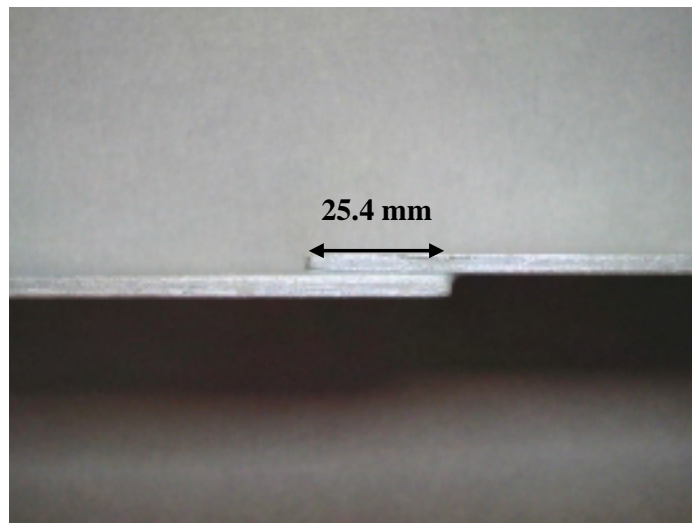


Figure 3.14 Specimen used in adhesive lap-shear tests.



Figure 3.15 Grips prepared for tensile testing of adhesives.

3.4. MICROSTRUCTURAL CHARACTERIZATION

For microstructural characterization of AA 2024 under optical microscope Keller's reagent (**Table 3.7**) was used. The surface of the target plates after surface treatment was investigated under scanning electron microscope (JEOL 6400[®]).

Table 3.7 Keller's Reagent

<i>Keller's Reagent</i>	<i>Vol. %</i>
HCl	1
HF	1.5
HNO ₃	2.5
H ₂ O	95

3.5. DYNAMIC MECHANICAL CHARACTERIZATION

The primary aim of this study was to investigate low velocity ballistic behavior of AA 2024 under drop weight testing machine and correlate the results with static mechanical properties. For this purpose, a drop weight test set-up was used. Moreover, notched-bar impact test was also performed to compare the outcomes from these two different dynamic tests.

3.5.1 Notched-Bar Impact Test

In this study, Charpy impact test apparatus was used and specimens were prepared according to ASTM E23 standards [44]. Other test parameters were given in **Table 3.8**.

Table 3.8 Charpy V-notch impact test parameters

<i>Thickness</i> (<i>mm</i>)	<i>h</i> (<i>mm</i>)	<i>h'</i> (<i>mm</i>)	<i>Impact Velocity</i> (<i>m/s</i>)
10	1625	290	5.11

45° V-notch

3.6. NOTATION FOR TARGET PLATES

In order to follow experimental results easier, a notation for AA 2024 target plates was developed as shown in **Table 3.9** - **Table 3.11**.

Table 3.9 Notations for monolithic targets.

<i>Notation</i> (<i>monolithic</i>)	<i>Target Thickness</i> (<i>mm</i>)	<i>Aging Temperature</i> (<i>°C</i>)	<i>Aging Time</i> (<i>hour(s)</i>)	<i>Explanations</i>
MA1	5	NA	NA	AA 2024-O Annealed
MA2	5	220	1	Peak Aged
MA3	5	220	3	Over Aged
MA4	5	220	5	Over Aged
MA5	5	220	24	Extremely Over Aged

Table 3.10 Notations for monolithic targets (continued).

<i>Notation (monolithic)</i>	<i>Target Thickness (mm)</i>	<i>Aging Temperature (°C)</i>	<i>Aging Time (hour(s))</i>	<i>Explanations</i>
M1	2.5	220	1	Peak Aged
M2	5	220	1	Peak Aged
M3	7.5	220	1	Peak Aged
M4	10	220	1	Peak Aged

Table 3.11 Notations for laminated targets.

<i>Notation (Laminated)</i>	<i>Target Thickness (mm)</i>	<i>Aging Temperature (°C)</i>	<i>Aging Time (hour(s))</i>	<i>Explanations</i>
LT1	2.5	220	1	Tape ¹
LT2	5	220	1	Tape ¹
LT3	7.5	220	1	Tape ¹
LT4	10	220	1	Tape ¹
LE1	2.5	220	1	Epoxy ²
LE2	5	220	1	Epoxy ²
LE3	7.5	220	1	Epoxy ²
LE4	10	220	1	Epoxy ²
LP1	2.5	220	1	Polyurethane ³
LP2	5	220	1	Polyurethane ³
LP3	7.5	220	1	Polyurethane ³
LP4	10	220	1	Polyurethane ³

¹ Loosely bound with tape.

² Adhered with epoxy (Sikadur 32N[®])

³ Adhered with polyurethane (Bison[®])

CHAPTER 4

EXPERIMENTAL RESULTS

There were two main objectives for this study. First one was to investigate the variation in low velocity ballistic response of monolithic AA 2024 target plates at different hardness, percent elongation, ultimate tensile and yield strength. The latter was to determine the low velocity ballistic behavior of laminated targets and compare the results with those of monolithic plates having the same thickness.

In order to obtain information about ballistic performance, drop-weight setup was used with several modifications (**Chapter 3**). Drop-weight test has several advantages in evaluation of ballistic characteristics. First of all, it is an easy test to perform in regards to time consuming ballistic tests. Secondly, the velocity of the impact can be easily determined since the height of free fall is precisely known. Finally, the weight of the hammer and the impacting bullet profile can be manipulated easily to obtain different impact conditions. Consequently, solid data can be generated for modeling of ballistic impact of materials at low velocities.

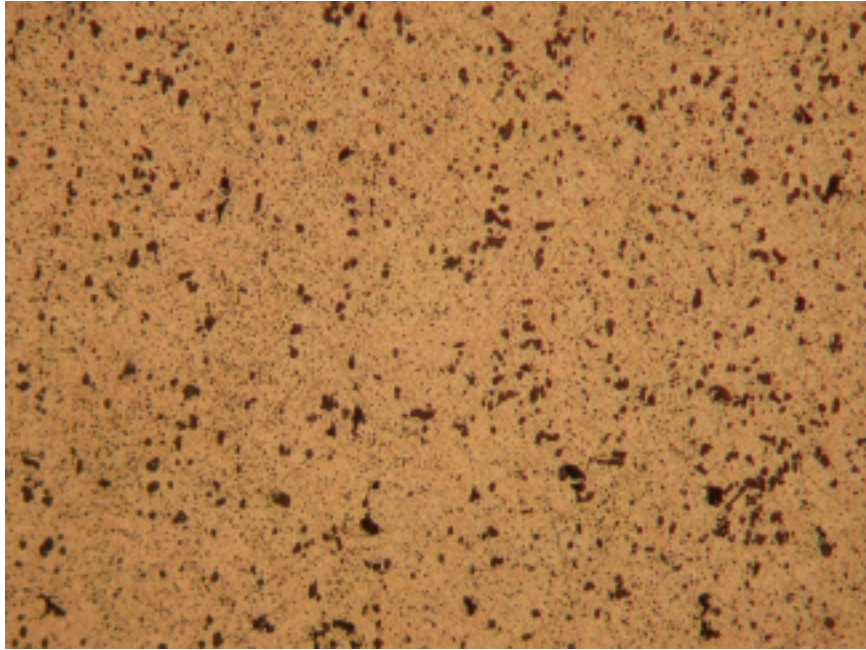
In the following part, firstly, microstructural characterization of target plates will be introduced. The effect of surface treatment and adhesion strengths will also be given both visually and quantitatively. Secondly, the results of static mechanical tests will be given and for visualization purpose, they will be converted into graphics where it is possible. Thirdly, quantitative results of drop-weight test will be presented and several graphs will be used to illustrate the relationships between the static mechanical test results and drop-weight

test results. The results obtained from notched-bar impact test (Charpy) will be introduced with drop weight test results to compare two different dynamic test methods. Moreover, the effect of increasing thickness of monolithic target plates will be introduced quantitatively. The results obtained from laminated and monolithic plates will be compared. Finally, qualitative macro inspection results will be presented.

4.1. MICROSTRUCTURAL CHARACTERIZATION OF AA 2024

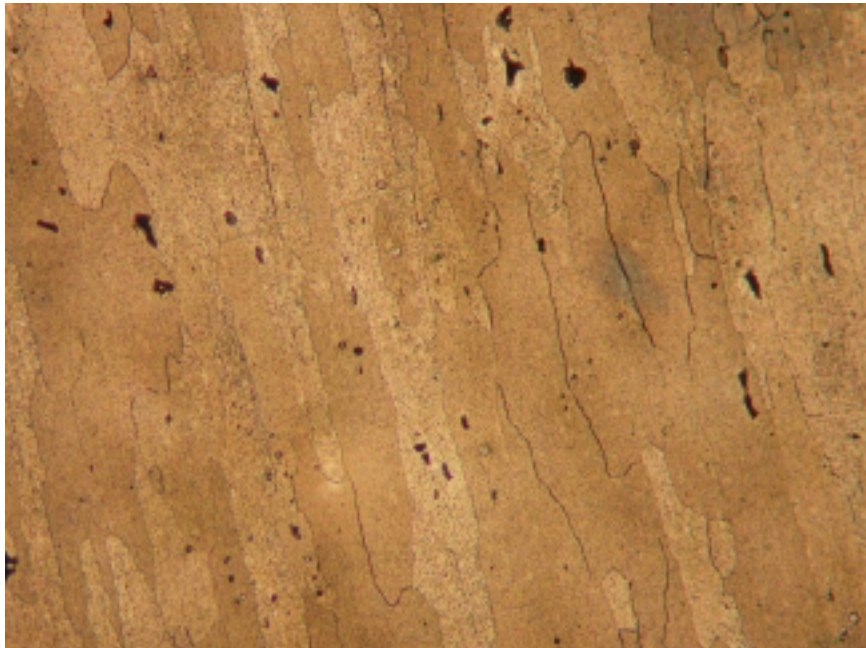
AA 2024 alloys are usually complex because of the many additives for strength, corrosion resistance, or grain structure control. AA 2024, with aluminum + copper + magnesium + manganese + iron + silicon, has a multiphase ingot structure. Microstructural characterization of artificially aged target plates was carried out under optical microscope.

AA 2024 was received in annealed condition with temper designation “0”. The typical microstructure of AA 2024 plate in annealed (“0”) condition can be seen in **Figure 4.1**. As seen, the microstructure consists of large black second phase particles. On the other hand, **Figure 4.2** shows the microstructure of an AA 2024 plate after solution heat treated at 490 °C and quenched in water. It is seen that most of the second phase particles are dissolved during solutionizing and supplied alloying elements to the matrix. Although, no attempt was made to characterize the second phase particles undissolved, they are most probably of CuMgAl_2 , $\text{Cu}_2\text{MnAl}_{20}$ or Cu_2FeAl_7 type. It is also seen that grain boundaries can be resolved easily after solution heat treatment. If solution heat-treatment was not performed properly, eutectic melting could occur which cause a considerable loss in mechanical properties. **Figure 4.3** and **4.4** shows the importance of the microstructural analysis. **Figure 4.3** shows an example, where eutectic melting took place at the three point junction of grain boundaries during solutionizing. These specimens behaved in a brittle manner during impact tests. Such a eutectic melting can be seen in **Figure 4.4** at a higher magnification.



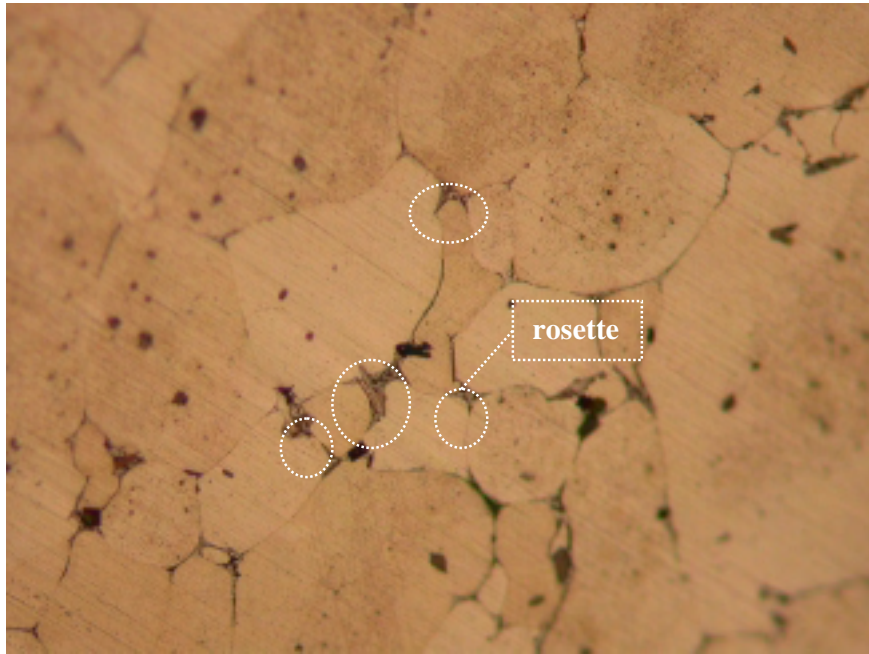
200 X

Figure 4.1 AA 2024-O (200X).



200 X

Figure 4.2 AA 2024-T6 (200X).



200 X

Figure 4.3 AA 2024-T6, showing rosettes formed by eutectic melting. Solidus temperature was exceeded during solution heat treatment (200X).

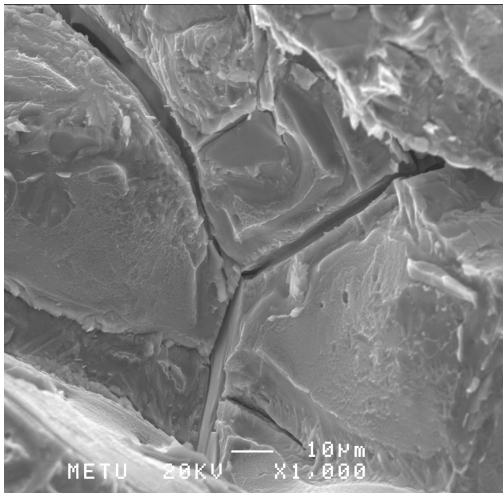


Figure 4.4 Fracture surface of AA 2024-T6 target specimen under SEM. Eutectic melting is evident at three point junctions.

4.2. EFFECT OF FPL TREATMENT ON SURFACE MORPHOLOGY OF AA 2024

Prior to adhesive bonding the AA 2024 plates were surface treated to increase the adhesion strength. If a layer of grease or oil on the surface is not removed, bonding strength can be dramatically reduced. The bonding used in lamination is very important as it must transmit the shock waves formed during impact to the other laminates without distortion. Largely tensile and shear stresses develop on the targets during impact. Probably a thick and or weak oxide layer present on AA 2024 target lowers joint strength and durability. Therefore, FPL surface treatment method replaces the existing layer with a thinner and/or stronger oxide layer and/or with different microroughness characteristics.

The initial grinding and toluene application was for removing gross organic contamination from the surface, whereas the alkaline cleaning was to remove some oxide coating formed during the aluminum heat treatment. The remaining oxide dissolves in the etching solution. The microroughness (pitting) formed on the surface may probably provide a means of mechanical interlocking between the adhesive and the oxide surface. Chemically, the FPL film is amorphous Al_2O_3 with some amount of MgO . Microroughness and thickness of oxide layer increase with FPL application duration.

The relationship between the time and the amount of microroughness is demonstrated in **Figures 4.5 – 4.9**. The recommended time for this process according to *ASTM standards* [37] is 15 minutes. In **Figure 4.5**, the grinded surface of the plate can be seen. After 2 minutes of FPL etching, a few amount of pitting started to form (**Figure 4.6**). A 10 minutes FPL application on the target surfaces resulted in an increase in size and numbers of pits (**Figure 4.7**). After 15 minutes, the size and numbers of pits reached an optimum value as it can be seen from **Figure 4.8**.

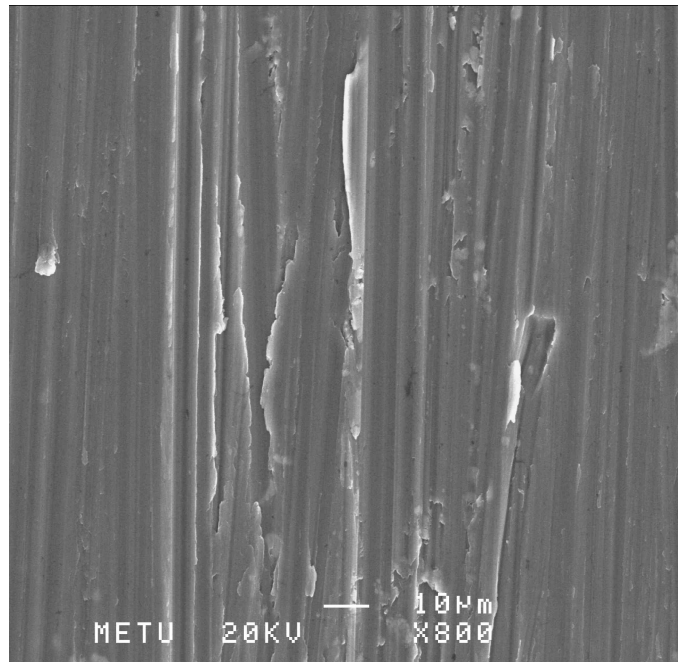


Figure 4.5 AA 2024-T6, as grinded with 100 grit abrasive paper (800X).

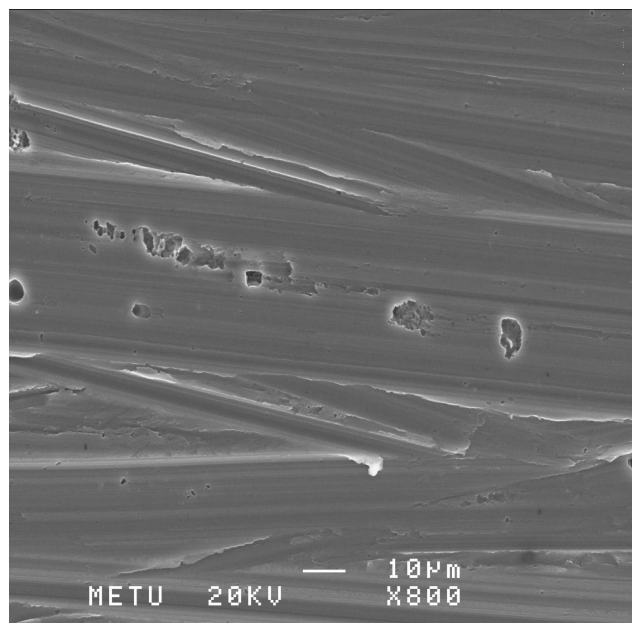


Figure 4.6 AA 2024-T6, as FPL etched for 2 minutes.
A few pitting can be observed. (800X).

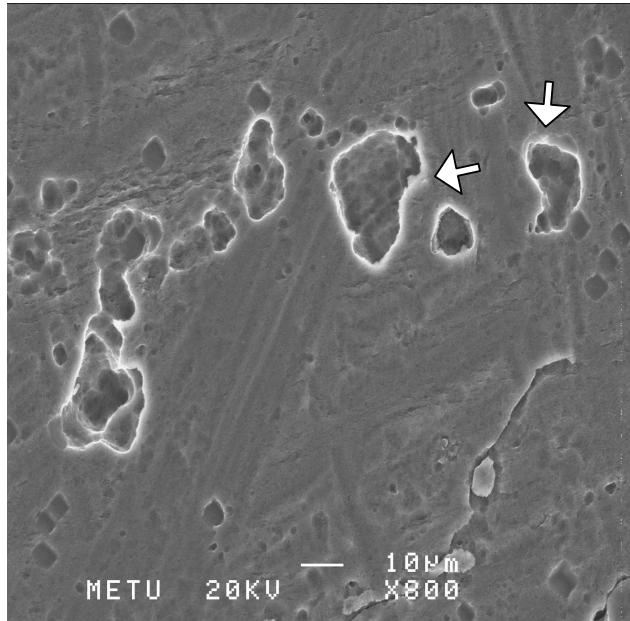


Figure 4.7 AA 2024-T6, as FPL etched for 10 minutes. Surface roughness increase. (Pits are shown) (800X).

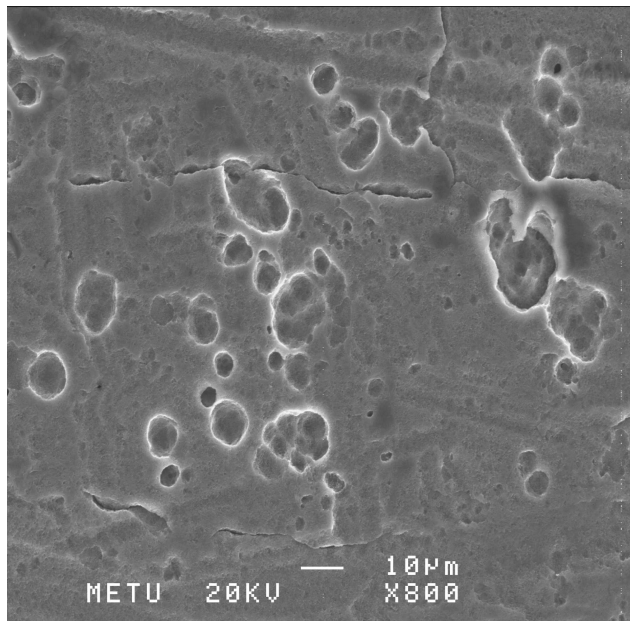


Figure 4.8 AA 2024-T6, as FPL etched for 15 minutes. Higher amount of pits exist on the surface. (800X).

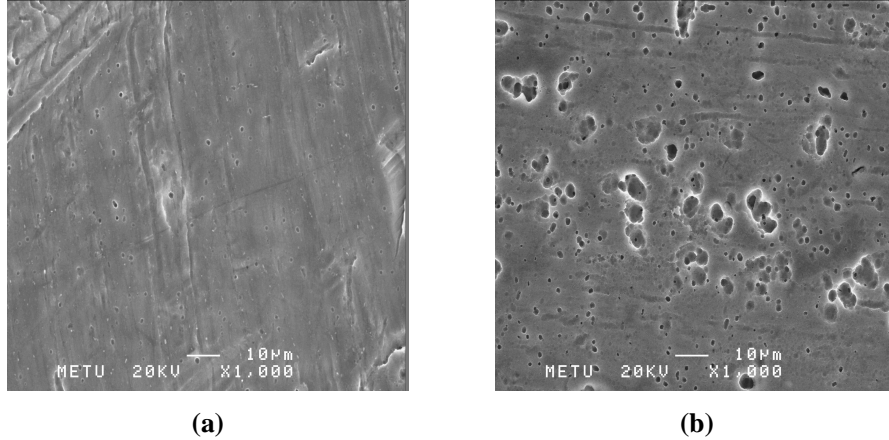


Figure 4.9 AA 1050 and AA 2024, as FPL etched for 15 minutes. (1000X)

Figure 4.9a shows the surface of an AA 1050 with min 99.50%Al and max 0.05 %Cu-Mg as FPL etched for 15 minutes. Similarly, **Figure 4.9b** shows the surface of an AA 2024 with 4.4%Cu and 1.8% Mg as FPL etched for the same duration. As it can be seen from **Figure 4.9a**, surface was virtually unaffected from FPL. However, FPL was highly effective and caused a large number of pits on the surface of AA 2024. The reason may be the difference in %Cu contents of these two alloys. The addition of the aluminum alloy seed optimizes the FPL solution by releasing copper into the solution. Moreover, the heat treatment of magnesium-containing alloys, like in the case of AA 2024, following the growth of an FPL oxide, can result in an outdiffusion of magnesium and formation of MgO [19].

The examination of FPL treated surfaces under scanning electron microscope gave an idea about surface microroughness. Its effect on degree of adhesion was measured by tensile and lap-shear testing. Three sets of specimens for tensile and two sets of specimens for lap-shear test were prepared. The tensile and lap-shear test results are given in **Table 4.1** and **Table 4.2**.

Table 4.1 Tensile and lap-shear tests results for polyurethane.

Surface Treatment	Polyurethane Tensile Strength (MPa)	Polyurethane Lap-Shear Strength (MPa)
P1 (grinded)	3,21	3,10
P2 (grinded + toluene)	3,72	3,59
P3 (FPL)	4,37	3,73

Table 4.2 Tensile and lap-shear tests results for epoxy.

Surface Treatment	Epoxy Tensile Strength (MPa)	Epoxy Lap-Shear Strength (MPa)
E1 (grinded)	17,26	9,16
E2 (grinded + toluene)	17,50	-
E3 (FPL)	26,26	17,55

According to the mechanical test results of adhesives, it was found that tensile strength of the epoxy adhesive is much higher than that of polyurethane adhesives. Similarly, lap-shear strength of the epoxy adhesive is higher than that of polyurethane based adhesive. Moreover, it can be concluded that FPL surface treatment is a very effective method to increase the adhesion efficiency for epoxy adhesive. However, the adhesion efficiency of polyurethane based adhesive did not improve applying FPL surface treatment. Finally, among the tested adhesives epoxy was found to be more effective as far as adhesion strength is concerned.

Figure 4.10 shows two different surfaces of jigs used in tensile testing of epoxy adhesive. A perfect adhesion of epoxy on jig surfaces, after application of FPL surface treatment can be seen in **Figure 4.10a**. However, an insufficient adhesion of epoxy on the jig surfaces was observed for the specimens that FPL method was not applied (**Figure 4.10b**). As it can be seen from **Figure 4.10b**, epoxy peeled up from the surface. Therefore, under tensile loading, adhesive bond strength is higher for FPL etched specimens.

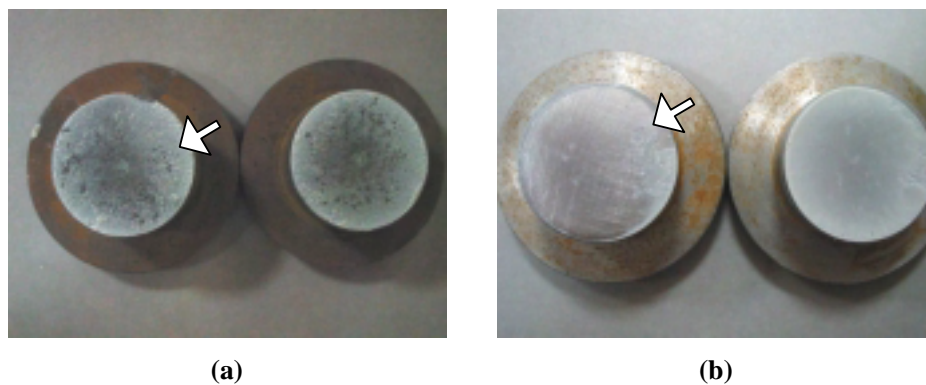


Figure 4.10 The surfaces of jigs of FPL applied (a) and not applied (b) specimens.

4.3. STATIC MECHANICAL TESTS

Static mechanical characterization in this study involves hardness, ultimate tensile and yield strength, ductility and elastic modulus. Except hardness, the other properties can be calculated from stress-strain curve obtained by simple tensile testing.

4.3.1 Hardness Test

The hardness test played a very important role in this study. It is not only important for the ballistic performance but also in performing the aging curve of AA 2024. The hardnesses of AA 2024 target plates after aging at 220 °C and 190 °C can be seen in **Figure 4.11** and **Figure 4.12** respectively. The hardness values are tabulated in **Table 4.3** and **Table 4.4**.

Table 4.3 Brinell hardness values of AA 2024 at 220°C.

<i>AA 2024</i> (Aging Temperature 220°C)	<i>Aging Time</i> (hours)					
	0	1	3	5	7	24
Hardness Values (BHN)	55	148	120	112	108	100
STD	2.0	2.2	4.0	3.6	2.7	2.2
25 indentations were taken for each condition.						

Table 4.4 Brinell hardness values of AA 2024 at 190°C.

AA 2024 (Aging Temperature 190°C)	Aging Time (hours)					
	0	1	3	5	7	150
Hardness Values (BHN)	55	126	131	138	142	110
STD	2.0	2.6	2.4	3.2	2.1	2.7
25 indentations were taken for each condition.						

An aging treatment at 190 °C caused an increase in hardness values. The hardness was increased from 50 BHN to nearly 145 BHN within 7 hours. A prolonged aging up to 24 hours did not cause a decrease in hardness but rather stayed nearly constant at 145 BHN.

Upon aging at 220 °C, the maximum hardness value was attained within 1 hour. A prolonged aging treatment, however, caused a decrease in peak hardness. A 24 hours aging at 220 °C yielded a hardness value of 100 BHN.

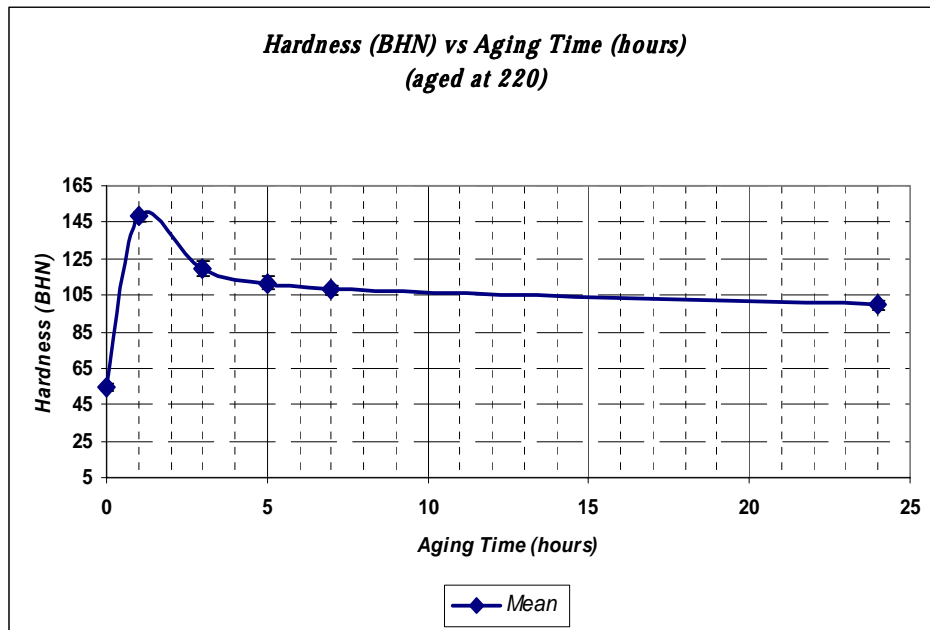


Figure 4.11 Aging curve of AA 2024 at 220°C.

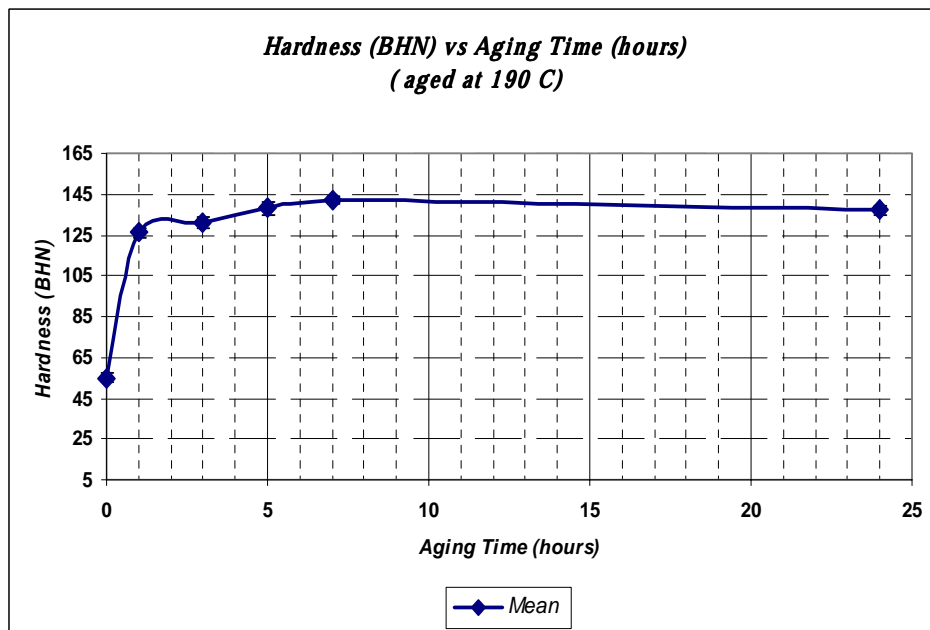


Figure 4.12 Aging curve of AA 2024 at 190°C.

4.3.2 Tensile Testing

Tensile testing was performed only for AA 2024 target specimens aged at 220 °C. The selection of 220 °C is mainly due to that a wide range of mechanical properties could be obtained by small variations in aging time. This can be seen from the hardness values. For example, at 190 °C hardness decreased from 142 HB to 110 HB in six days. However upon aging at 220 °C, one can easily obtain a wide range of mechanical properties within a reasonable time interval. The tensile test values of all heat treated specimens are tabulated in **Table 4.5**.

These data are plotted in **Figure 4.13** to **Figure 4.16**. Minimum tensile and yield strength was seen in annealed condition. Maximum tensile and yield strength were attained with 1 hour aging at 220 °C. After 24 hours aging there is a virtual decrease in tensile and yield strength.

Table 4.5 Tensile test values of AA 2024 at 220°C.

<i>Aging Time</i> (Aging Temperature 220°C)	<i>UTS</i> (MPa)	σ_y (MPa)	<i>%EL</i>	<i>Log(SHR)</i> [†]	<i>E</i> (GPa)
0	195	90	19	2,874	73
1	500	400	10	3,176	73
3	402	340	8	3,071	73
5	395	333	8	3,068	73
24	344	310	6	2,959	73

3 specimens were tested for each condition.

[†] *SHR = Strain Hardening Rate = (UTS*(1+%EL)- σ_y)/(%EL) [45]*

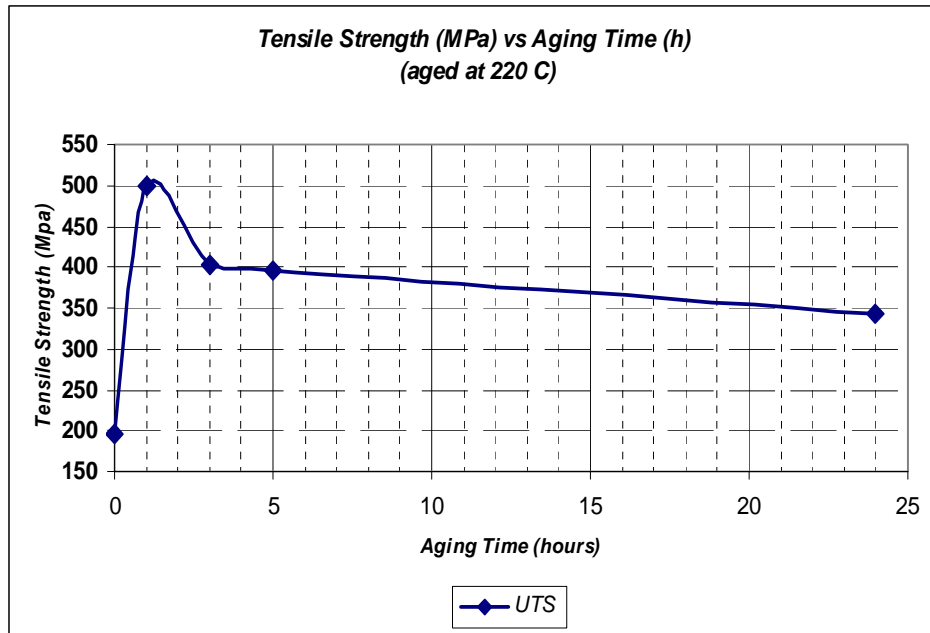


Figure 4.13 The change in UTS of AA 2024 plates after aging at 220 °C.

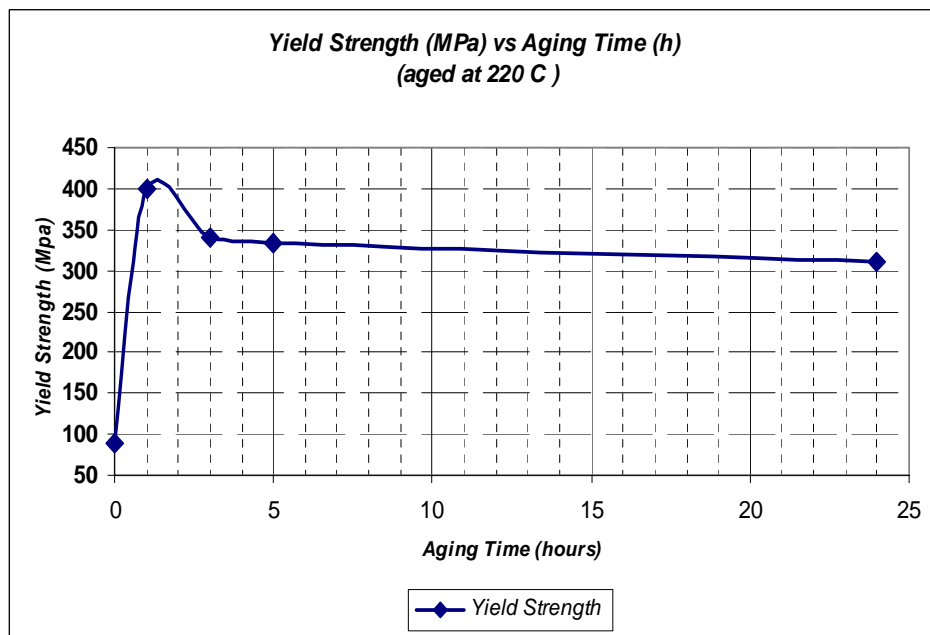


Figure 4.14 The change in yield strength of AA 2024 plates after aging at 220 °C.

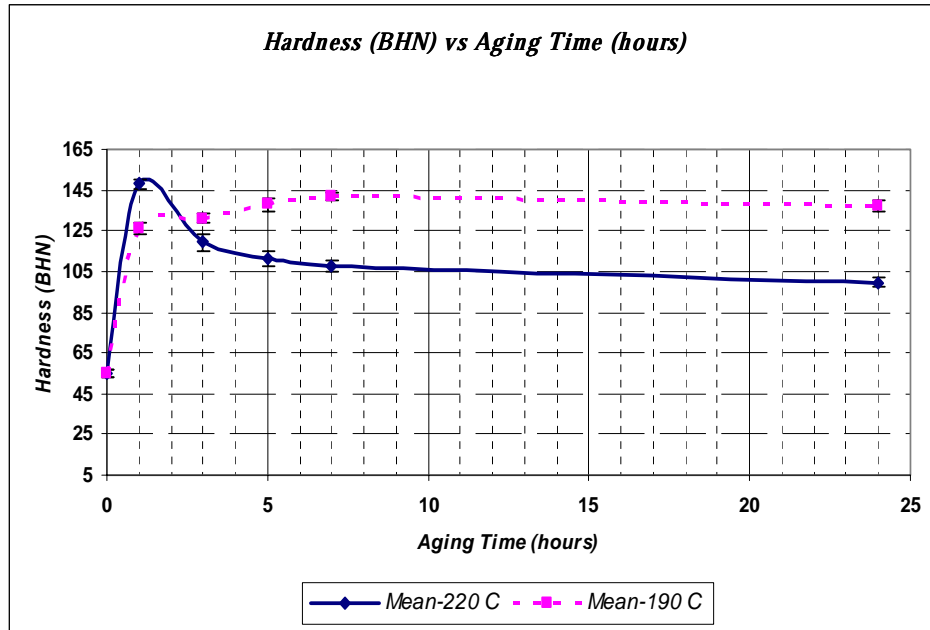


Figure 4.15 Comparison of hardness values of AA 2024 plates after aging at 190 and 220 °C.

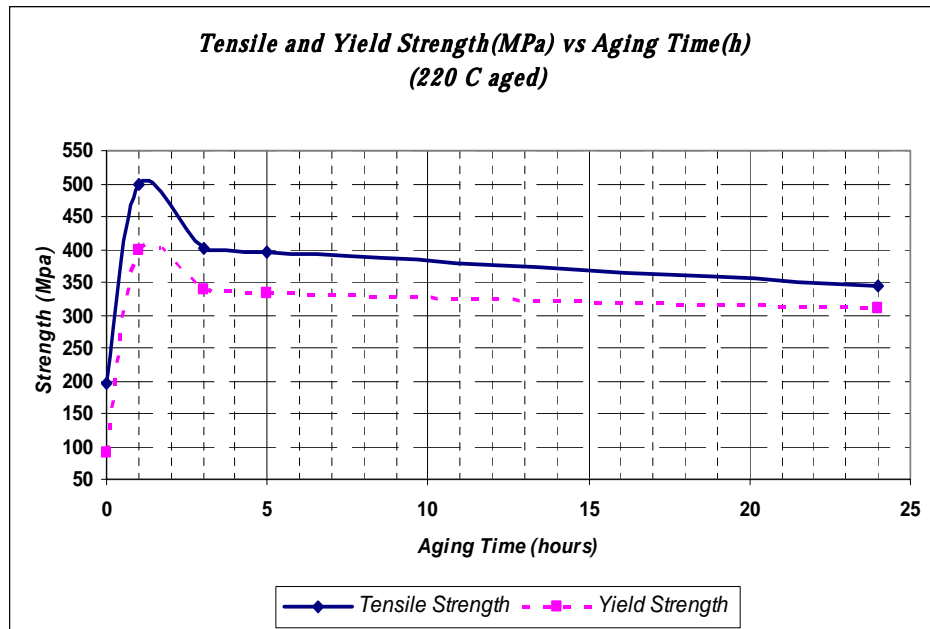


Figure 4.16 Comparison of tensile and yield strength values of AA 2024 plates after aging at 220 °C.

4.4. DYNAMIC MECHANICAL TESTS

4.4.1 Charpy Impact Test

The results obtained from Charpy impact tests are tabulated in **Table 4.6**.

Table 4.6 Impact energy values of AA 2024.

<i>Aging Time</i> <i>(hours)</i> <i>(at 220°C)</i>	<i>Impact Energy</i> <i>(Joules)</i>	<i>STD</i>	<i>Testing Temperature</i> <i>(°C)</i>
0	27	0,49	<i>Room Temp.</i>
1	11	0,40	<i>Room Temp.</i>
3	15	0,40	<i>Room Temp.</i>
5	15	0,49	<i>Room Temp.</i>
24	19	0,40	<i>Room Temp.</i>
5 specimens were tested for each condition.			

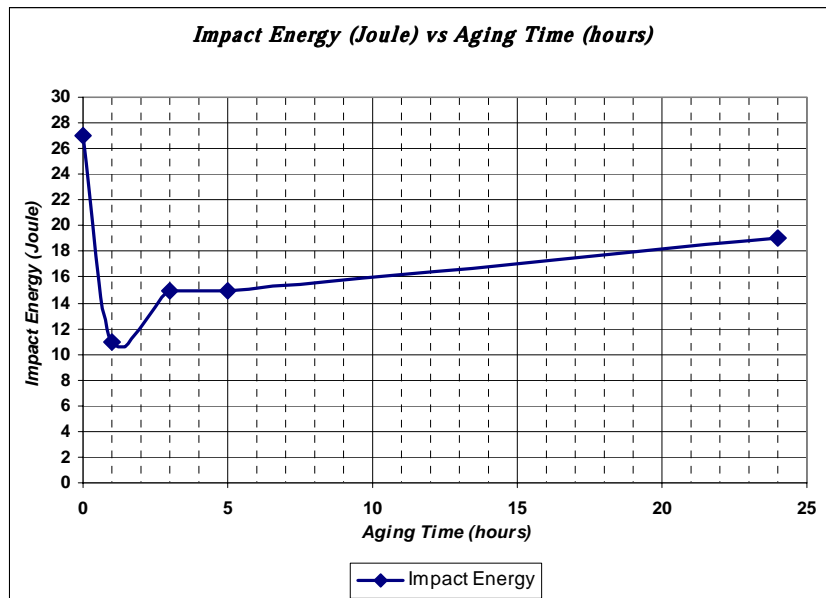


Figure 4.17 Impact energy versus aging time.

4.4.2 Determination of Ballistic Limits of AA 2024 Plates

In this study, drop weight test was used to determine low velocity terminal ballistic properties of AA 2024 plates.

Primary aim of this study, in the sense of drop weight testing, was to find the ballistic limit velocities. Ballistic limit velocities were determined by making iterative shots from different heights until finding the height at which perforation just occurred. This was performed by relating the changes in deformation mechanism to initial geometry rather than the instantaneous geometry. Determined heights are converted to velocities by using calibration chart given in **Figure 3.3**. The bars of the drop-weight testing machine were well lubricated. However, there is a 3 % error [17] due to change in coefficient of friction. This error was carefully considered in every calculation.

After ballistic limit velocity determination, results were connected with those of static and dynamic tests. Following, the graphs were plotted in order to investigate this connection.

Figure 4.18 shows the ballistic limit versus hardness of the plates. This relationship is nearly linear. Ballistic limit increases almost linearly with an increase in hardness within 50 - 150 BHN hardness range. **Figure 4.19** illustrates the behavior of ballistic limit with respect to ultimate tensile strength. It can be seen that with an increase in ultimate tensile strength, ballistic limit increases. The same is true for the yield strength which can be seen from **Figure 4.20**. However, these relationships are not linear as in the case of hardness. Especially, the situation between the yield strength and ballistic limit is quite complex.

The UTS, yield strength and percent elongation data can be converted into “*strain hardening rate*” by using a suitable formula. Strain hardening rate (SHR) of material is defined as:

$$SHR = \frac{UTS(1 + \%EL) - \sigma_y}{\%EL} \dots\dots\dots \text{Equation 4.1}$$

where, UTS is the ultimate tensile strength (MPa) ; %EL is the fractional elongation or %Elongation/100 ; σ_y is the yield strength (MPa) [45] .

Strain hardening rate is an important property. Because, it combines the information about UTS, yield strength and percent elongation. **Figure 4.21** indicates almost a perfect linear behavior between the ballistic limit and strain hardening rate in 2,8 – 3,2 range. Ballistic limit increases almost linearly with an increase in strain hardening rate values.

Besides static mechanical test results, Charpy impact test results were also investigated in relation to ballistic limit values. Ballistic limit decreases with increasing impact energy. The behavior is almost perfectly fitted to second degree polynomial as it can be seen from **Figure 4.22**. This relationship is quite interesting and will be discussed in **Chapter 5**.

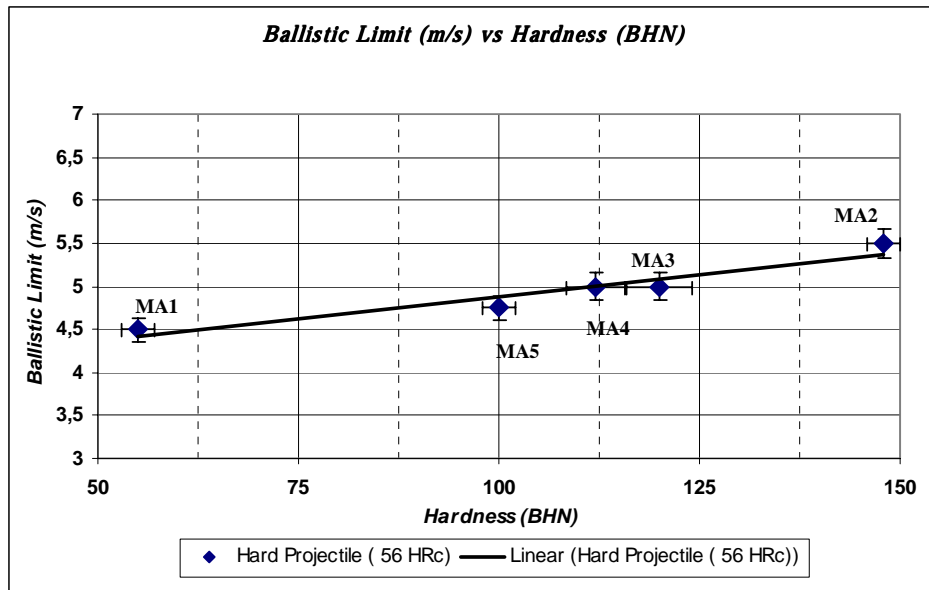


Figure 4.18 The change in ballistic limit of AA 2024 with respect to hardness.

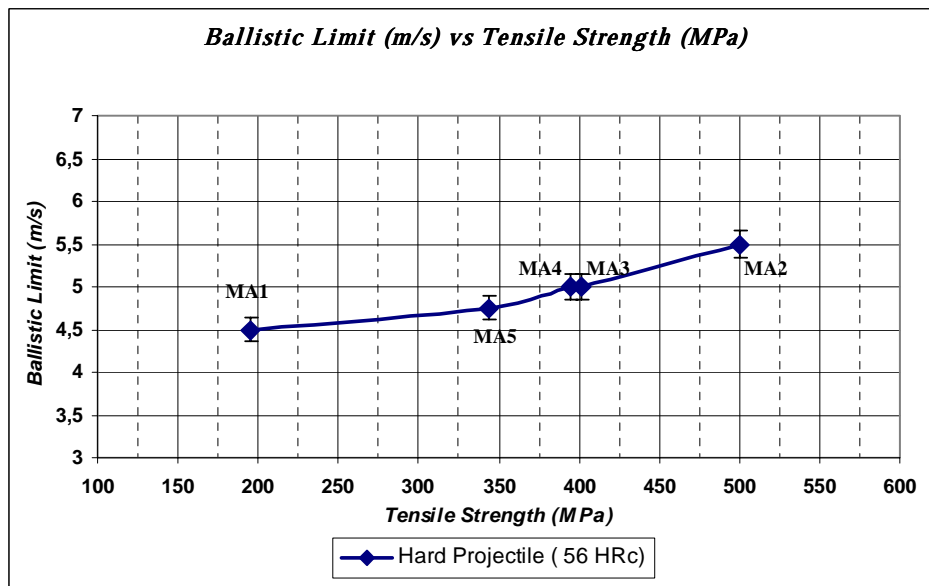


Figure 4.19 The change in ballistic limit of AA 2024 with respect to tensile strength.

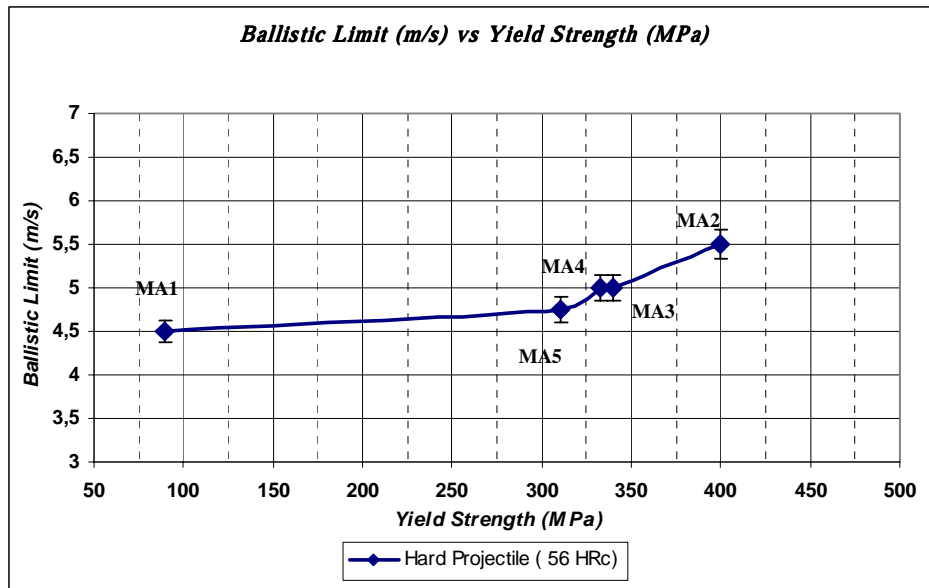


Figure 4.20 The change in ballistic limit of AA 2024 with respect to yield strength

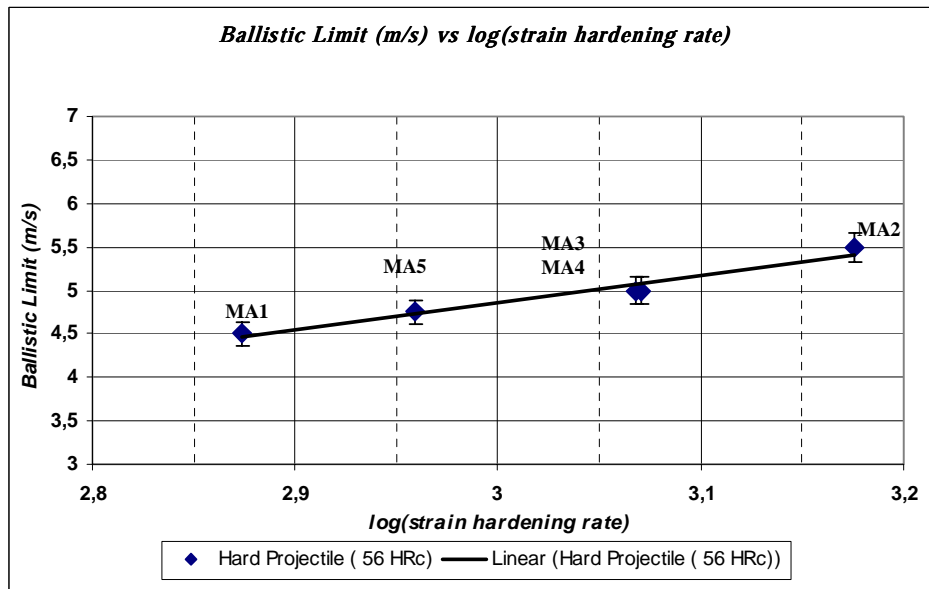


Figure 4.21 The change in ballistic limit of AA 2024 with respect to SHR

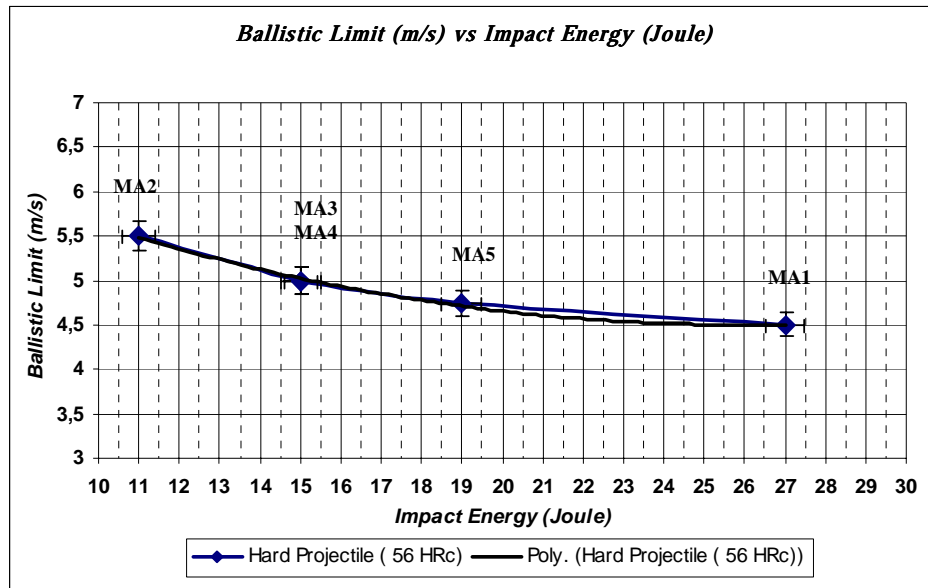


Figure 4.22 The change in ballistic limit of AA 2024 with respect to impact energy.

The thickness of AA 2024 target plates was an important parameter studied in this work. The thickness of a target was increased in two different ways.

- (1) The 2.5 mm thick plates were successively brought together to obtain a total thickness of 2.5, 5.0, 7.5 or 10.0 mm.
- (2) The monolithic 2.5, 5.0, 7.5 or 10.0 mm plates were use.

Figure 4.23 shows the relationship between ballistic limit and target thickness for a monolithic plate. Ballistic limit increases in a linear manner with target thickness. Ballistic limit for 10 mm thick target could not be determined due to the limited capacity of the drop weight test machine.

Figure 4.24 shows the effect of lamination in ballistic limit. Whatever the type of adhesive used between the plates, all the laminated targets yielded very

similar ballistic limit values. Either using a strong epoxy adhesive or bringing the plates loosely together did not affect the results. However, an important result which can be deduced from the graph is that at identical total thickness values, monolithic targets have higher ballistic limits. The ballistic limits of all laminated plates tend to increase linearly with an increase in thickness. However, the slope of this linear relationship is smaller than in the case of monolithic targets as it can be seen from **Figure 4.25**.

Like the monolithic targets, the ballistic limit values for 4-layer targets (10 mm thick), could not be found by using the drop weight testing machine.

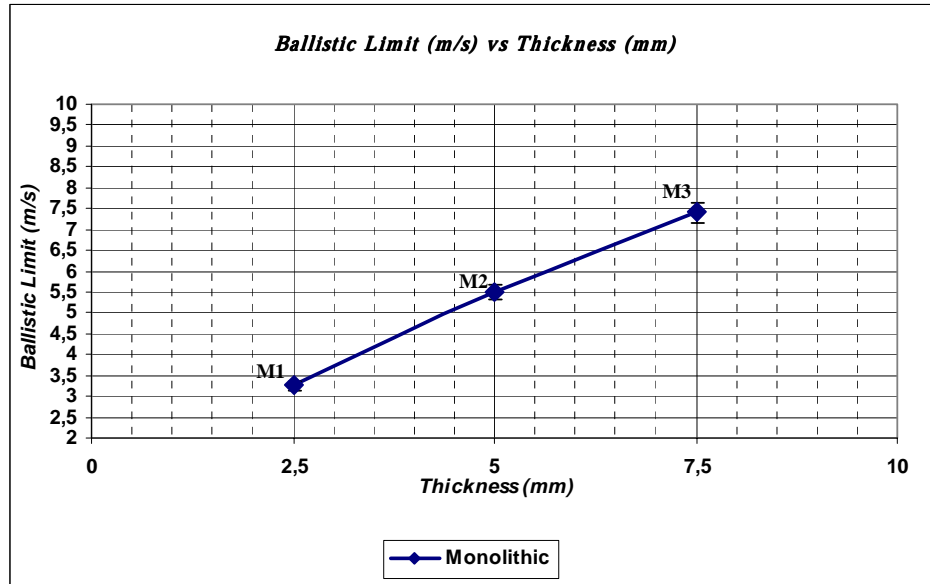


Figure 4.23 Ballistic limit versus Thickness (Monolithic).

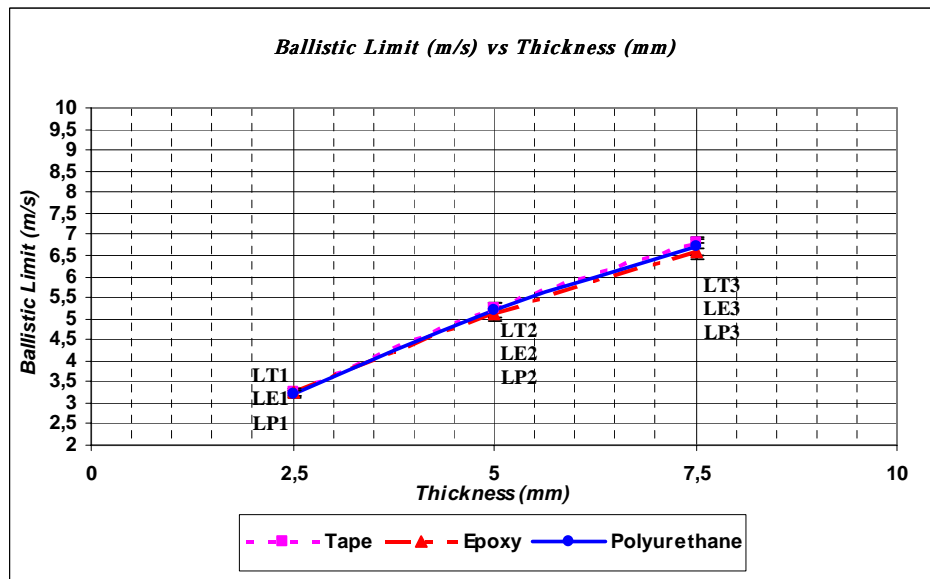


Figure 4.24 Ballistic limit versus Thickness (Laminated).

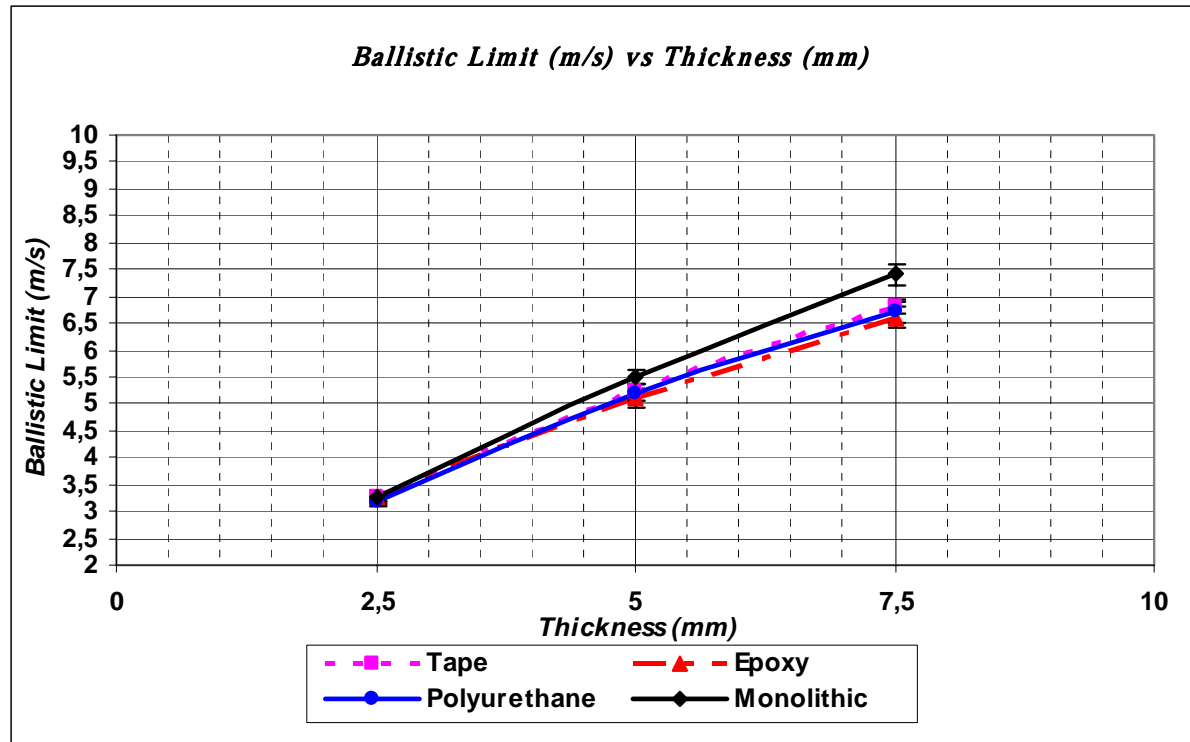


Figure 4.25 Ballistic limit versus Thickness (Both monolithic and laminated).

4.5 MACROSCOPIC INSPECTIONS

In this part of the study, macroscopic inspections of projectile, monolithic and laminated targets were carried out. These investigations gave valuable information about the failure mechanisms of AA 2024 targets tested under drop weight testing machine. In the case of kinetic energy projectiles, the failure mechanisms of drop weight tested targets are quite similar to those of real ballistic tests. Some representative examples of impacted targets were given in the following sections.

4.5.1 Macroscopic Inspection of Projectile

Projectile is one of the very important parameter in terminal ballistic aimed researches. Projectile hardness, density, nose geometry, size are the major criterion effective on ballistic limit velocities of armor targets. During this study, projectile was considered as a non-deformable solid and an 115CrV cold work tool steel penetrator was used. However, due to some maladjustment in drop weight test or metallurgical impurities in steel penetrator, unwanted plastic deformations were taken place. **Figure 4.26** shows, the deformations that can take place after the drop weight test. The results obtained from the buckled (b) and fractured (c) specimens were not considered in the calculations. In order the test to be valid the penetrator should not be plastically deformed.

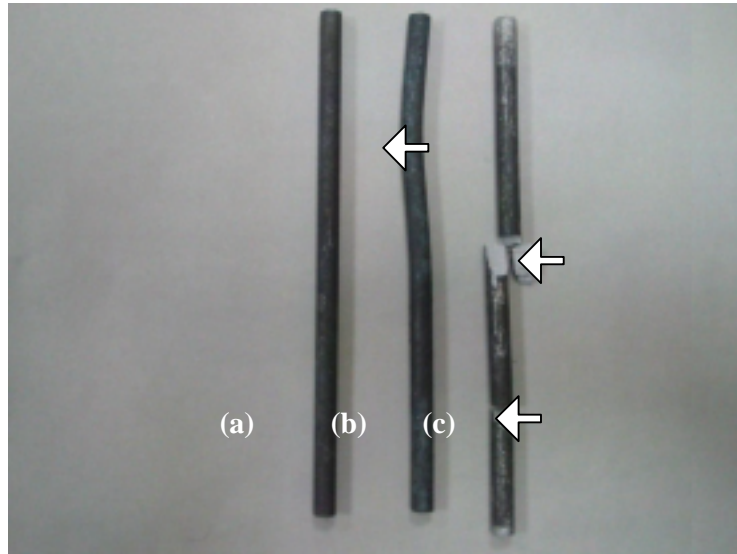


Figure 4.26 Penetrators after the impact (a) In good condition
(b) Buckled
(c) Fractured



Figure 4.27 Ballistic limit reached after an impact. The plug could not be separated.

4.5.2 Macroscopic Inspection of Monolithic Targets

For monolithic targets the leading projectile-target interaction was plugging. A specimen at its ballistic limit is given in **Figure 4.27**. The plate could not be perforated and the plug is still on the specimen. A perforated specimen with its plug can be seen in **Figure 4.29**. **Figure 4.28** shows the section of an AA 2024-O target having 5 mm thickness. Plug is seen at the centre. Front face of the plug where projectile was impacted was relatively flat. However the rear face of the plug was concave. Radial expansion is seen at the rear face of the target. For thin targets (2.5 mm thick), *plugging* type failure was again favored. Another important macroscopic investigation was a slight shortening of the plug thicknesses. All the observed failure mechanisms for monolithic targets impacted by flat-ended projectile were characteristic for a ductile failure of AA 2024 aluminum alloy.

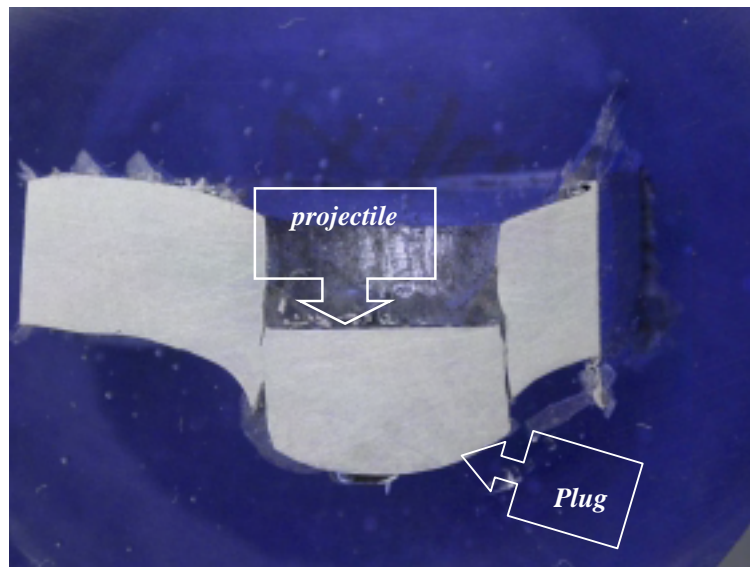


Figure 4.28 Sectioned AA 2024-O target after impact.
Plugging type failure with some radial expansion.

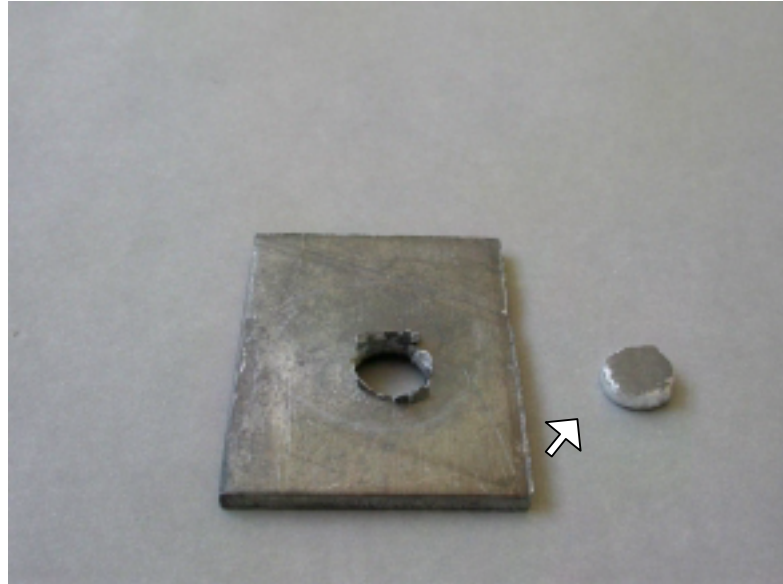


Figure 4.29 Front face of AA 2024-T6 with 2.5 mm thickness.
Plugging type failure.

4.5.3 Macroscopic Inspection of Laminated Targets

AA 2024-T6 having 2.5 mm thickness was used to form laminated composites. Three different types of adhesive were used.

- (1) Several laminates were loosely held by adhesive tapes from the edges,
- (2) An epoxy adhesive was applied between the plates.
- (3) A polyurethane adhesive was applied between the plates.

After the macroscopic investigation of epoxy and polyurethane adhered targets impacted under drop weight testing machine, it was observed that almost 90 % of targets that were adhered with epoxy were delaminated, that is, the laminates were separated from each other. It is interesting to note that none of targets adhered with polyurethane were delaminated.

When the mechanism of the failure was investigated, *plugging* type deformation was seen for the layer 1 (The notation for layers can be seen in **Figure 4.30**). For layers 2, 3 and 4, firstly *bending* was observed. As the kinetic energy of the projectile increased, a *dishing* type failure was favored for these layers. **Figure 4.31** shows a 2-layer target held with a tape. At the first layer at which projectile was impacted, a plug formation was seen. At the rear layer, again a plug formation was seen. However, in this case plug is elliptical in shape and its size is bigger than the plug formed at the front layer. **Figure 4.32a** shows a 10 mm monolithic target after impact. No perforation or ballistic limit could be obtained under drop weight test machine. Similarly, in 4-layer target, perforation and ballistic limit values could not be obtained again under drop weight test. When the test was conducted for 4-layer targets, a plug formation was seen in the first layer, and for other layers extensive bending and bulging were observed as in **Figure 4.32b**.

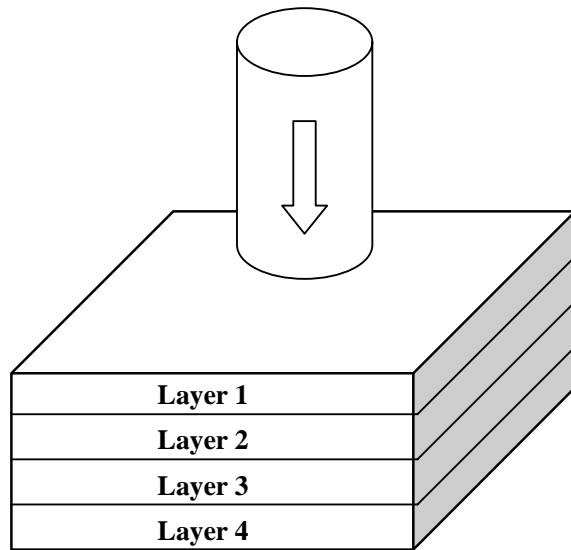


Figure 4.30 Notation of layers with respect to impact side.

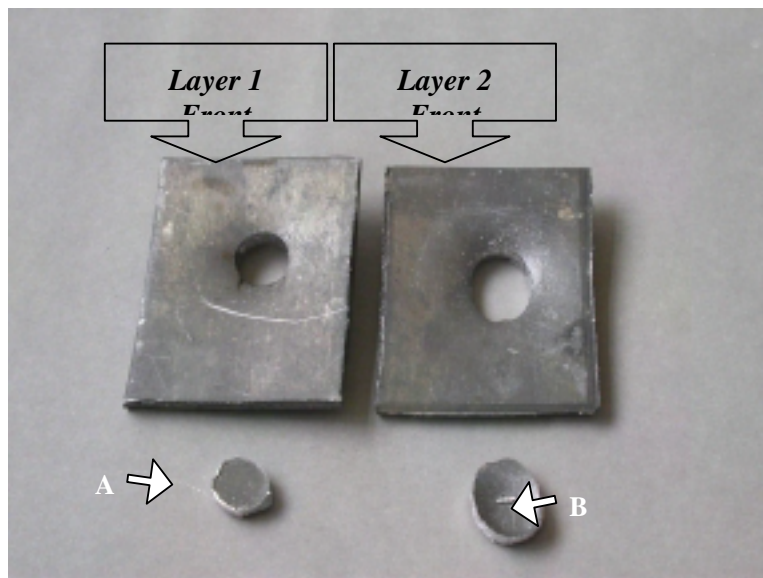
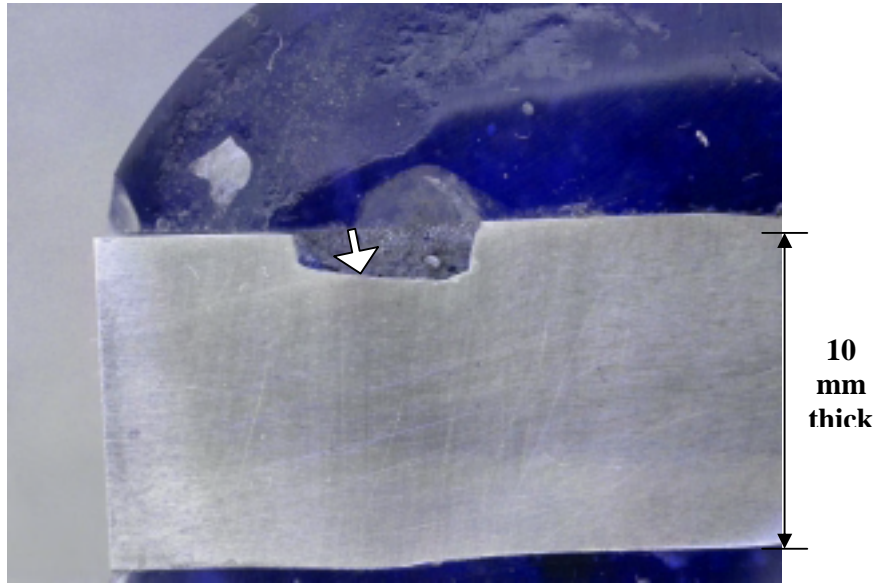
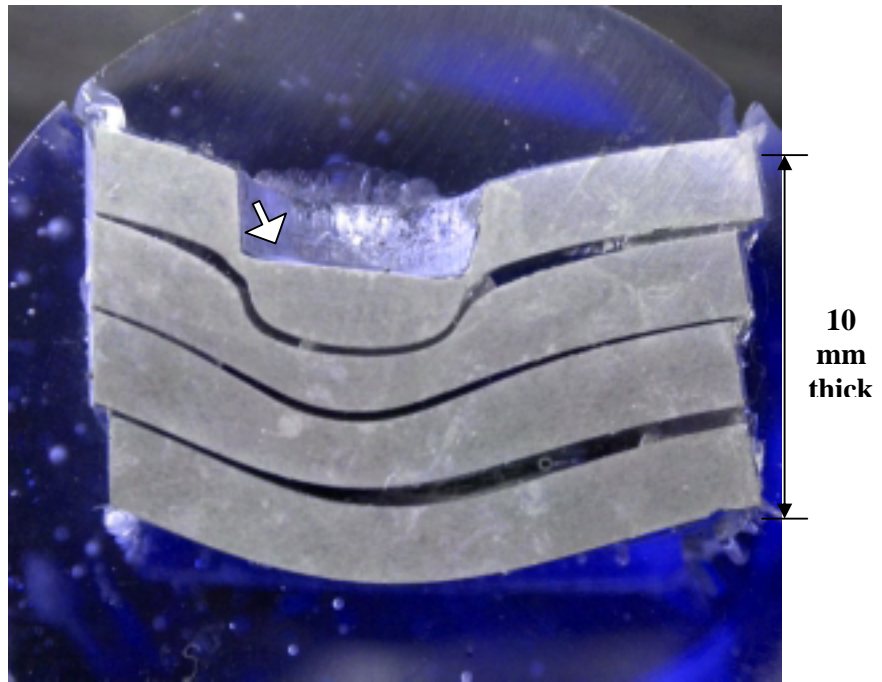


Figure 4.31 Two layers AA 2024-T6 after impact.
Plug B is in elliptical shape.



(a)



(b)

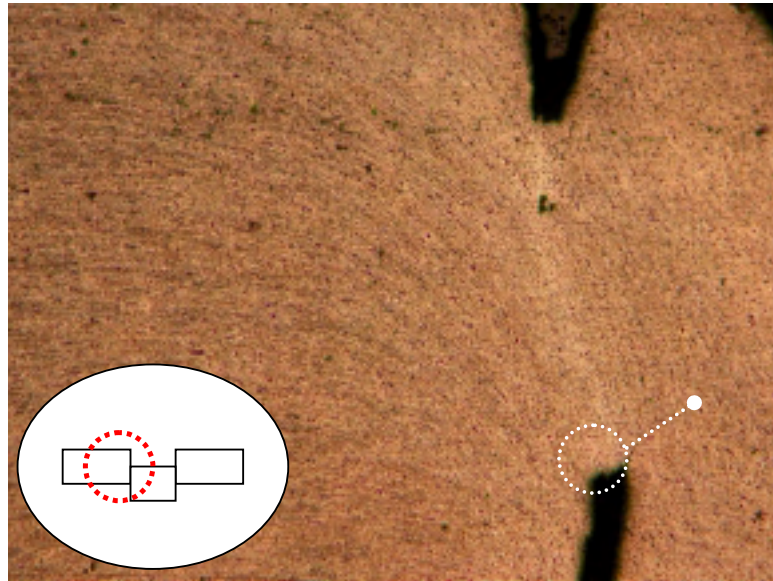
Figure 4.32 The sectioned view of an impacted 10 mm thick (a) Monolithic and (b) Layered target. In both cases perforation could not be achieved.

4.6. MICROSCOPIC INSPECTIONS

Failure mechanisms occurred in terminal ballistic studies are highly dependent on microstructure. Therefore, a microstructural analysis was performed for both monolithic and laminated targets. For this analysis, a set of perforated and penetrated AA 2024 targets were prepared. Perforated samples gave very few information about failure mechanism as cracks were already propagated and resulted in failure. In order to perform micro examinations, representative samples were selected and sectioned. Inspections were carried out under an optical microscope at different magnifications. The regions close to deformation zones were examined.

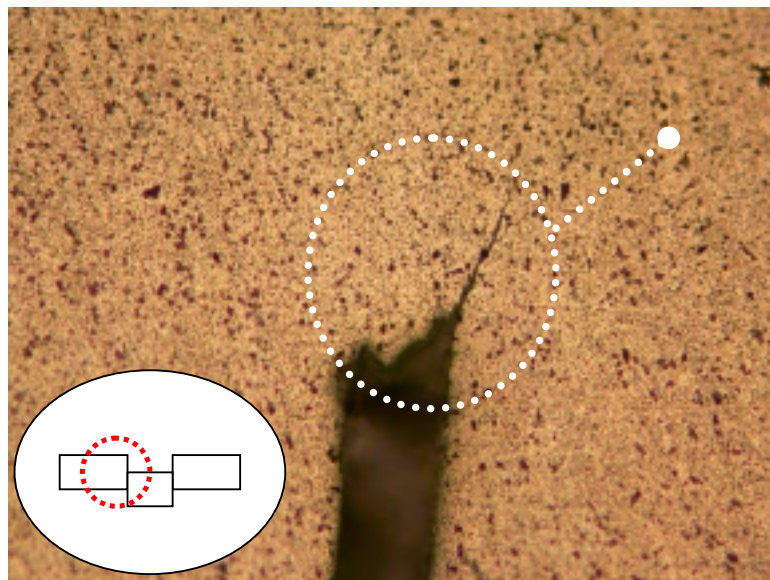
In macro examination, it was seen that for monolithic targets tested under drop weight, the principal dynamic deformation process is plugging. In plugging type deformation process, shear bands play a very important role. The formation of shear bands establishes the shear failure path. Some representative examples of micro examined zones are as follow.

Figure 4.33 shows the sectioned zone between the plug and the target. This was an AA 2024-O target impacted nearly by its ballistic limit velocity. Shear bands can not be resolved but shear localization zone can be seen clearly. Impacting with a blunt tip projectile resulted in formation of these shear localization zones due to imposed strain concentration at the projectile edges. The large dark points are most probably voids causing failure. One very large void is seen just between the plug and the target. Another very interesting object is a crack formed, which is shown in **Figure 4.33a**. This crack was formed due to shear forces and will probably propagate in a path including these voids spending minimum energy. **Figure 4.33b** shows the view of this crack at higher magnification. The propagation path is easily seen from the figure.



50 X

(a)



200 X

(b)

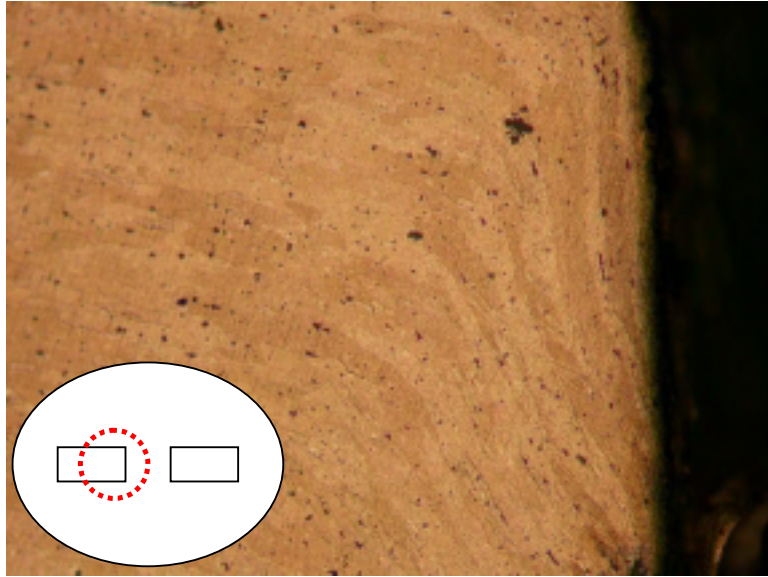
Figure 4.33 (a) The sectioned view of an impacted AA 2024-O plate (50X)

(b) The crack propagation at a higher magnification (200X)

Figure 4.33 is an example for annealed AA 2024 targets. **Figure 4.34** shows the microstructure of an aged AA 2024 target perforated by a blunt tip projectile. Its microstructure is a little bit different from annealed one. Shearing of grains is easily seen at the intense shear zone.

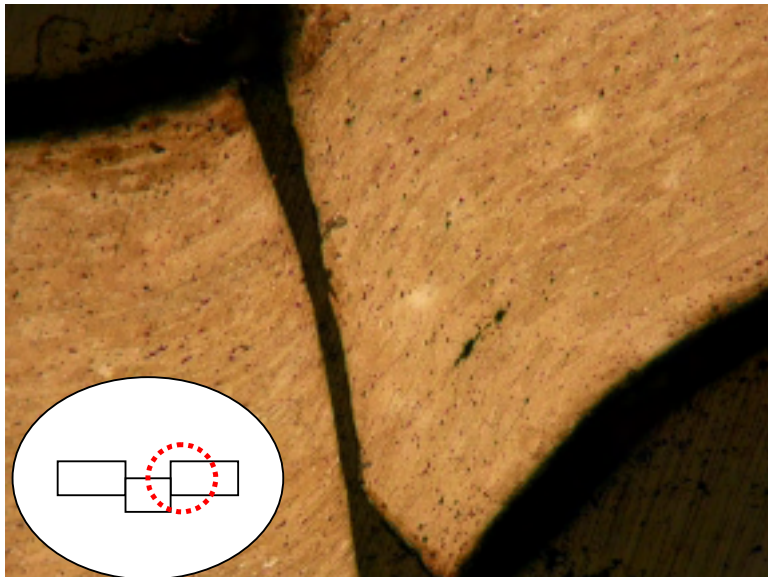
Figure 4.35 shows the microstructure of an aged AA 2024 target at its ballistic limit. Plug is located at the left side of the figure. Grains in the target were sheared parallel to the deformation direction.

Figure 4.36 and **Figure 4.37** shows the microstructure of a laminated AA 2024-T6 target. **Figure 4.37** shows the layer number 1 at which the blunt projectile was impacted. There is a large amount of plastic deformation in the target. Intense shear localization is clearly seen in **Figure 4.36**. This shear localization is a precursor to fracture and indicates plugging type failure. **Figure 4.37** shows the rear layer number 2 and the plug interaction. In the rear layer a shear localization zone is not seen but the structure is slightly bended. This bended structure may cause a dishing type of failure by tensile stretching at high stress level. A further discussion will be carried out in detail in **Chapter 5**.



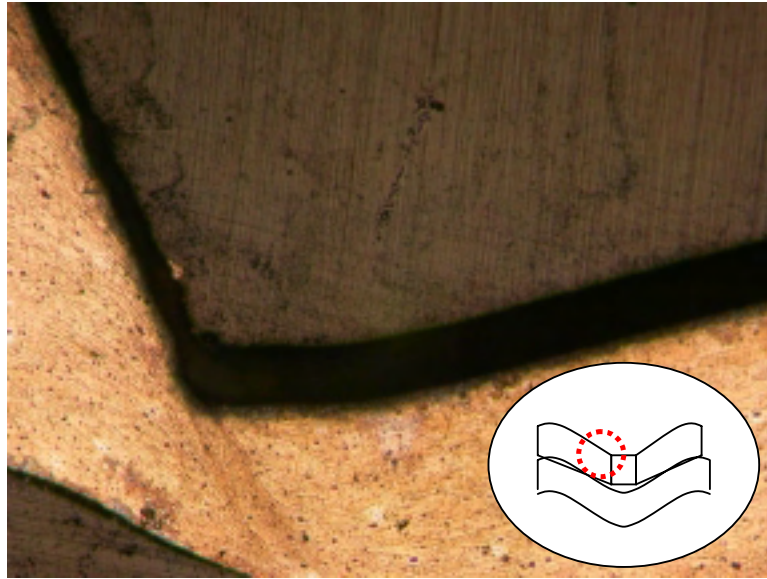
200 X

Figure 4.34 AA 2024-T6 plates. Intense Shear Zone (200X)



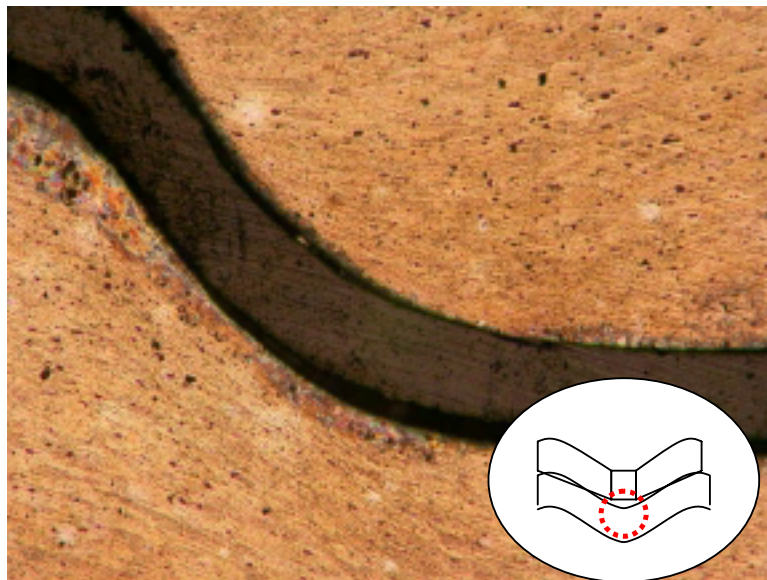
100 X

Figure 4.35 AA 2024-T6 plates and plug. Shear and Compression Zone (100X)



100 X

Figure 4.36 AA 2024-T6 laminated plate. (Front Faces) (100X)



100 X

Figure 4.37 AA 2024-T6 laminated plate. (Plug and Rear Faces) (100X)

CHAPTER 5

DISCUSSION

There are three major categories related to the impact velocity of the projectile. Namely, these are low-velocity impact, subordnance-ordnance velocity regime and high-velocity impact [46]. In this study, a drop-weight test apparatus was used in order to perform low velocity impact tests on AA 2024 plates. An 8 mm diameter non deformable blunt tip steel rod was attached to a hammer weighing 8 kg. The hammer could be dropped from any height, therefore a velocity regime between 0 to 8 m/s is available with a 3% error in velocity.

Penetration and perforation through the metal targets are known as a complex problem, both from experimental, analytical and numerical point of view. Even only for the penetration and perforation of targets by kinetic energy projectiles Backman and Goldsmith [6] identified eight possible perforation mechanisms for brittle and ductile targets in a range of target thickness. Also more than one perforation mechanism may lead under impact loading. Therefore, in this chapter firstly, investigated failure mechanisms for monolithic and laminated targets will be discussed. Secondly, some of the important material properties affecting the ballistic performance will be argued and experimental results will be compared with analytical models present in the literature.

5.1 FAILURE MECHANISMS

In a penetration and perforation process different types of failure may be seen. These failures are due to the interaction of a variety of mechanisms with one predominating, depending on material properties, geometric characteristics, and impact velocity. The most frequent types consists of fracture resulting from the initial compression wave, fracture in radial direction, spalling, scabbing, plugging, front or rear petaling, or fragmentation in the case of brittle targets and ductile hole enlargement [6].

Blunt projectiles normally cause failure by shear plugging [6, 10, 46]. However, for a blunt projectile, shear plugging is not only failure mode to dominate the perforation of a metallic plate. Dishing may also be formed for a thin plate subjected to a low velocity impact, which eventually leads to a tensile failure [10, 47]. In this study, plugging type failure was observed for thick monolithic plates. On the other hand, plugging followed dishing failure mixed mode was seen for laminated thin plates. For either two –or three- layered laminates, the first layer is seen to fail by pure shear. However, the second and third layers were bended and tensile fracture dominated the failure, which is typical for dishing type of failure. The failure modes encountered during this study were summarized in **Figure 5.1**.

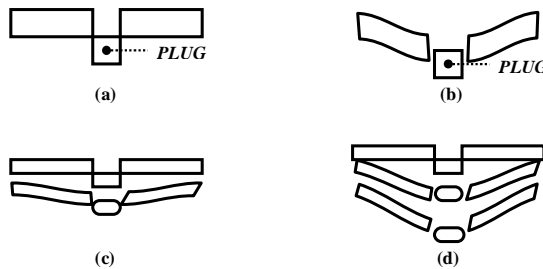


Figure 5.1 Schematic views of failure mechanisms investigated (a) Plugging type failure without bending for monolithic plates (b) Plugging type failure with large amount of bending for monolithic plates (c) Plugging and dishing type failure for two layers plates (d) Plugging and dishing type failure for three layers plates

5.1.1 Failure Mechanisms in Monolithic Targets

A series of 5 mm thick AA 2024 targets were tested for failure mechanisms investigations. Two different types of failure were dominated. Shear plugging was the dominating failure mechanism in age hardened AA 2024 species. **Figure 4.27** and **4.29** shows the plug formation in AA 2024-T6 plates with 5 mm and 2.5 mm thickness respectively. This is totally in agreement with the results obtained in this study. On the other hand, for the ductile plates in annealed condition like in case of MA1, some plastic deformation in the form of bending or radial expansion around the plug crater was analyzed (**Figure 4.28**).

The failure of AA 2024 monolithic plates having different thicknesses and strengths, with a blunt non-deformable projectile can be considered as a multi-stage event [10, 48 - 51]. These multi-stages are involved elements of target compression and acceleration followed by the ejection of a plug by shear deformation of fracture [10, 52, 53].

If the force required to indent the target is less than the resistance of the plug to forward movement by shear, then indentation and compression of the target material occurs initially [10]. **Figure 4.32a** shows the case in which the blunt tip non deformable projectile caused the indentation of the 10 mm thick monolithic target. Target resisted forming a plug under a velocity of 8 m/s and only indentation took place.

When the force to achieve forward movement of target plug is less than the force to indent the target, then indentation ceases. At this point it is necessary to consider how exit-side failure of the target may occur. Two alternative failure modes are considered either:

- (1) Ejection of a plug by shearing or,
- (2) Dishing failure [10].

In this study shear plugging was the dominating failure mechanism for monolithic targets. Due to the high relative velocity between the accelerated material in front of the projectile and the rest of target, the deformation localizes in narrow shear bands.

In these localized zones, very large strains, strain rates and temperature appear, causing material damage [46]. A similar behavior was also observed in this study, in which shear localizations were obvious in impacted AA 2024 plates (**Figure 4.33** to **Figure 4.35**).

Figure 4.33a is regenerated in **Figure 5.2** in which shear localization is marked. For the penetration of a target by a projectile, the formation of a shear concentration alters the defeat mechanism. If no shear bands are formed, one has a better distributed plastic deformation. The formation of the shear bands establishes the shear failure path and is responsible from the clean “plugging” of the target [53]. A similar behavior was also observed in this study, in which shear localizations were observed in impacted AA 2024 plates (**Figure 4.34** to **Figure 4.35**). When the strains especially localized at the edge of the blunt projectile reaches a critical value, a crack starts to grow towards the rear side of the target, and a plug is finally formed. **Figure 5.1a** and **5.1b** illustrate schematically the failure mechanisms observed for homogeneous AA 2024 plates in T6 and annealed condition. **Figure 5.3** and **Figure 5.4** show the stress modes developed in these plates. It can be stated that the microstructural observations in this study are all in agreement with the schematic drawing given in **Figure 5.3** and **Figure 5.4**.

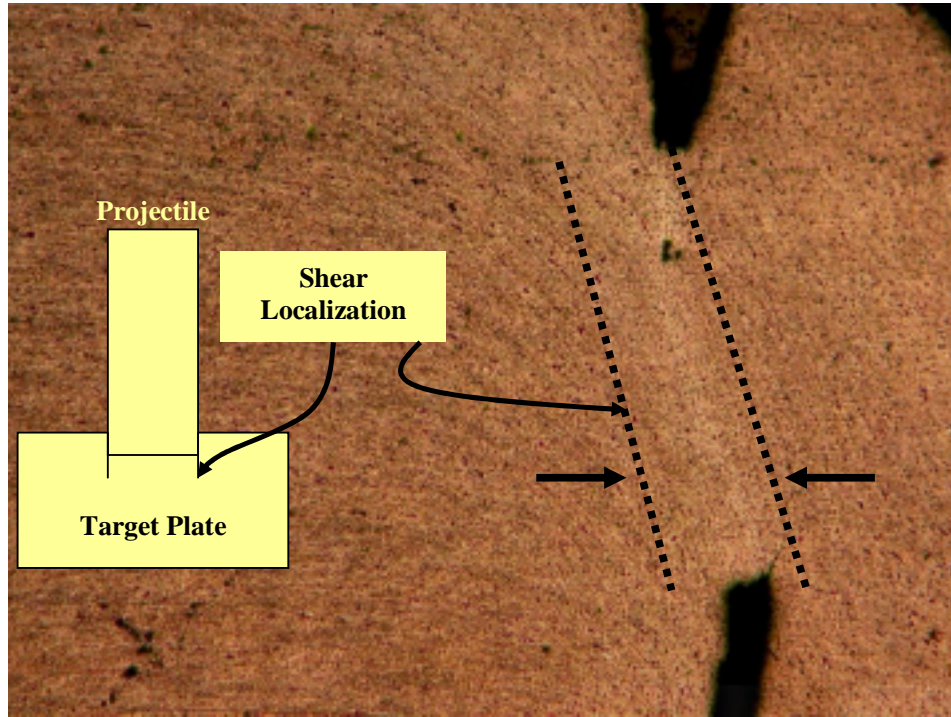


Figure 5.2 Shear localization

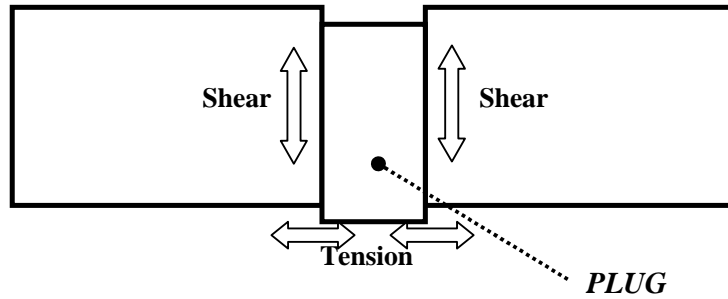


Figure 5.3 Schematic view of failure mechanisms by pure shear plugging [10].

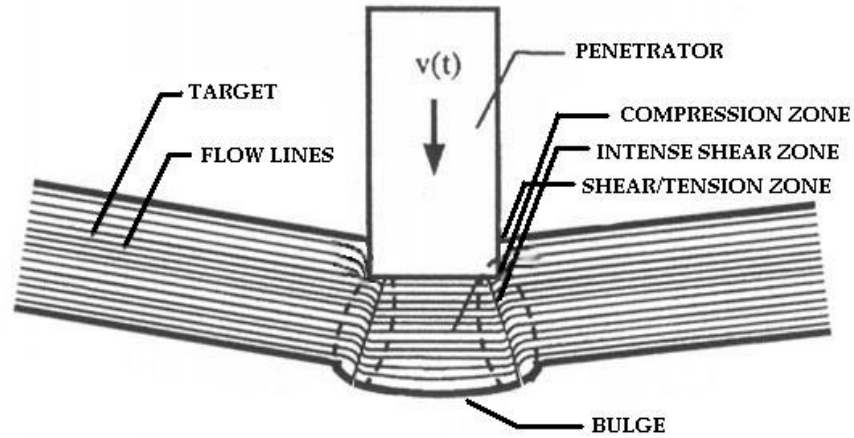


Figure 5.4 Schematic view of failure mechanisms by bending and plugging [55].

5.1.2 Failure Mechanisms in Laminated Targets

Three series of laminated AA 2024 were constructed by using epoxy, polyurethane and tape type adhesives. Both series consist of 2.5, 5.0, 7.5 and 10.0 mm thick targets constructed from 2.5 mm thick AA 2024-T6 plates. Although different types of adhesives were used, the failure mechanisms were identical. A schematic drawing of failure mechanisms for 2 and 3 layer composites were given in **Figure 5.1c** and **5.1d**.

In the front layer 1 of the laminated composites where the penetrator is first interacted, a shear plugging was seen (**Figure 4.31** and **Figure 4.32b**). This was actually what expected. However, the mode of failure for second, third and fourth layers were quite different. Again a plug was formed from these layers. However the size and shape of these plugs were different from that of the first layer. The sizes of the plugs belonging to rear plates were bigger than those of the front layers. In addition they were in elliptical shape that longer diameter in the rolling direction of the target. Moreover, as it can be seen from **Figure 4.32b**, a large amount of bending and stretching were occurred in the second, third and fourth layers unlike the first one. This type of failure is most probably a *dishing* type failure. Same type

of failures have been reported by Woodward and Cimpoeru [10] and Levy and Goldsmith [56] for thin aluminum targets impacted by hardened steel projectiles of a variety of diameters and nose shape.

The reason for the differences in the failure mechanisms between the front layer and rear layers may actually be the change in nose shape of the impact rod. On the front layer a blunt tip non-deformable projectile was impacted. However, the second layer was impacted by a plug in hemi-spherical shape rather than the impact rod. Deformation mechanisms as indicated in **Chapter 2** are highly dependent on projectile nose geometry.

The localized intense shear zones in the target are characteristic for blunt projectiles. For blunt projectiles flow lines running parallel to the surface of the target as a result of the manufacturing process are cut straight off and hardly distorted near the impact surface. As the material in front of the projectile starts to move, the flow lines indicate intense shear inside localized bands, while limited bending is seen outside the bands. Once the deformation localizes, the material is constrained to flow in the direction of the moving projectile [46].

On the other hand, bulging and dishing in the target is typical for hemispherical projectiles. When a hemispherical projectile impacts the target, the flow lines deflect and the material flows up to form a frontal bulge. However, this stage is rapidly overcome and the flow changes direction towards the rear side as the projectile indents the target. As the indentation continues, the material in front of the projectile stretches and bends, giving parallel and dense flow lines. This results in a region of intense tensile strain, where failure finally is initiated due to necking [46]. In this study although a blunt tip projectile impacted laminated targets, actually it is the hemispherical plug which indents the rear layers. Therefore, the results obtained from laminated targets seem to be in accordance with dishing type failure originated from a hemispherical projectile.

The plastic flow during the penetration process is further illustrated in micrographs given in **Figure 5.5**. In **Figure 5.5a**, a sharp and distinct indentation was clearly seen for 10 mm thick monolithic AA 2024-T6. A tiny crack prior to plug formation was formed and most probably will propagate through the localized shear zone. **Figure 5.5b** shows stretching and bending of second layer of laminated composites due to hemispherical shape of the plug indentation. The mode of plugging for the layer 2 is most probably necking and tensile type failure.

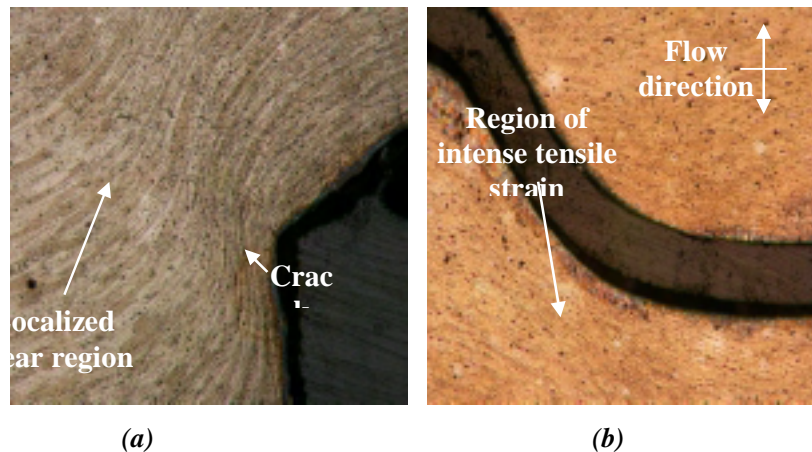


Figure 5.5 Micrographs of (a) monolithic and (b) laminated targets close to perforation (not in scale)

5.1.3 Effects of Artificial Aging on Failure Mechanisms

In this study a subsequently artificial aging was performed in order to change the mechanical properties of AA 2024 targets. Significantly, yield strengths of these plates were increased from 90 MPa to 400 MPa. However, not only the mechanical properties but also the failure mechanism was slightly changed. For annealed targets having yield strength of 90 MPa, shear plugging was formed by radial expansion and bending to some degree due to the large amount of ductility in annealed condition. In contrast, for aged specimens, almost pure shear plugging was observed and ballistic limit velocities were increased.

Artificial aging resulted in an increase in ballistic limit velocity which has vital importance in terminal ballistic. However, if aging were not done correctly it would end with catastrophic results. **Figure 4.3** and **Figure 4.4** shows AA 2024-T6

samples which were not properly solution heat treated. Due to that eutectic melting occurred during solutionizing AA 2024 plates behave like a brittle material (**Figure 5.6**).



Figure 5.6 AA 2024 target solution heat treated at 540°C impacted under drop-weight test machine

5.2 FACTORS AFFECTING BALLISTIC PERFORMANCE

Structural impact, due to excess number of physical parameters involved that may cause highly non-linear and sometimes unexpected structural behavior, is a very complex problem. In terminal ballistic, physical parameters are mostly projectile, impact and target related [57]. These parameters can broadly be classified as:

- 1) **Projectile related:** Projectile size, geometry, density, hardness, etc.
- 2) **Impact related:** Impact velocity and angle.
- 3) **Target related:** Hardness, tensile strength, yield strength, toughness, ductility, microstructure, thickness, and lamination.

In a more detailed analysis, the number of these factors increases. As an example, Baker et al. [58] identified nearly 30 possible and relevant input parameters in the general problem of metal plates. Fortunately, several of those parameters are problem-dependent and can be neglected in certain situation [57].

In this study, projectile related parameters like projectile size, nose geometry, density and hardness were keep constant. The only variable impact related parameter was the impact velocity. Impact angle was also fixed. In contrast, this study was concentrated on the target related parameters. The effect of hardness, tensile and yield strength, strain hardening rate, Charpy impact energy, thickness and lamination effects on ballistic performance of AA 2024 target plates were investigated.

5.2.1 Effect of Hardness

Hardness which can be described as the measure of a material's resistance to deformation by surface indentation is one of the major property as far as the ballistic performance is concerned. This is because of the fact that the projectile contacts with the surface of the target prior to indent in the case of kinetic energy projectiles. Therefore, increase in the hardness means higher resistance to indentation [59, 60]. However, it is also pointed out that after reaching a certain level of hardness, ballistic performance is getting worse. This behavior can be explained by formation and propagation of adiabatic shear bands at high velocity impacts.

When the force to achieve forward movement of target plug is less than the force to indent the target, indentation ceases [10] and plugging or dishing start to occur depending on the nose geometry or target size and strength. Therefore, as the hardness of AA 2024 targets increase, the initiation of plugging or dishing would become harder so ballistic limit velocities should increase. As shown in **Figure 4.18**, the results obtained in this study support this claim, such that the ballistic limit velocities tend to increase linearly with increasing hardness in the range of 50-150 BHN.

In conclusion, whether failures occurred by pure shear plugging or plugging with some radial expansion and bending ballistic limit velocities increase linearly with hardness.

5.2.2 Effect of Tensile and Yield Strength

Tensile and yield strengths are the major static mechanical properties of the target elements. Their relationship with ballistic properties is very important because of two reasons. First one is the fact that the availability of static mechanical properties. By conventional tensile testing static mechanical properties can be easily obtained. Secondly by applying different aging treatments, tensile and yield strength can be further improved.

As seen in **Figure 4.19**, ballistic limit velocities increase with an increase in tensile strength within range of 150-500 MPa. Similarly, in the range of 90-400 MPa ballistic limit velocities tend to increase with yield strength as illustrated in **Figure 4.20**. The increase in ballistic limit values with strength can be explained by resistance to plastic deformation as strength increases. As stated in section 5.1.1, when the targets were impacted with a blunt tip projectile, the material in front of the projectile started to move, until a plug form. If the yield strength of the material increases, this movement becomes harder due to increase in shear strength. Moreover, as indicated in **Figure 5.3**, towards the rear side the flow lines are severely stretched, indicating the presence of tensile stress in the bulge. At this stage, tensile strength becomes important to prevent this stretching.

As a concluding remark, it can be stated that the ballistic limit of AA 2024 increases with an increase in both tensile and yield strength. However the relationship is not linear, but rather complex. The reason may be the slight change in failure mode from MA1 to MA2. As indicated before, besides plugging, bending up to some degree was also observed in MA1. Whereas for MA2 to MA5 almost a pure shear plugging was observed. This effect can be seen from **Figure 4.19** and **Figure 4.20**. For aged targets, whose deformation modes are pure shear plugging (MA2 to MA5), ballistic limit velocities tend to increase linearly with strength values.

Yield strength is also widely used in constructing analytical models. Analytical models give good results in several conditions. However, they greatly depend on failure mode. Ideally, a combination of simple analytical models that quantitatively describes a wide range of failure modes is desired [10]. Unfortunately, ductile and shear fracture processes, especially in combination with such complex laminate geometries, are poorly understood. Moreover, the number of analytical models giving ballistic limit velocities is very limited. Chen and Li proposed an analytical model involving yield strength and density as a material property of targets [61].

In this model assuming that the plug is cylindrical with same diameter as projectile, ballistic limit of flat-nosed projectiles impacting on thick target plates can be determined as follows:

$$V_{BL}^2 = \frac{A\sigma_y}{B\rho} \left\{ \left[1 + \frac{8B\chi\eta}{A\sqrt{3}} \left(1 + \frac{Hp}{H} \eta \left(\frac{Hp}{H} \right)^2 \right) \right] \exp \left[2\eta B \left(1 - \frac{Hp}{H} \right) \right] - 1 \right\} \dots \text{Equation 5.1}$$

where A and B are dimensionless material constants of target materials, in which A is given by

$$A = \frac{2}{3} \left\{ 1 + \ln \left[\frac{E}{3(1-\gamma)\sigma_y} \right] \right\} \dots \dots \dots \text{Equation 5.1a}$$

where γ is Poisson's ratio and $B = 1.5$ for incompressible materials. σ_y is the yield strength of the target. H and H_p are the thicknesses of the target plate and plug respectively. χ is dimensionless thickness of the plate (ratio of plate thickness and projectile diameter) and η is the ratio of the plug mass to the projectile mass. Since, the model assumes that the plug is cylindrical with same diameter as projectile, η can be expressed as

$$\eta = \frac{\rho H \pi d^2}{4M} \dots \dots \dots \text{Equation 5.1b}$$

where ρ is the density of the target material, d is projectile diameter and M is mass of the projectile.

This analysis proposed by Chen and Li is actually a two stage model, i.e., penetration/indentation and shear plugging. It is assumed that a central plug is formed beneath the projectile at a critical condition when the compressive force on the projectile nose reaches the fully plastic shear force on the plug. As soon as the plug is formed, it moves with the projectile under the constant shear resistance.

During this study, it was observed that for the 5 mm thick targets, the thicknesses of the plugs were slightly smaller than the original target thicknesses, which shows an indentation occurred prior to plugging. Therefore, the model of Chen and Li is suitable to apply to experimental data as the model was constructed on the basis of a two stage model, i.e., penetration/indentation and shear plugging. Experimental parameters and constants used in **Equation 5.1** are summarized in **Table 5.1**.

When this model is applied for AA 2024 targets tested in this study, the plot in **Figure 5.7** is obtained. The dashed line indicates the model of Chen and Li.

Table 5.1 Experimental parameters used in **Equation 5.1**.

Parameters	Values
σ_y (MPa)	300 to 450
ρ^\dagger (g/cm ³)	2.77
M (g)	8000
H_p (mm)	4,8
H (mm)	5,0
d (mm)	8,0
γ^\dagger	0,33
[†] These values are taken from ASM specialty handbook of “Aluminum and Aluminum Alloys” [19].	

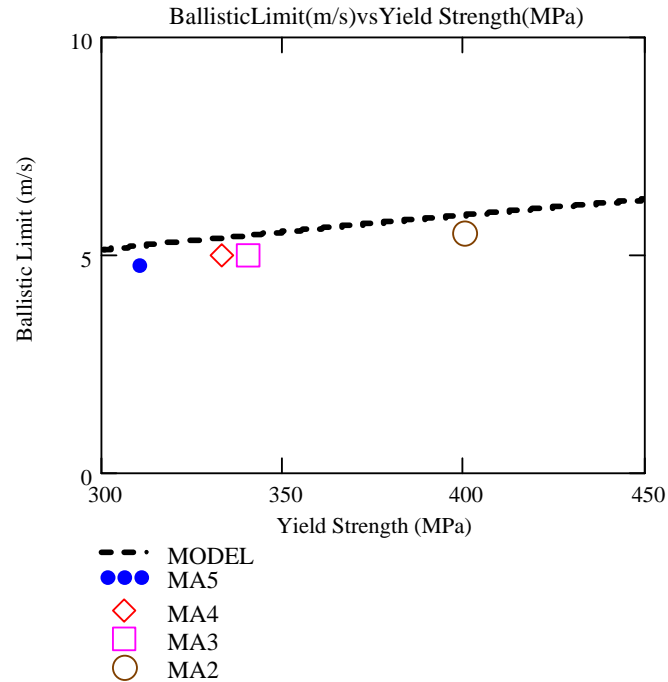


Figure 5.7 Comparison of experimental results with analytical model of Chen and Li [61]

Table 5.2 Comparison of experimental results with analytical model of Chen and Li [61]

Target	Ballistic Limit(m/s) -Experimental-	Ballistic Limit(m/s) -Analytical-	Percent Error %
MA2	5,50	5,90	7
MA3	5,0	5,44	9
MA4	5,0	5,38	8
MA5	4,75	5,19	9

As it can be seen from the **Figure 5.6**, the experimental results are in good agreement with those of analytical results proposed by Chen and Li. There is an approximately 8% error between the analytical and experimental results as it is indicated in **Table 5.1**. MA1 was not compared with this analytical model. The reason is the excess amount of bending occurred for the target MA1. This model

constructed on the basis of indentation and shear plugging was happened, however in the case of perforation of MA1 some extra energy was consumed in the bending of target. Due to several assumptions [61] the ballistic limit values obtained from this analytical model are higher than those of found from this study. The model is therefore useful, but it is still far from a complete solution and care must be taken in its use.

5.2.3 Effect of Strain Hardening Rate

Strain hardening rate is defined as [45];

$$SHR = \frac{UTS(1 + \%EL) - \sigma_y}{\%EL} \dots\dots\dots \text{Equation 5.2}$$

The formula gives the slope of the flow curve of the target material. As the formula represents all major mechanical properties like UTS, σ_y , and percent elongation, SHR may probably yield a better relationship with ballistic impact velocity.

In this study, as the strain hardening rate increases, ballistic limit velocity increases. More important, there is a linear relationship between the logarithmic strain hardening rate values and ballistic limits. A high rate of strain hardening implies mutual obstruction of dislocations gliding on intersecting systems. This can come about (1) through interaction of the stress fields of the dislocations, (2) through interactions which produce sessile locks, and (3) through the interpenetration of one slip system by another which results in the formation of dislocation jogs [16]. The obstruction of dislocation motion at high strain rates increase ballistic limit velocities for plugging type failure for which a material flow is needed in front of the blunt projectile. By preventing the dislocation motions this movement might possibly obstructed.

Therefore it can be stated that there is a more clear relationship between the SHR and ballistic limit in comparison to UTS or yield strength. The plot does not exhibit a discontinuity, rather a good linear relationship was observed. Additionally, SHR

may be suitable for comparison of ballistic performance of other metallic armor other than aluminum armor. Thus, SHR may be useful parameter for evaluation of a more universal criterion for the ballistic performance of metallic armor.

5.2.4 Effect of Charpy Impact Energy

It is well-known fact that the static test properties of materials are different than dynamic properties of materials. To get some quantitative information about the deformation of AA 2024 at high strain rate and under triaxial stress state (by the presence of a notch), Charpy impact tests were carried out. Although fracture energy measured by the Charpy test is only a relative energy [16], it gives some idea about the impact energies and toughness of AA 2024 aged at different conditions. Therefore the impact energy values measured in this study are of interest mainly in a relative sense and for making comparisons in AA 2024 targets in O and T6 conditions.

As indicated in **Figure 4.22**, ballistic limit velocities tend to decrease with increasing impact energy. At first it seems unusual to obtain such a result, because as it was mentioned before, high impact energy and toughness are the important parameters to reach high ballistic performance. This statement is still true; however ballistic performance is highly dependent on failure modes. That is ballistic limit velocities are decreasing with increasing impact energy in the range of 10 to 30 joules for which a plugging type failure is dominating. The two important points in plugging is; (1) the indentation of projectile until a plug start to form and (2) failure with shear plugging. In order to resist these two stages, target elements must have high hardness and yield strength. However both of these properties are inversely proportional to toughness. Therefore, as the impact energies are increased, ballistic limit velocities tend to decrease in range of 10-30 joules of impact energy and for plugging type failure of AA 2024.

5.2.5 Effect of Thickness and Lamination

Target thickness is one of the most important parameters in terminal ballistic. By changing thickness, ballistic performance may change abundantly. Moreover, failure mode can be changed with thickness. For example Woodward and Cimpoeru indicated that with thin targets having low strength dishing type failure may be seen yet for thick targets plugging dominates [10].

In this study monolithic targets notated as M1, M2 and M3 were peak aged prior to impact tests. After testing, it was observed that plugging type failure was led in these targets. **Figure 4.23** indicates the relationship between the target thickness and ballistic limits for monolithic targets. As seen ballistic limit velocities increase linearly with thickness. The results are in good agreement with Wen [62] which tested for different materials at ordnance velocities with blunt tip projectiles.

For the target named as M4 (10 mm thick), ballistic limit data could not be obtained using drop-weight test machine. If the thickness versus ballistic limit relationship were considered to be linear, ballistic limit value for M4 would correspond to almost 9.5 m/s which is beyond the speed limit of drop weight test machine (**Figure 5.8**). The same statement is true for laminated targets. As it is illustrated in **Figure 5.9**, the ballistic limit velocity for a four layered target is higher than 8.5 m/s.

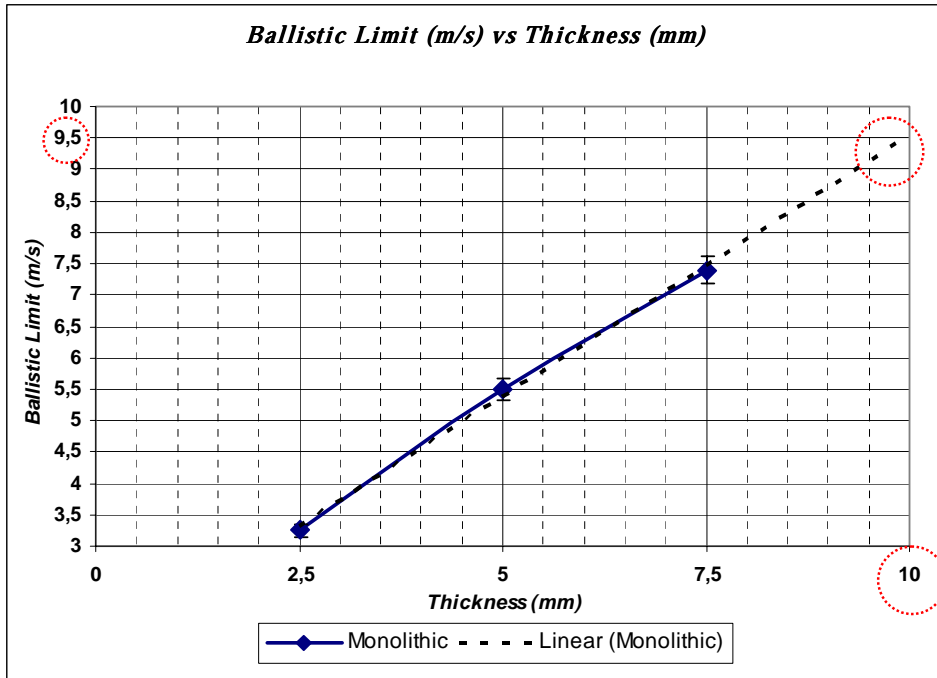


Figure 5.8 Ballistic limits versus Thickness (Monolithic).

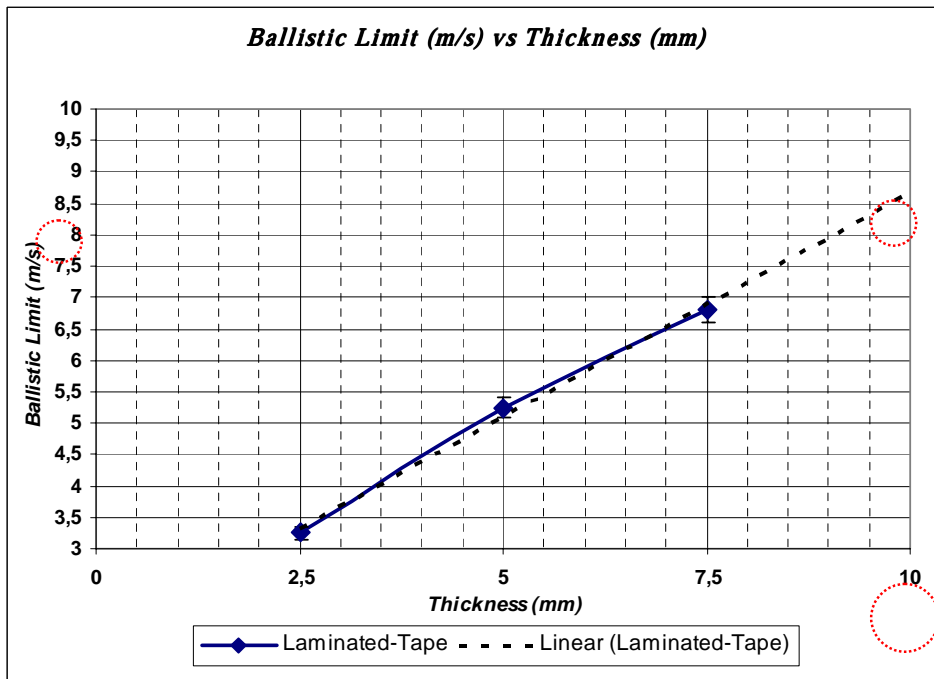


Figure 5.9 Ballistic limits versus Thickness (Laminated)

As it was mentioned earlier, if the force required to indent the target is less than the resistance of the plug to forward movement by shear, then indentation and compression of target material occurs initially. The indentation force is the area of the projectile impact face times the target flow stress times a constraint, K to account for the lateral confinement provided by surrounding target material [10]. Then indentation force becomes;

$$F_{indent.} = K.Y.(\pi.\frac{D^2}{4}) \dots\dots\dots \text{Equation 5.3}$$

Therefore the work performed during an indentation for an indentation depth of H_i becomes;

$$W_{indent.} = K.Y.(\pi.\frac{D^2}{4}).(H_i) \dots\dots\dots \text{Equation 5.4}$$

Woodward and Cimpoeru [10] stated the work performed during shear plugging as;

$$W_{plug.} = (\frac{\pi.Hp^2.DY}{2.\sqrt{3}}) \dots\dots\dots \text{Equation 5.5}$$

When the force to achieve forward movement of target plug is less than the force to indent the target, then indentation ceases. At this point it is necessary to consider how exit-side failure of the target may occur. For a plugging type failure, the total work for penetration of a target can be obtained by combining **Equation 5.4** and **5.5**. When equated to projectile kinetic energy, a limit velocity can be estimated.

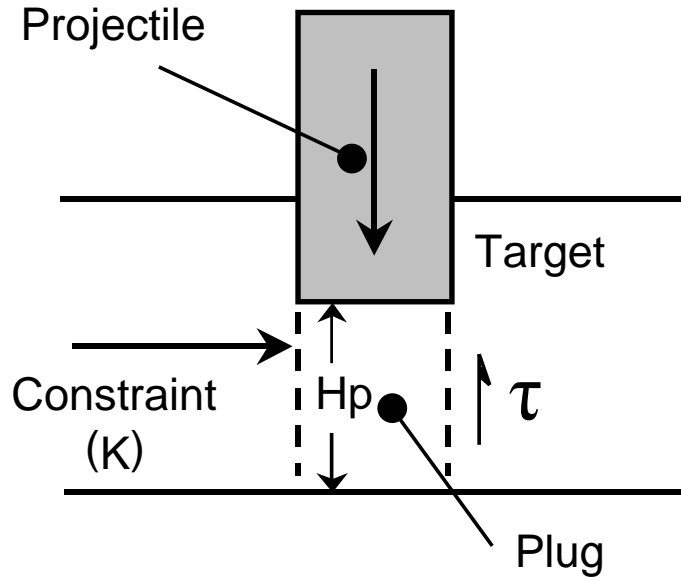


Figure 5.10 Simple force equilibrium model for plugging [10]

In the **Equations 5.3 to 5.5** as a material property flow stress was used. In this study, for the targets with notations M1 to M4 the values of uniform compressive strain ϵ_c [53] (**Equation 5.6**), were found to be close to the true strains at the yield point determined from the tension test[†]. The reason for that can be the low velocity regime of the experiments. Therefore, flow stresses were assumed to be equal to yield stresses. By combining **Equation 5.4** and **5.5** and equating to projectile kinetic energy, limit velocities were estimated in **Table 5.2**.

$$H_p = H \cdot \exp(-\epsilon_c) \dots\dots\dots \text{Equation 5.6}$$

[†] The Bauschinger effect is ignored.

Table 5.3 Comparison of experimental results with analytical model of Woodward and Cimpoeru [10]

Target	Ballistic Limit(m/s) -Experimental-	Ballistic Limit(m/s) -Analytical-	Percent Error %
M1	3,25	2,13	34
M2	5,50	4,41	20
M3	7,40	6,60	11
M4	9,50 [•]	8,54	10
• Estimated from Figure 5.8.			

For such a simple approach, the agreement can be considered successful. As it can be seen from **Table 5.2**, percent error is decreasing with increasing thickness of the target. The reason may be the decrease in amount of work of bending as the thickness increases. For relatively thick target, impact energy was mostly consumed for indentation of target and shear plugging. Therefore, equating the equations indicating the required energy for indentation and shear plugging to projectile energy for thicker plates seem to be more logic.

In **Figures 4.23 to 4.25** it is seen that ballistic limit velocities for monolithic targets are higher than those of laminated ones. Same statement was reported by Zukas and Scheffler [62] who concluded that layering weakened the thin targets, such that monolithic targets were more effective against perforation than equal weight multi-layered targets. Although metallic laminates have some potential advantages over monolithic armors, including the ability to be fabricated into thicker structures than is possible with monolithic plates of the same material for a given strength level, they seem to be weaker than monolithic targets under low velocity impact. A possible explanation may be the difference between their failure mechanisms. For laminated targets dishing provided by tensile stretching was dominated, whereas for monolithic targets pure shear plugging provided by shear forces was dominated [10]. However it must be stated that this claim is true for the conditions given in this

study. Dishing as a deformation mechanism in multi-layered targets is directly dependent on target thickness and number of layers [10].

As far as adhesive type is concerned, a remarkable change was not seen in ballistic limit values between the different type's adhesives. The reason for that may be the same failure mechanisms led for all laminated targets under low velocity impact. At ordnance or high velocity impacts this situation may change due to the change in failure mechanism [4, 63, 64, 65]. However, polyurethane based adhesive seems to be more effective in holding the laminates after the impact. After the tests under drop weight test machine, almost 90% of the epoxy adhered laminates were delaminated. However, none of the polyurethane adhered laminates were separated. The reason can be higher amount of percent elongation of polyurethane (nearly 300%) than epoxy based adhesives (nearly 2-5 %). The high amounts of percent elongation may allow polyurethane based adhesive to behave flexible.

CHAPTER 6

CONCLUSION

After a drop-weight testing was used to perforate AA 2024 targets the following conclusions can be withdrawn:

- 1) Monolithic targets were failed with *plugging* type of failure. Whereas, *dishing* was dominated for laminated targets.
- 2) The relationship between *hardness and ballistic limit* was found to be linear in the range of *50 to 150 BHN*. Moreover, a linear behavior was observed between *logarithm of strain hardening rate and ballistic limit* as well.
- 3) On the other hand the relationship between *UTS and ballistic limit* with *yield strength and ballistic limit* were *complex*. A discontinuity is present rather than being line.
- 4) In both *monolithic and laminated target*, the *ballistic limits* of the targets *increase linearly with an increase in thickness*. At *identical thickness*, the *resistance of monolithic targets* is found to be *higher* than *laminated targets*.
- 5) Using either an *epoxy or polyurethane* adhesive to join the laminates *did not affect the resistance to perforation*.

- 6) Due to its brittle nature, 90% of the *epoxy* adhered targets were *delaminated*. However a delamination was not observed in targets bonded by *polyurethane* based adhesive.

- 7) It has been shown that *experimental observations* for the ballistic limit velocities of AA 2024 targets are in good agreement with *recently proposed models*.

- 8) *The ballistic limits of monolithic targets* were *inversely proportional* to Charpy *impact energies* in the range of *10 to 30 joules* and for *plugging* type failures.

REFERENCES

- [1] **Thomas J.H.**, “*Elements of Ordnance*”, New York, *John Wiley & Sons, Inc.*, 1938.

- [2] **Lowry E.D.**, “*Interior Ballistics*”, New York, *Doubleday & Company*, 1968.

- [3] **Ryan J.W.**, “*Guns, Mortars & Rockets*”, Shrivenham, *Brassey’s Publishers Limited* a member of the Pergamon Group, 1981.

- [4] **Zukas J.A., Nicholas T., Swift H.F., Greszczuk L.B., Curran D.**, “*Impact Dynamics*”, pp. 155-214, *John Wiley & Sons, Inc.*, 1982.

- [5] **Zukas J.A., Jonas G.H.**, “*Mechanics of Penetration; Analysis and Experiment*”, *International Journal of Engineering Science*, Vol. 16, pp. 879-903, 1978.

- [6] **Backman M.E., Goldsmith W.**, “*The Mechanics of Penetration of Projectiles into Targets*”, *International Journal of Engineering Science*, Vol. 16, pp. 1-99, 1978.

- [7] **Ipson T.W., Recht R.F., Schmelling W.A.**, Ppt. NWC TP 5607, *Naval Weapons Center, California*, 1973.

- [8] **U.S. Army Ballistic Research Laboratories**, “*A Penetration Equations Handbook. (Joint Technical Coordination Group)*”, Aberdeen Proving Ground, Maryland, 1977.
- [9] **Woodward R.L.**, “*Penetration Behavior of a High Strength Aluminum Alloy*”, *Metals Technology*, Vol. 6, pp. 106-110, 1979.
- [10] **Woodward R.L., Cimpoeru S.J.**, “*A Study of the Perforation of Aluminum Laminate Targets*”, *International Journal of Impact Engineering*, Vol. 21, No. 3, pp. 117-131, 1998.
- [11] **Air Force Flight Dynamics Lab.** “*Tech. Rpt. JTTCG/AS-74-D-002.*” Wright-Patterson Air Force Base, Ohio, 1976.
- [12] **AMCP 706-161** “*Elements of Terminal Ballistics, Part II, Collection and Analysis*”, Washington D.C., U.S. Army Material Command, 1962.
- [13] **Throop J.F., Fujezak R.R.**, “*Fracture Resistant Titanium-Aluminum Laminate. In Toughness and fracture Behavior of Titanium*”, ASTM-STP-651, ASTM, pp. 246-266, 1978.
- [14] **Lambert J.P., Ringers B.E.**, Ballistic Research Laboratory, ARBRL-TR-02066, 1978.
- [15] **ASTM Standards**, pt. 31, pp. 582-601, “*Designation E208-69*”, 1969.
- [16] **Dieter G.E.**, “*Mechanical Metallurgy, SI Metric Edition*”, McGraw-Hill Inc, 1988.

- [17] **Çolakoğlu A.**, “*Design and Construction of a Gravity Drop Hammer*”, M.Sc. Thesis, Mechanical Engineering Department, METU, 2002.
- [18] **H.P. White Laboratory**, “Sharp Instrument Penetration of Body Armor”, Inc. Test Procedures, HPW-TP-0400.03, 1994.
- [19] **ASM Specialty Handbook**, “Aluminum and Aluminum Alloys”, Materials Information Society, 1996.
- [20] **Van Horn K.R.**, “Aluminum, *VOL.I. PROPERTIES, PHYSICAL METALLURGY AND PHASE DIAGRAMS*”, American Society for Metals, 1968.
- [21] **Altenpohl D.**, “*Aluminum Viewed from Within*”, Aluminum-Verlag, Dusseldorf, 1982.
- [22] **ASM Handbook**, “Heat Treating of Aluminum Alloys vol. 4”, ASM International, 1991.
- [23] **Aluminum Company of America**, “*Adhesive Bonding: Alcoa Aluminum*”, 1967.
- [24] **Cagle C.V.**, “*Handbook of Adhesive Bonding*”, McGraw-Hill Book Company, 1973.
- [25] **Wilkes, Joseph A.**, “*Encyclopedia of Architecture, Design, Engineering and Construction*”, New York, John Wiley & Sons, 1988.
- [26] **Amstock J. S.**, “*Handbook of Adhesives and Sealants in Construction*”, McGraw-Hill, 2000.

[27] **Dormish J.**, “*Polyurethane Adhesives*”, Technology and Development Trends, Bayer Corp. Akron OH 44236.

[28] **Sealant, Waterproofing & Restoration Institute**, “*Sealants: The Professionals’ Guide*”, 1995.

[29] **Eichner H.W., Schowalter W.E.**, Report 1813, Forest Products Laboratory, 1950.

[30] **Rodgers N.L.**, Society for the Advancement of Material and Process Engineering, 13th National SAMPE Technical Conference, pp. 640, 1981.

[31] **Desai A., Ahearn J.S., Namara D.K.**, “*Cleanliness of External Tank Surfaces*”, MML TR-85-65, Martin Marietta Laboratories, 1985.

[32] **Kabayashi G.S., Donnelly D.J.**, Report D6-41517, The Boeing Company, 1974.

[33] **Military Specification**, MIL-A-862C.

[34] **Brockman W., Hennemann O.D.**, Society for Advancement of Material and Process Engineering, 11th National SAMPE Technical Conference, pp. 804-816, 1979.

[35] **Brockman W., Hennemann O.D., Kollek H., Matz C.**, International Journal of Adhesion, Vol. 6, pp. 115, 1986.

[36] **Guttman W.H.**, “*Concise Guide to Structural Adhesives*”, New York, Reinhold Publishing Corporation, 1961.

[37] **ASTM Standards**, “*Designation D 2651-90*”, “*Standard Guide for Preparation of Metal Surfaces for Adhesive Bonding*”, 1993.

- [38] **Hardy H.K., Heal T.J.**, Prog. Met. Phys. 5, pp. 143-278, 1954.
- [39] **Bagaryatskii I.A.**, Zh. Tech. Fiz. 18 pp. 827, 1948.
- [40] **Şimsir C.**, “*Low Velocity Ballistic Characterization of Steel Armor Plates by Drop-Weight Test*”, M.Sc. Thesis, Metallurgical and Material Engineering Department, METU, 2002.
- [41] **ASTM Standards**, “*Designation E 8M, ‘Tension Test’*”, 1993.
- [42] **ASTM Standards**, “*Designation D 897-78 (Reapproved 1983), ‘Standard Test Method for Tensile Properties of Adhesive Bonds’*”, 1993.
- [43] **ASTM Standards**, “*Designation D 1002-72-78 (Reapproved 1983), ‘Standard Test Method for Strength Properties of Adhesives in Shear by Tension Loading (Metal-to Metal)’*”, 1993.
- [44] **ASTM Standards**, “*Designation E 23, ‘Impact Test’*”, 1993.
- [45] **Srivatsa B., Ramakrishan N.**, “Ballistic Performance for Thick Metal Armor”, Journal of Materials Processing Technology, 96, pp. 81-96, 1999.
- [46] **Borvik T., Hopperstad O. S., Langseth M., Malo K.A.**, “Effect of target thickness in blunt projectile penetration of Weldox 460 E steel plates”, International Journal of Impact Engineering, 28, pp. 413-464, 2003.
- [47] **Chen X.W., Li Q.M.**, “Shear plugging and perforation of ductile circular plates struck by a blunt projectile” International Journal of Impact Engineering, 28, pp.513-536, 2003.

- [48] **Awerbuch J.A.**, “Mechanics approach to projectile penetration”, Israel J. Tech., 8, pp.375-383, 1970.
- [49] **Goldsmith W., Finnegan S.A.**, “Penetration and perforation processes in metal targets at and above ballistic velocities”, International Journal of Mechanical Science, 13, pp.843-866, 1971.
- [50] **Ravid M., Bodner S.R.**, “Dynamic perforation of viscoplastic plates by rigid projectiles”, International Journal of Engineering Science, 21, pp.577-579, 1983.
- [51] **Liss J., Goldsmith W., Kelly J.M.**, “A phenomenological penetration model of plates”, International Journal of Impact Engineering, 1(4), pp.321-341, 1983.
- [52] **Awerbuch J.A., Bodner S.R.**, “Analysis of the mechanics of perforation of projectiles in metallic plates”, International Journal of Solids Structure, 10, pp.671, 1974.
- [53] **Woodward R.L., deMorton M.E.**, “Penetration of targets by flat-ended projectiles”, International Journal of Mechanical Science, 18, pp.119, 1976.
- [54] **Meyers M.A.**, “Dynamic Behavior of Materials”, John Wiley and Sons, Inc., 1994.
- [55] **Borvik T., Leinum J.R., Solberg J.K., Hopperstad O.S., Langseth M.**, “*Observations on Shear Plug Formation in Weldox 460 E Steel Plates Impacted by Blunt-Nosed Projectiles*”, International Journal of Impact Engineering, **25**, pp 553-573, 2001.

- [56] **Levy N., Goldsmith W.**, “Normal impact and perforation of thin plates by hemispherically-tipped projectile-II. Experimental results”, International Journal of Impact Engineering, 2, pp. 299, 1984.
- [57] **Borvik T., Hopperstad O. S., Langseth M., Malo K.A.**, “Perforation of 12 mm thick steel plates by 20 mm diameter projectiles with flat, hemispherical and conical noses” Part I : Experimental study”, International Journal of Impact Engineering, 27, pp. 19-35, 2002.
- [58] **Baker W.E., Westine PS., Dodge FT.**, “Similarity methods in engineering dynamics”, Theory and practice of scaling modelling, Amsterdam, Elsevier, 1991.
- [59] **Wingroove A.L., Wulf G.L.**, “Some aspects of target and projectile properties on penetration behavior”, Journal of Aust. Inst. Metals, 18, pp. 167-173, 1973.
- [60] **Mangelo J., Abbott K.H.**, “Metallurgical factors affecting the ballistic behaviour of steel targets”, Journal of Materials, JMLSA, 17, pp. 231-239, 1972.
- [61] **Chen X.W., Li Q.M.**, “Perforation of a thick plate by rigid projectiles” International Journal of Impact Engineering, 28, pp.743-759, 2003.

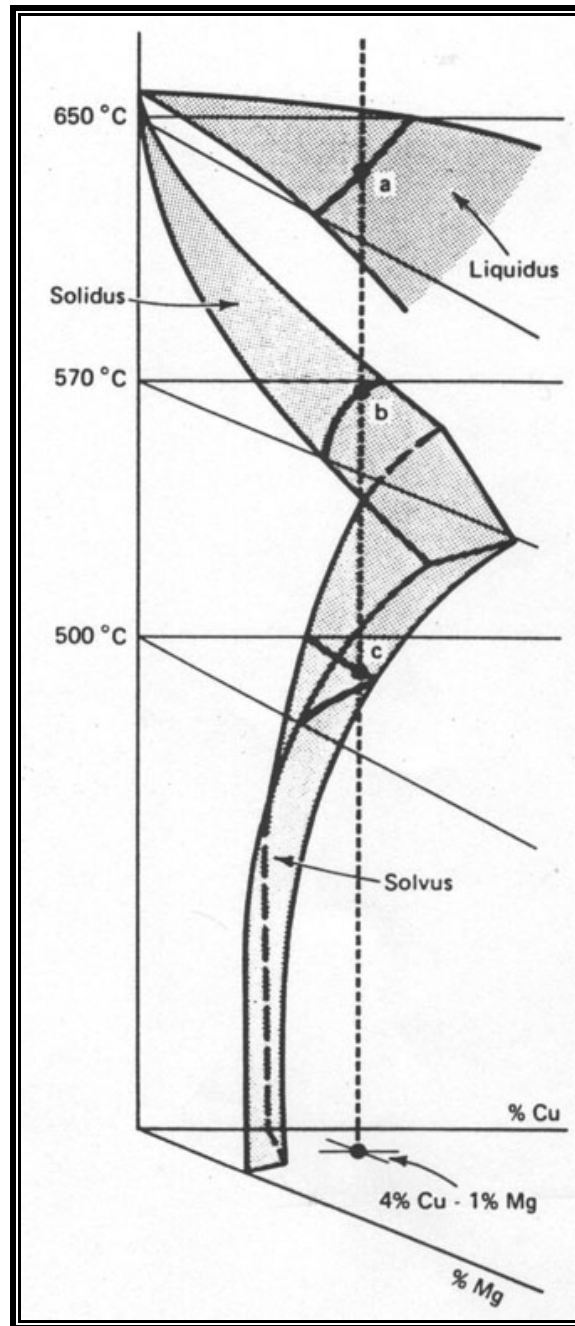
[62] **Wen H.M.**, “Predicting the penetration and perforation of targets struck by projectiles at normal incidence” *Mechanics of Structures and Machines*, 30, pp.543-577, 2002.

[63] **Zukas J.A., Sheffler D.R.**, “Impact Effects in Multi-Layered Plates”, *International Journal of Solids and Structures*, 38, pp. 3321-3328, 2001.

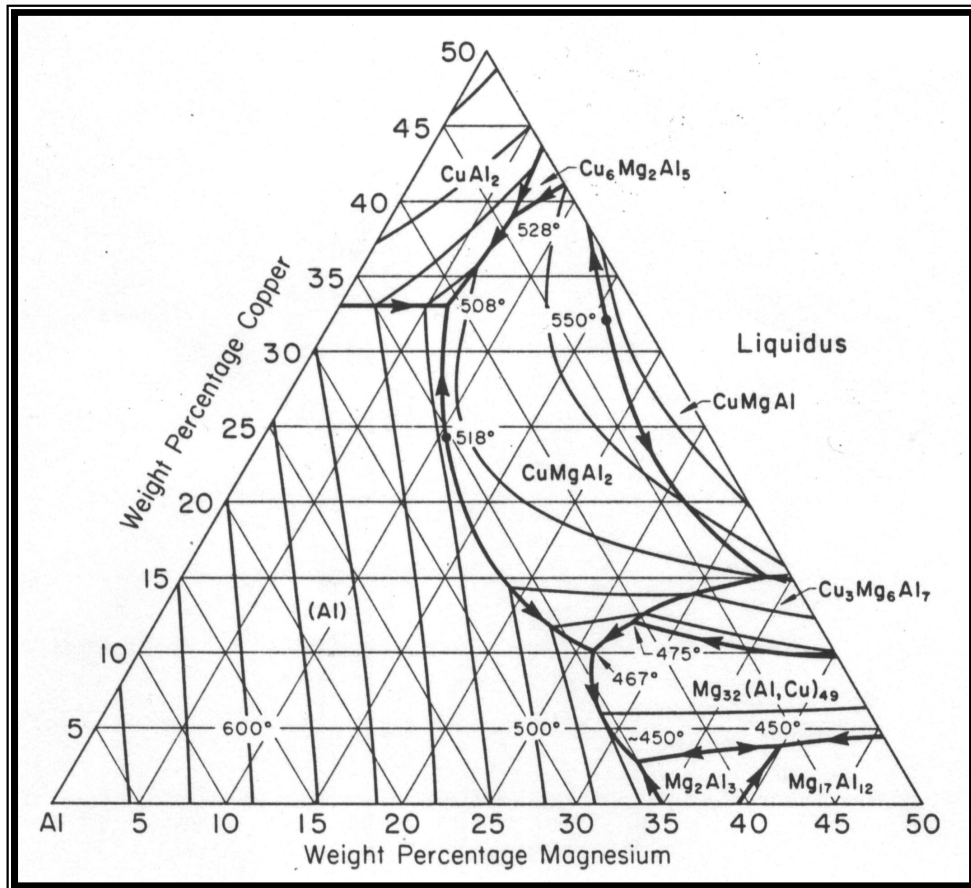
[64] **Blazynski T.Z.**, “Materials at High strain Rates”, Elsevier Applied Science Publishers LTD., 1987.

[65] **Woodward R.L.**, “*The interrelation of failure modes observed in the penetration of metallic targets*”, *International Journal of Impact Engineering*, Vol. 2, pp. 121-129, 1984.

APPENDICES



Appendices I Three Dimensional Phase Diagram of Al-Cu-Mg



Appendices 2 Ternary Phase Diagram of Al-Cu-Mg

Unit Conversion Factors

Length

1 cm 0.394 in.

1 m 3.28 ft

Area

1 cm² 0.1550 in²

1 m² 10.76 ft²

Mass

1 kg 2.205 Ib_m

Force

1 N 10⁴ dynes

1 N 0.2248 Ib_f

Stress

1 MPa 145 psi

1 Pa 10 dynes/cm²

1 kg/mm² 1422 psi

Appendices 3 Unit Conversion Factors